



UNITED NATIONS EDUCATIONAL, SCIENTIFIC AND CULTURAL ORGANIZATION  
INTERNATIONAL ATOMIC ENERGY AGENCY  
INTERNATIONAL CENTRE FOR THEORETICAL PHYSICS  
I.C.T.P., P.O. BOX 586, 34100 TRIESTE, ITALY, CABLE: CENTRATOM TRIESTE



**SMR.998a - 7**

Research Workshop on Condensed Matter Physics  
30 June - 22 August 1997  
**MINIWORKSHOP ON**  
**QUANTUM MONTE CARLO SIMULATIONS OF LIQUIDS AND SOLIDS**  
**30 JUNE - 11 JULY 1997**  
**and**  
**CONFERENCE ON**  
**QUANTUM SOLIDS AND POLARIZED SYSTEMS**  
**3 - 5 JULY 1997**

---

**"Vacancies and phonons in solid 4He"**

**R. SIMMONS**  
**University of Illinois @ Urbana-Champaign**  
**Department of Physics**  
**1110 West Green Street**  
**IL 61801-3080 Urbana**  
**U.S.A.**

---

**These are preliminary lecture notes, intended only for distribution to participants.**

# Study of quantum solid heliums by X-ray and neutron scattering

Ralph O. Simmons

Physics Department and Frederick Seitz Materials Research Lab  
University of Illinois at Urbana-Champaign  
Urbana, IL 61801 USA

Conference on Quantum Solids and Polarized Systems  
International Centre for Theoretical Physics  
Trieste, Italy

3-5 July 1997

## **Dynamical studies using neutron and X-ray scattering probes**

Momentum distributions from neutron scattering

Limitations of self-consistent phonon theories

Conceptual

Disagreements with experiment

Path-integral Monte Carlo and related methods

Some agreements achieved with experiments

Projects in process

X-ray studies of dense helium solids

Debye-Waller  $\langle u^2 \rangle$

Dynamic diffuse scattering elastic response

Phonon spectroscopy (works for  $^3\text{He}$ !) dispersion

## **Equilibrium studies using X-ray diffraction**

*PVT*

Point defects and disorder

Differences from indirect techniques (Pressure,  
NMR... )

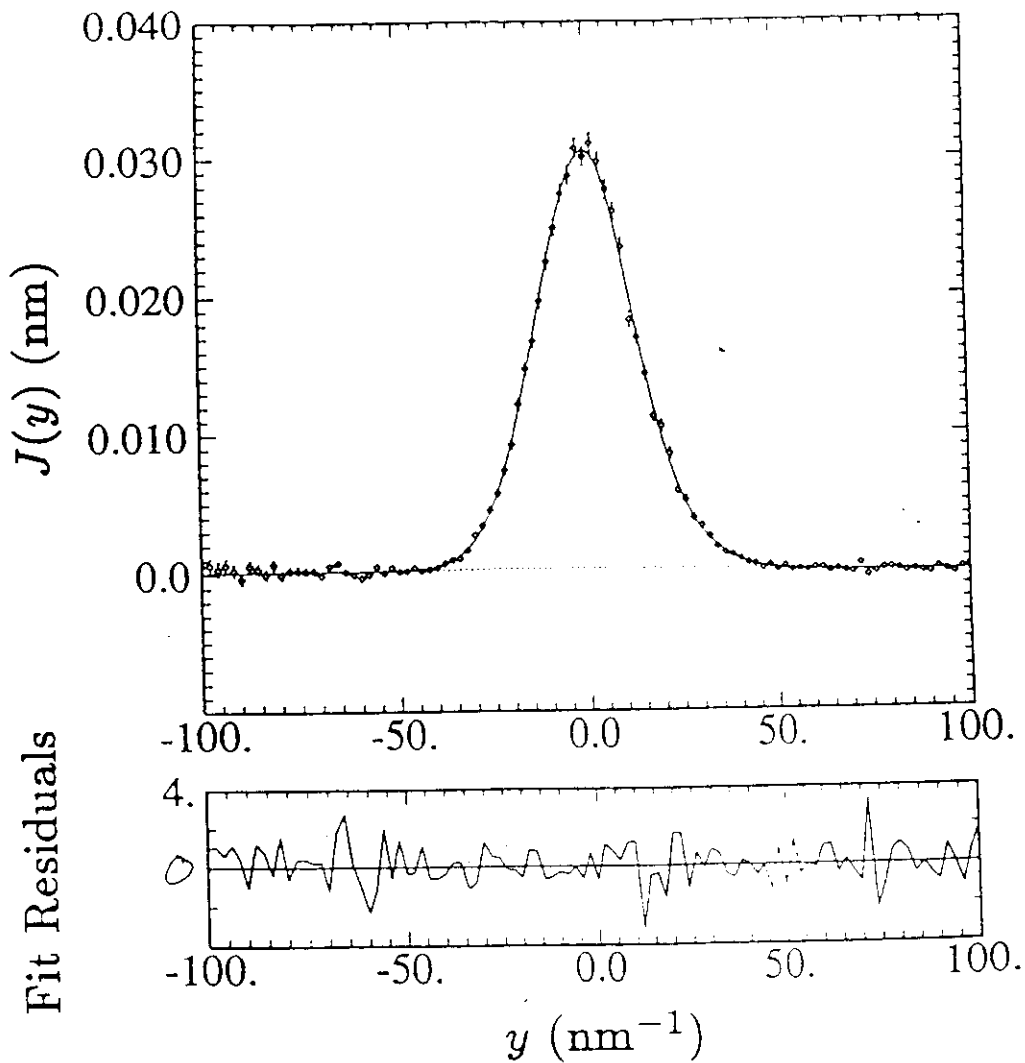
The  $^3\text{He}$ - $^4\text{He}$  mixture zoo

## **Future possibilities**

The kinetic energy,  $E_k$ , of a condensed system can be measured directly, by careful measurement of the ‘longitudinal neutron Compton profile’  $J(y)$

(“careful” means proper accounting for spectrometer resolution and final-state effects in the scattering)

$$S(Q, \omega) = \frac{m}{\hbar Q} \int n(p_{\parallel}, p_{\perp}, y) dp_{\parallel} dp_{\perp} \equiv \frac{m}{\hbar Q} J(y), \text{ where } y = \frac{m}{\hbar Q} \left( \hbar \omega - \frac{\hbar^2 Q^2}{2m} \right)$$



(liquid  $^4\text{He}$  at  $32.74 \text{ nm}^{-3}$  and  $4.20 \text{ K}$ )

Ceperley, Simmons, Blasdel, Phys. Rev. Lett. **77**, 117 (1996)

A comprehensive picture is now available of the kinetic energy,  $E_k$ , of solid and normal liquid  $^4\text{He}$

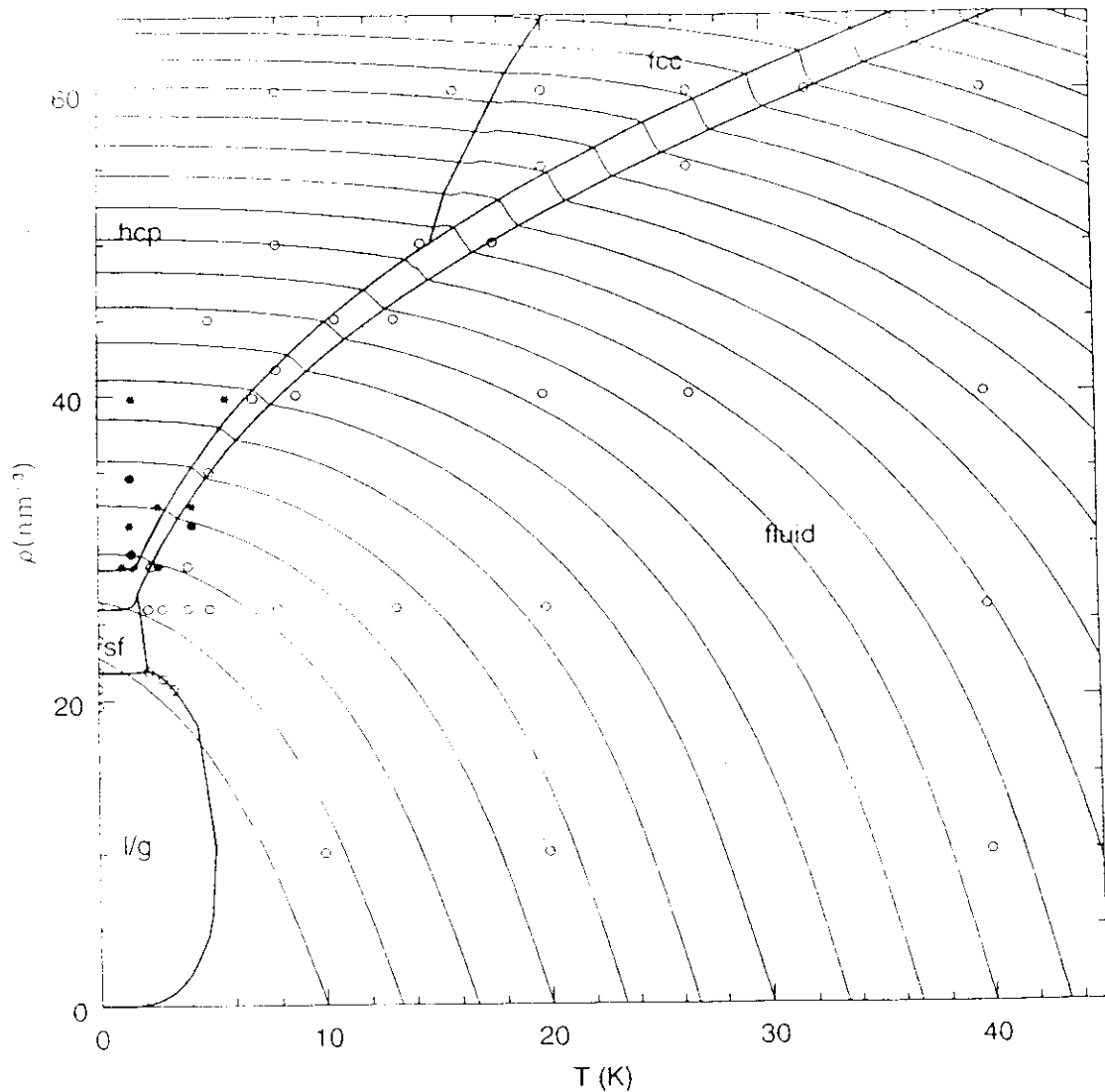
Values of  $E_k$  are not affected much by phase:

bcc, hcp, normal liquid

At constant density,  $E_k$  increases slightly at melting

Helium at high densities remains a 'quantum liquid'

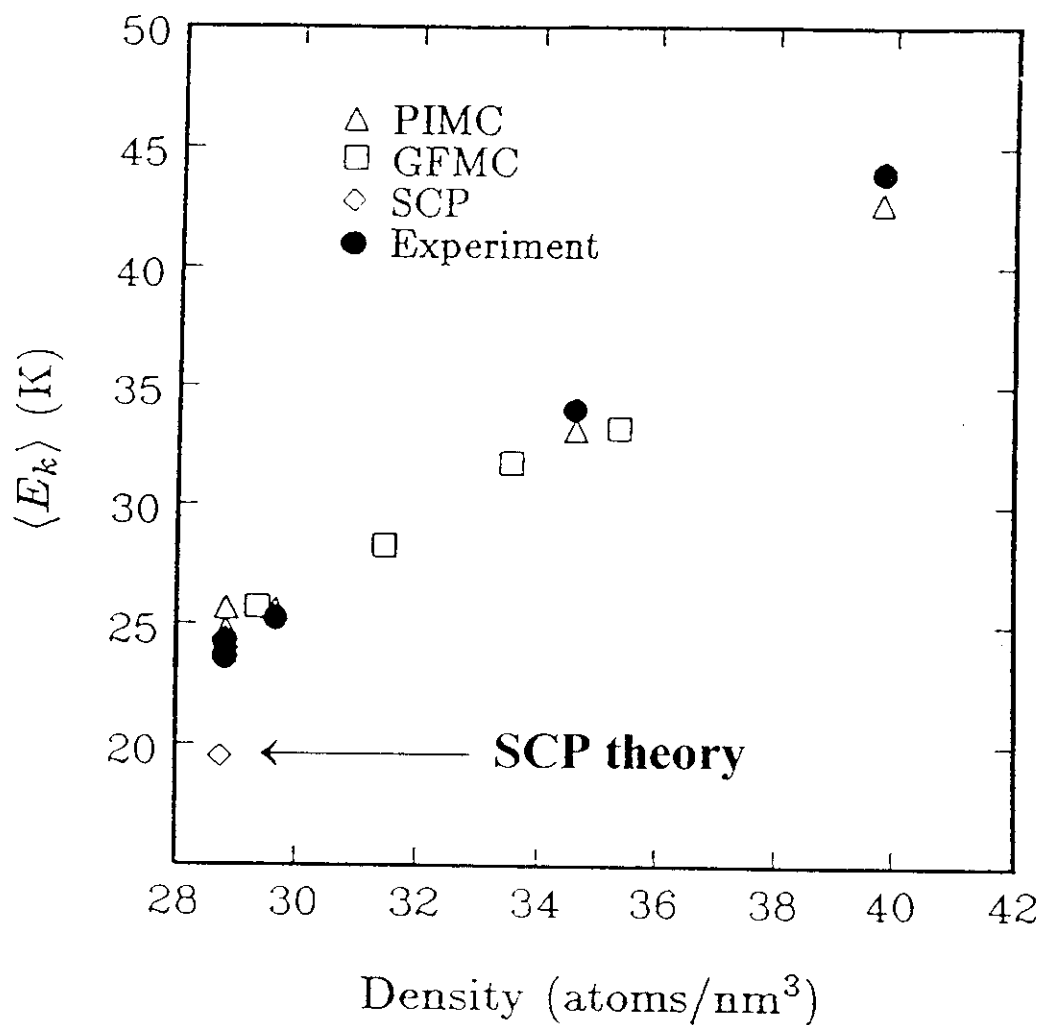
up to high temperatures



Ceperley, Simmons, Blasdel, Phys. Rev. Lett. 77, 117 (1996)

# Single-Particle Kinetic Energies $\langle E_k \rangle$

$^4\text{He}$



PIMC values agree with experiment within 3%

Self-Consistent Phonon (SCP) value differs by 20%

R.S. Blasdell, D.M. Ceperley, R.O. Simmons  
Z. Naturforsch. **48a** (1993) 433

## Self-Consistent Phonon Theory

- Qualitative success with one-phonon dispersion.
- Explains *some* excitation curve shapes as multi-phonon interference effects.
- Explains *some* explicit anharmonicities (i.e.  $T$  dependence of phonon energies at constant  $V$ ).
- 20% errors common in one-phonon energies. This is larger than raw isotope mass effect  $(4/3)^{1/2} = 1.15$ , and doesn't sensitively test potential changes.
- No consistent link to properties of liquid phases.
- No link to point- or line-defect properties.

## Path-Integral Monte Carlo

- Obtains accurate melting curves of both  $^3\text{He}$  and  $^4\text{He}$  over density range of factor 5. Note, this is an extremely sensitive test for very accurate values of total energy of both liquid and crystal phases.
- Obtains kinetic energies to a few percent accuracy, in both solid and liquid phases.
- Obtains  $S(hkl)$  values to predict Debye-Waller factors.
- Applicable to liquid and to point defect calculations on a consistent basis.

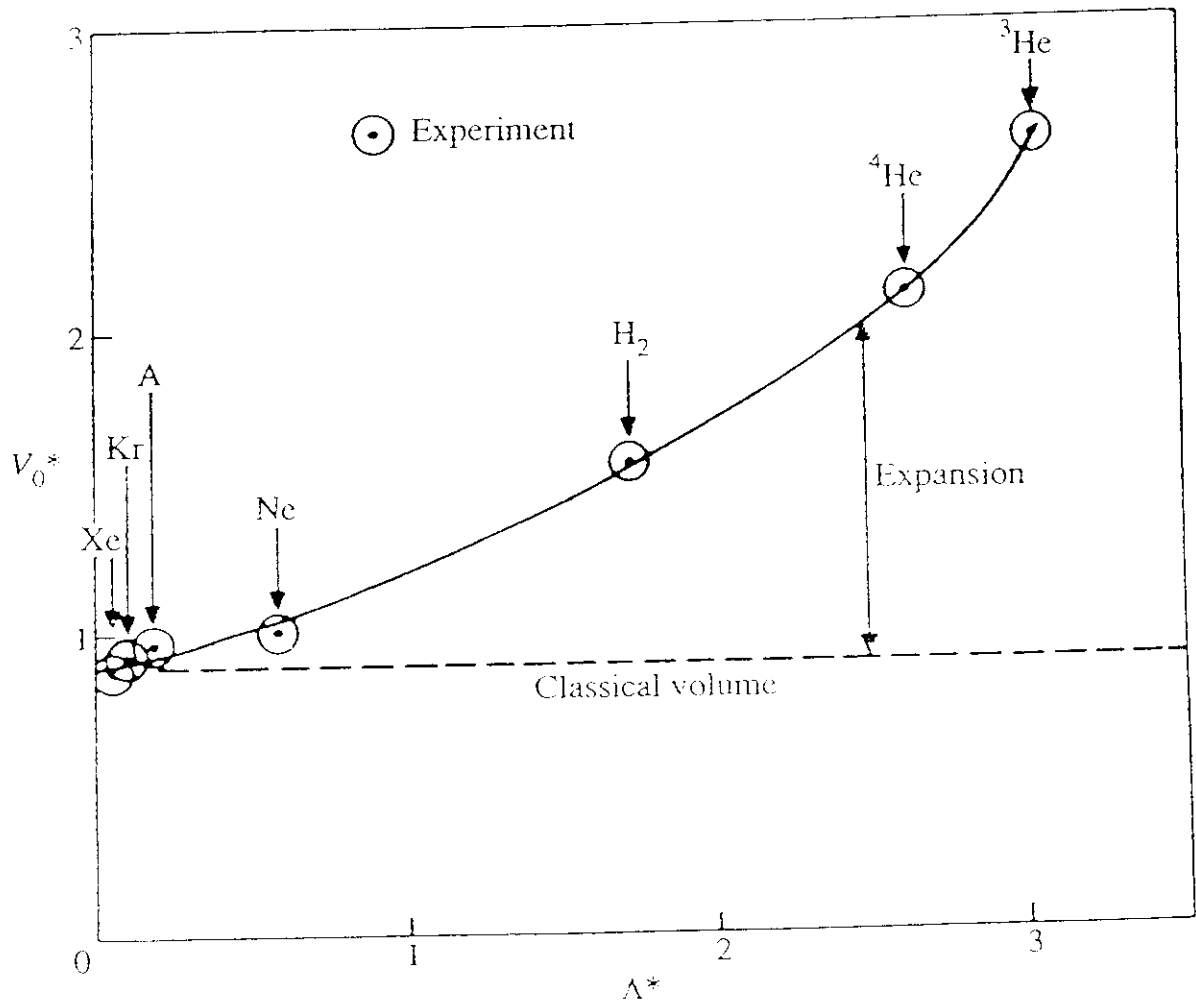
# Quantum Corresponding States

de Boer defined a quantum parameter

$$\Lambda^* = \Lambda / \sigma \equiv h / p \sigma = h / (\sigma m^{1/2} \epsilon^{1/2})$$

and could then form 'reduced' parameters, e.g.

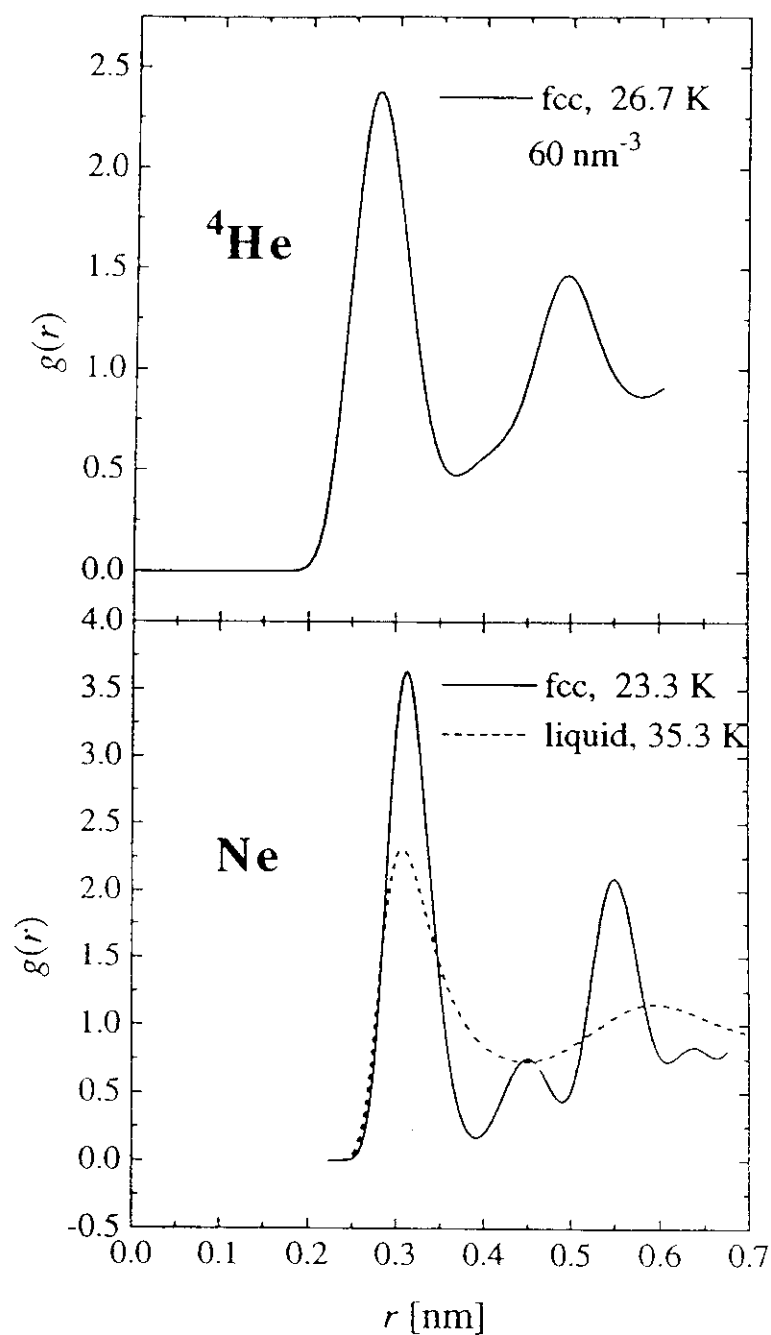
$$V_0^* = V_0 / (N_A \sigma^3)$$



Molar volumes of crystals plotted in de Boer's reduced units ( $V_0^*$ ) against a reduced de Broglie wavelength ( $\Lambda^*$ ) to show the quantum expansion of the lighter inert gas and molecular crystals compared with the classical molar volume of the heavier inert crystals (after de Boer 1948).



Pair distributions  $g(r)$  by Path-Integral Monte Carlo  
crystal He is **highly delocalized**

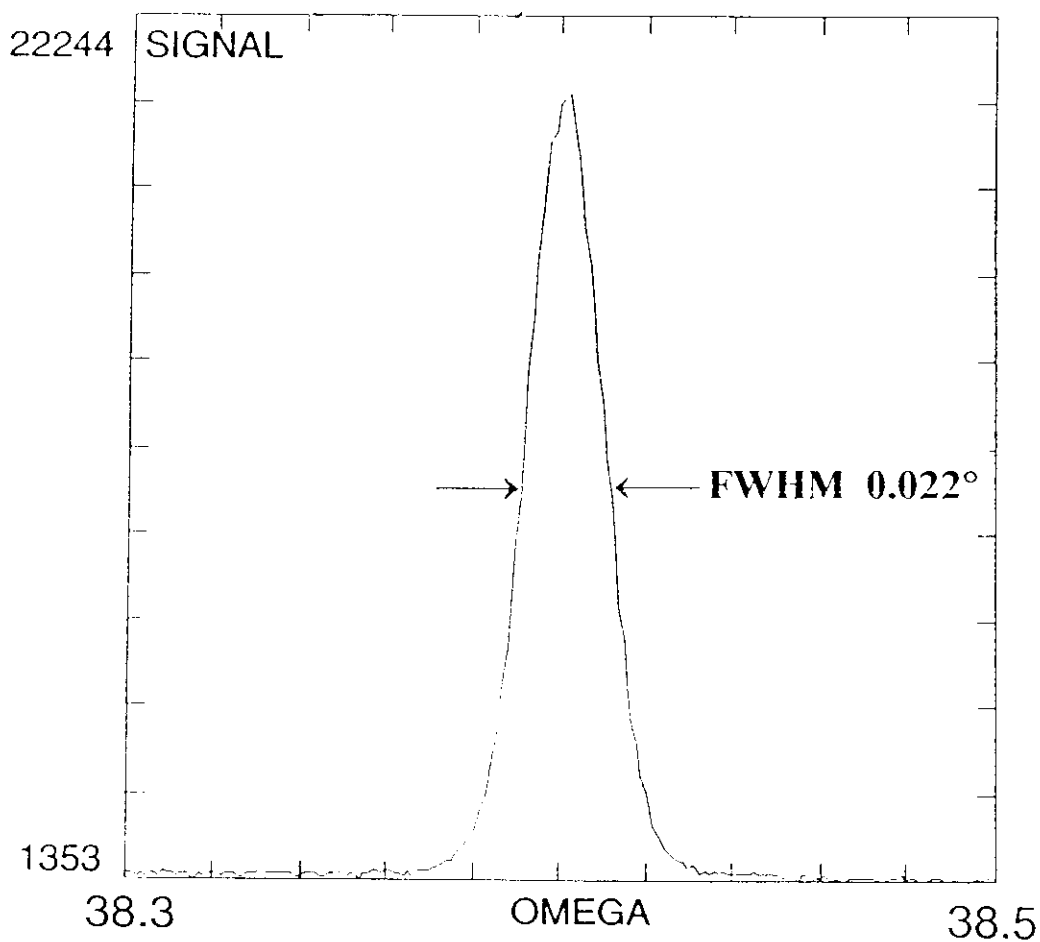


D.M. Ceperley, Rev. Mod. Phys. **67** (1995) 279

Excellent helium crystals can be grown over a wide range of densities

**(300) rocking curve hcp  $^3\text{He}$**

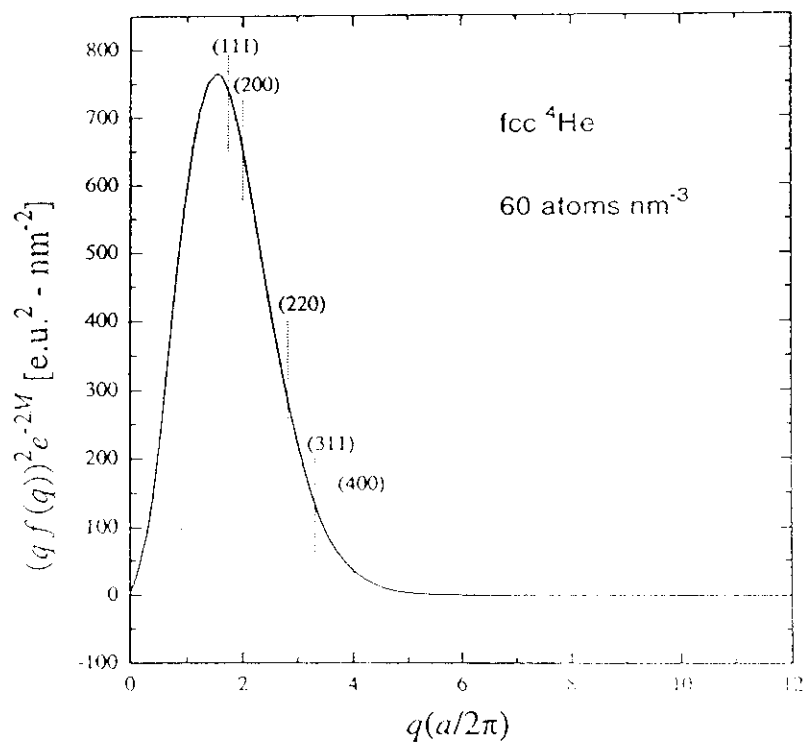
$V = 11.594 \text{ cm}^3$ ,  $T = 13.5 \text{ K}$



D.A. Arms, R. Shah, M. Schwoerer-Böhning, R.O. Simmons  
Brookhaven NSLS X-14A (1996)

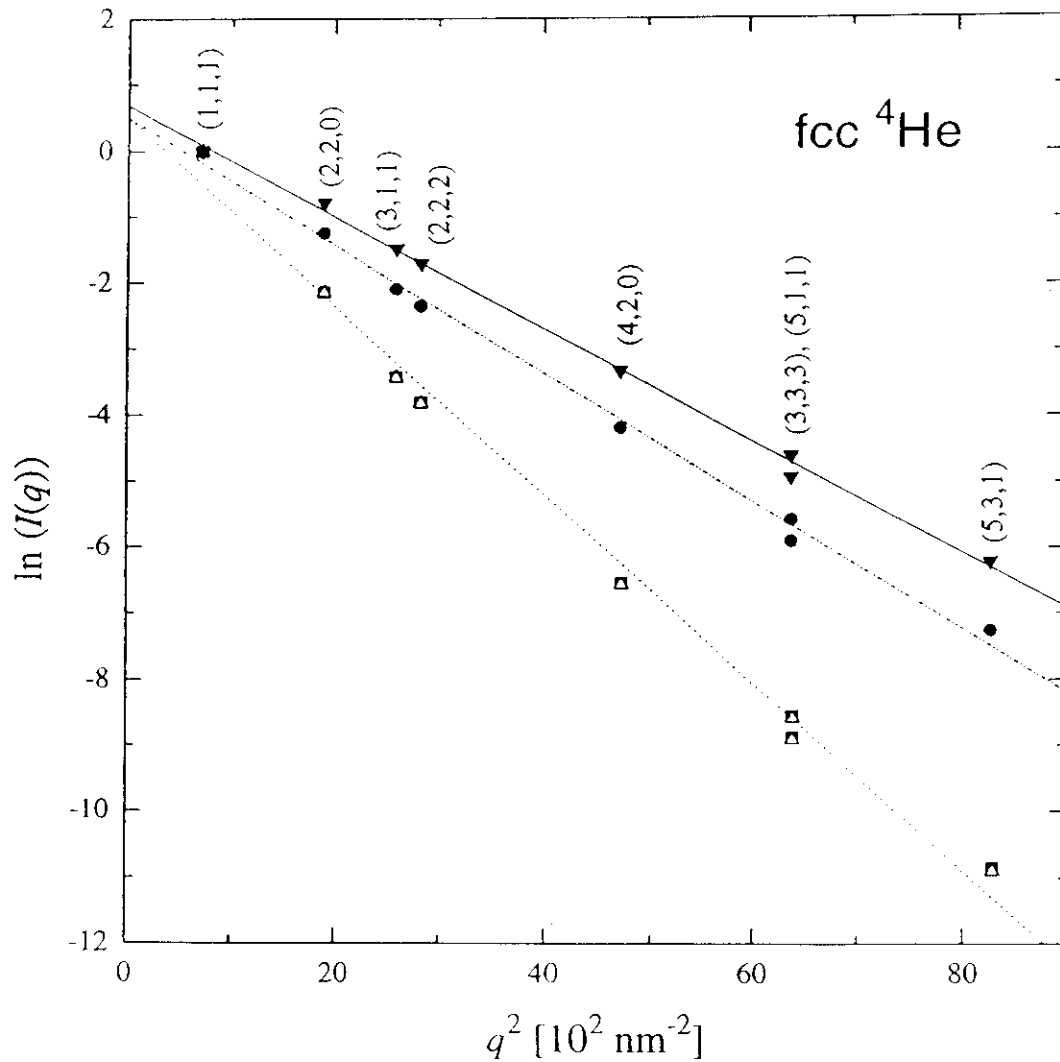
# $q$ -dependence of scattering intensities a problem in studying helium by X-rays

Restricted range for  
diffuse scattering studies  
phonon studies



# Debye-Waller effects in fcc $^4\text{He}$

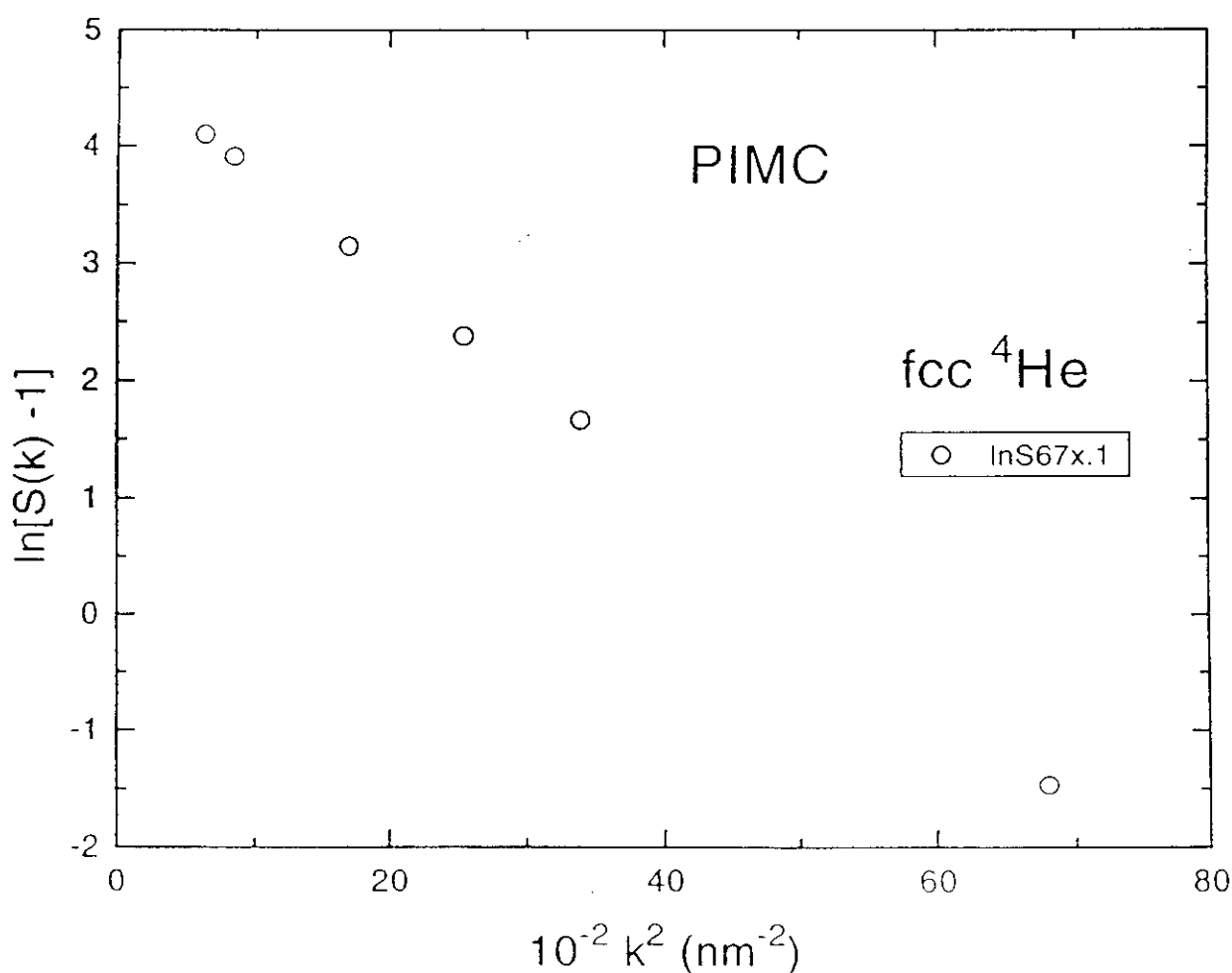
The  $q$ -dependence is extraordinarily large.  
 $q$ -dependent corrections (e.g.  $f(q)$ ) are important.



Venkataraman and Simmons, Czech. J. Phys. **46**, 461 (1996)

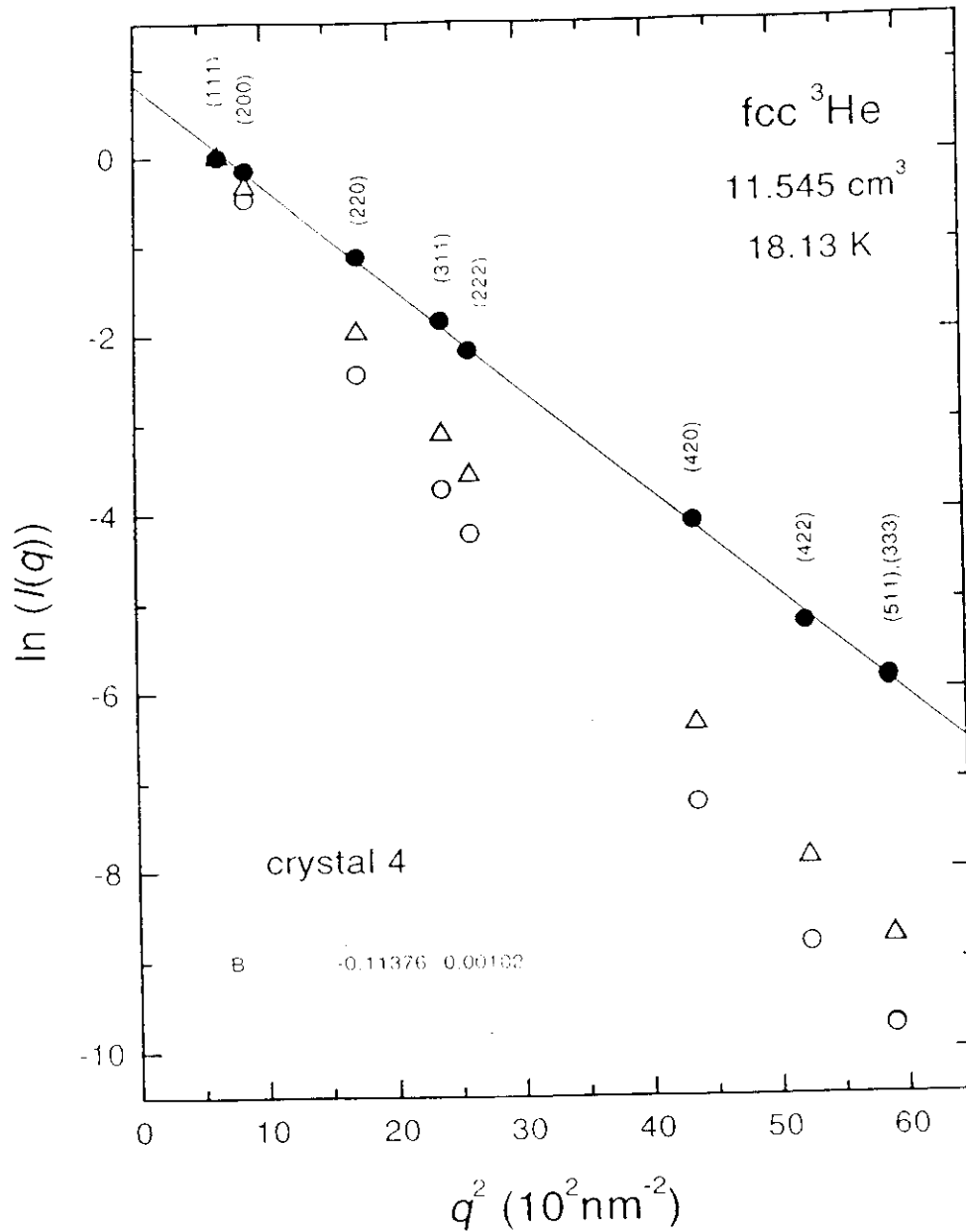
# **Path-Integral Monte Carlo** **calculation of crystal structure factors** **at particular densities and temperatures** $S(hkl)$

D.M. Ceperley (1996)



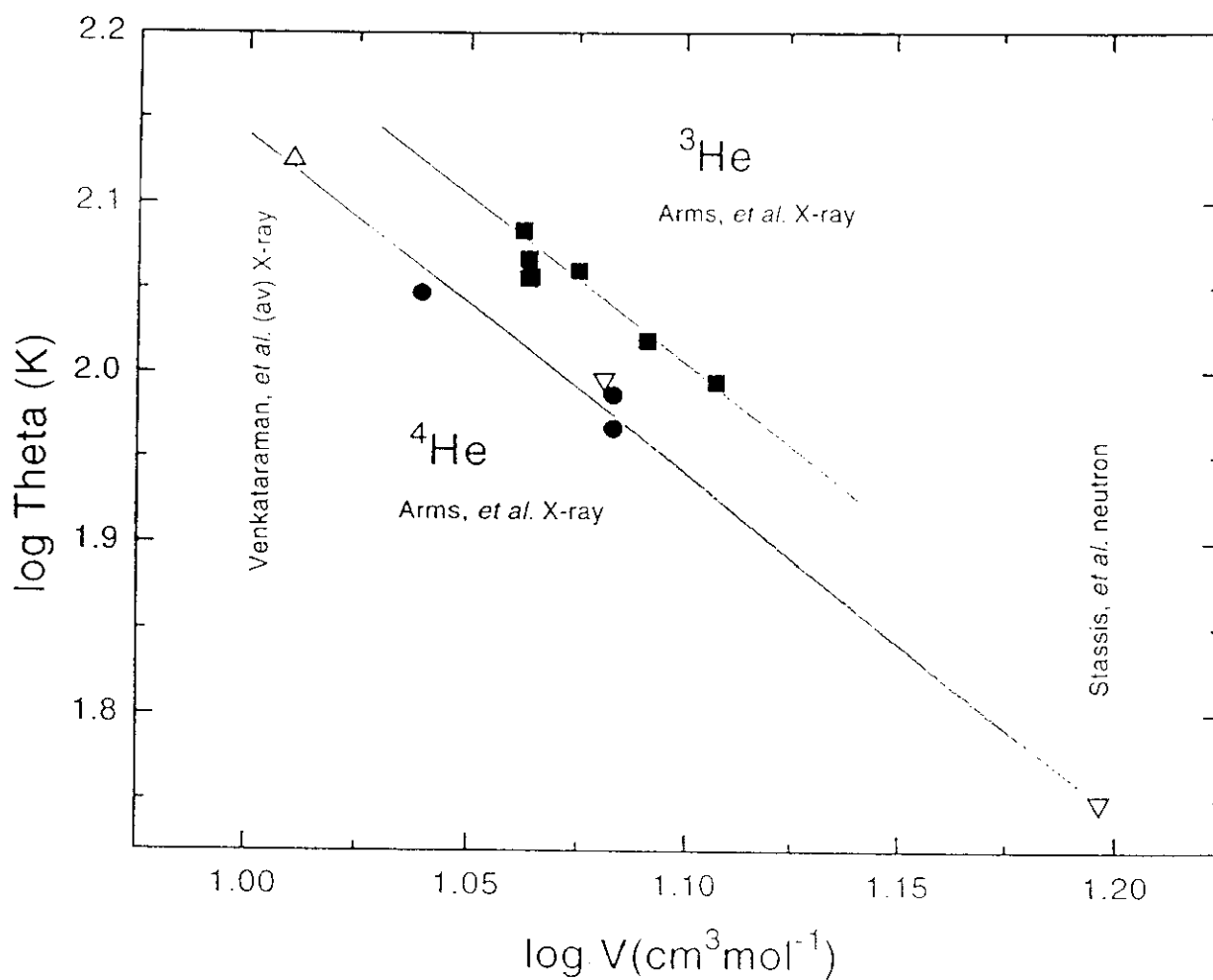
Agreement with Venkataraman data is very good.

Precise synchrotron X-ray Debye-Waller results  
provide direct measure of  $\langle u^2 \rangle$  as function of density and  $T$



Arms, Shah, Simmons, Schwoerer, Brookhaven NSLS (1997)

X-ray Debye Waller Factors  
can be converted to  
Equivalent Debye Characteristic Temperatures  
 $\Theta_M(V)$



Arms, Shah, Schwoerer-Böhning, Simmons (1996) NSLS X-14A

Venkatarman (Illinois thesis 1996)

Stassis, Khatamian, Kline, Solid State Comm. **25** (1978) 531

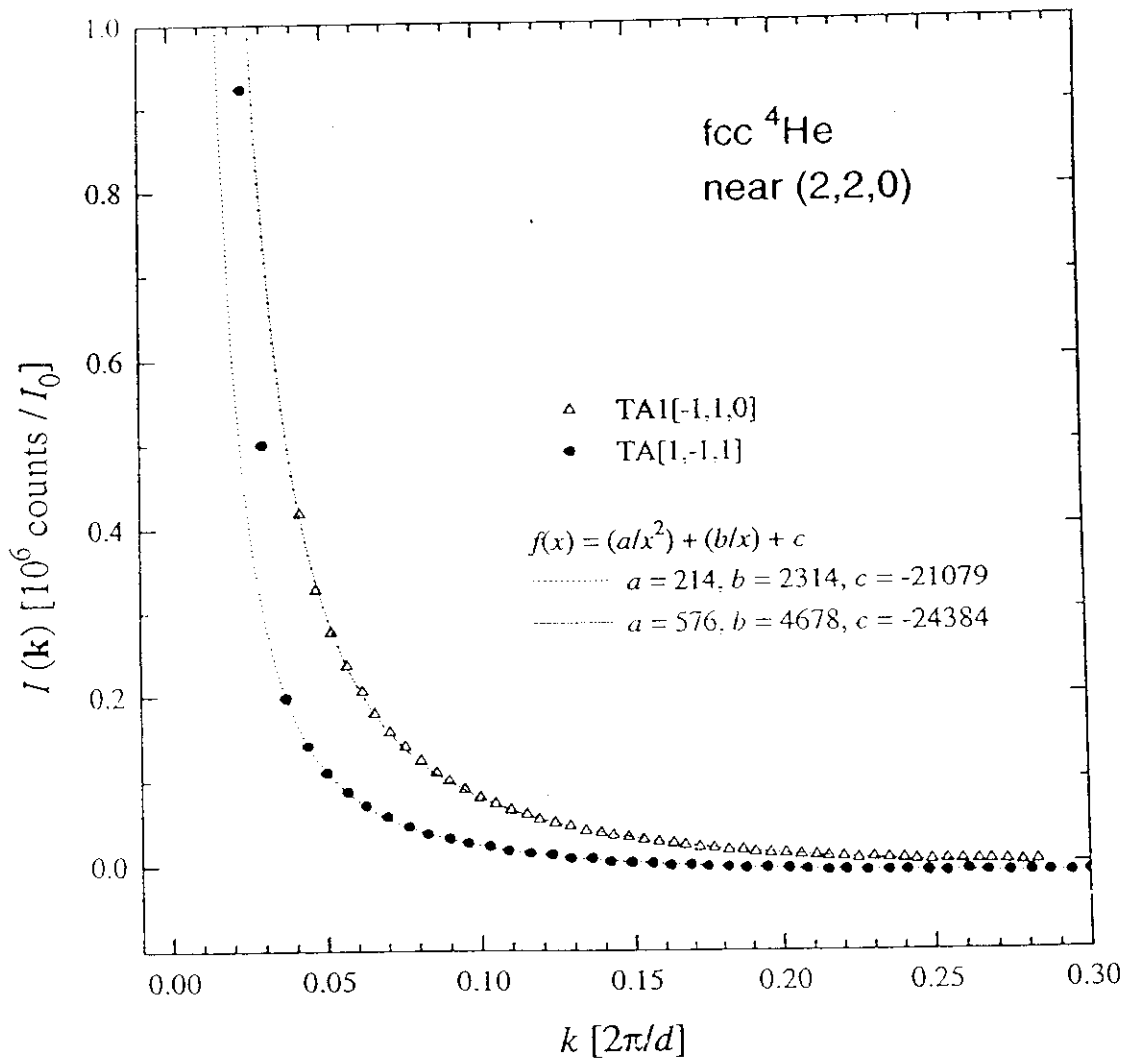
## Dynamic Diffuse Scattering (DDS)

For phonons propagating in  $\langle 110 \rangle$  directions

$$I_{TA2} \approx f^2(q) q^2 e^{-2M} \frac{(|\mathbf{K}|)^2}{\sqrt{(C_{44}) / \rho} |\mathbf{k}|}$$

For phonons propagating in  $\langle 111 \rangle$  directions

$$I_{TA} \approx f^2(q) q^2 e^{-2M} \frac{(|\mathbf{K}|)^2}{\sqrt{(C_{11} - C_{12} + C_{44}) / 3\rho} |\mathbf{k}|}$$



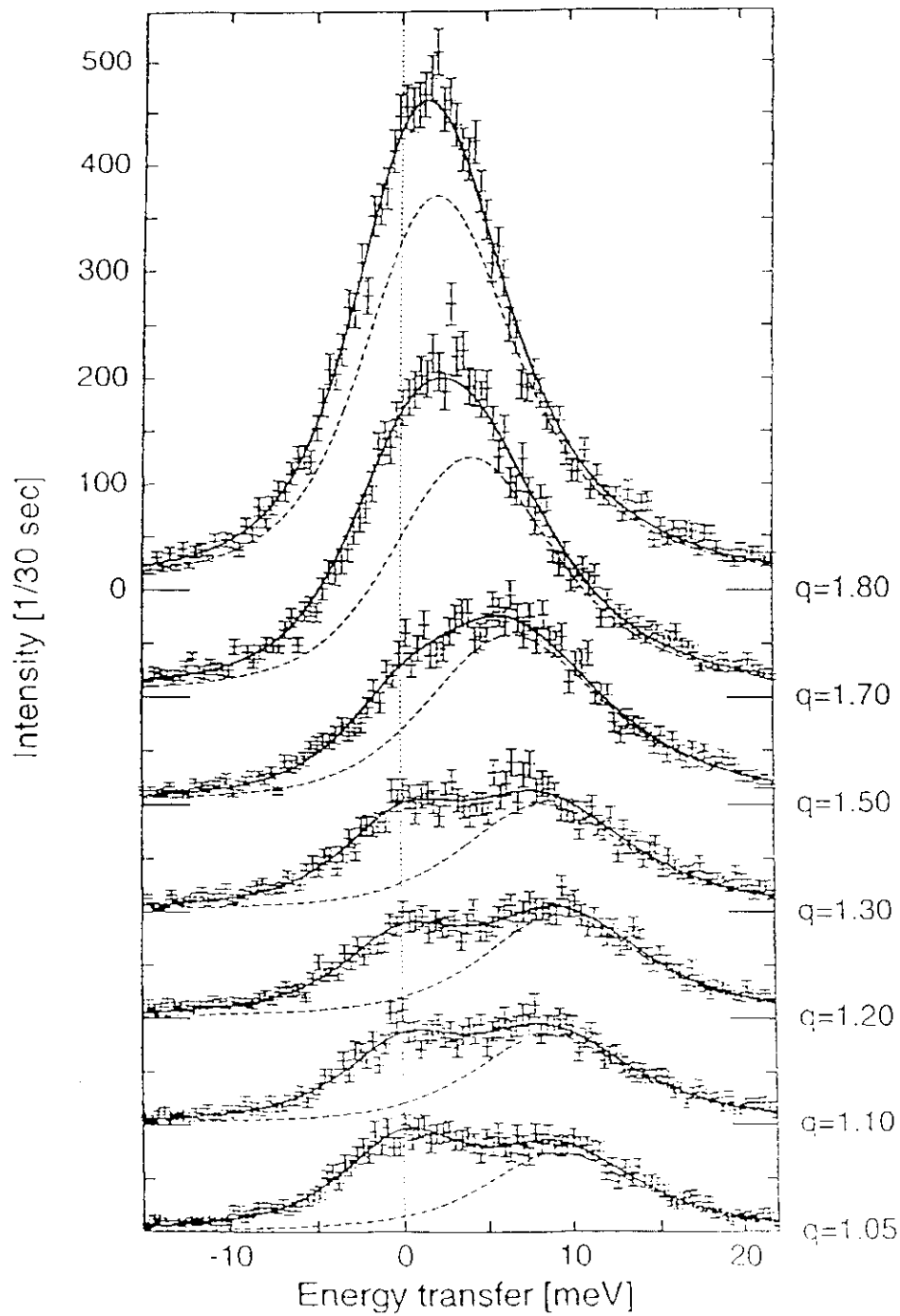
Schwoerer-Böhning, Venkataraman, Simmons (1996)

Brookhaven NSLS X-14A (1996)



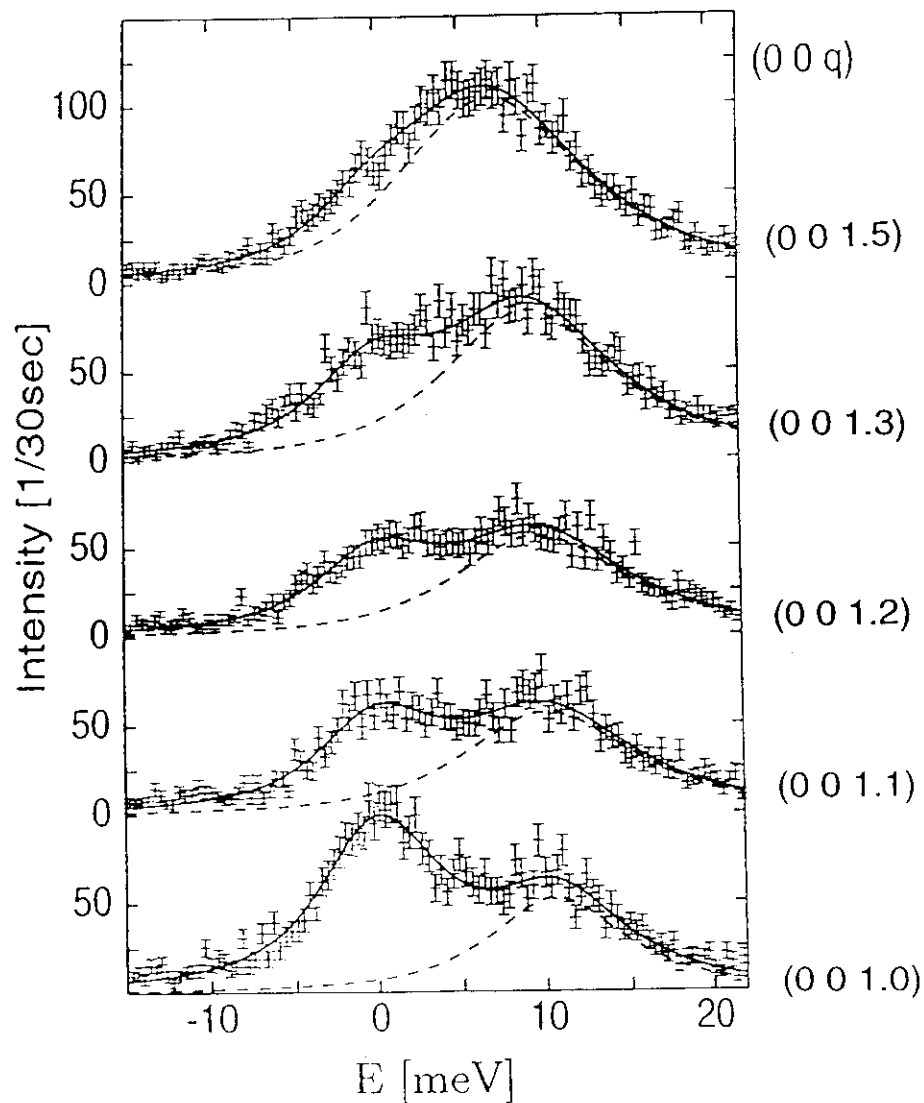
# Phonon Spectroscopy in hcp $^4\text{He}$ using X-rays

ID-16 at ESRF



Seyfert, Arms, Sinn, Simmons, Burkel  
Czech. J. Phys. **46**, 471 (1996)

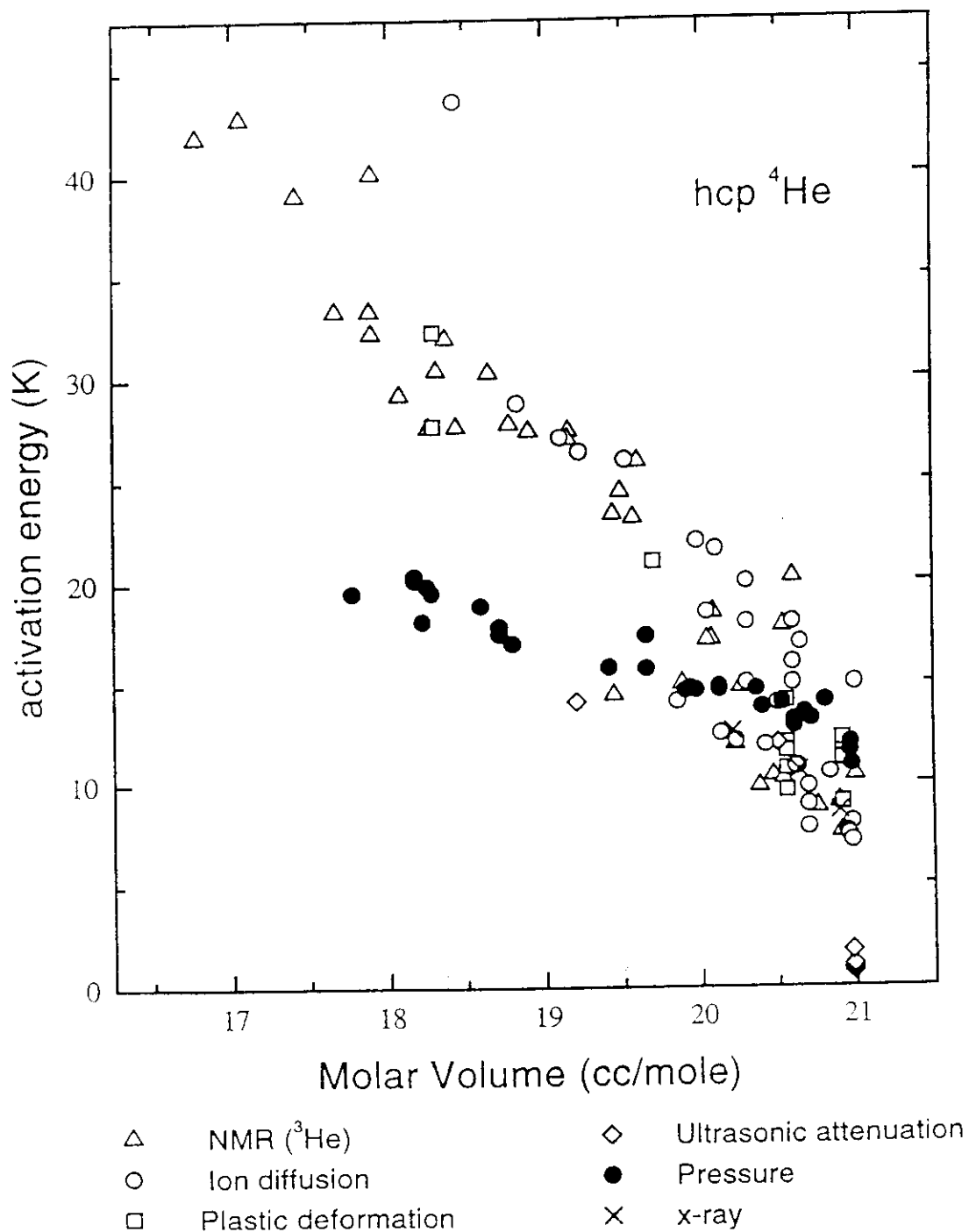
**Phonon Spectroscopy in hcp  $^3\text{He}$  using X-rays**  
 $13.2 \text{ cm}^3 \text{ mole}^{-1}$ ,  $T = 11 \text{ K}$   
**ID-16 at ESRF**



-----phonon fit using Fåk & Dörner model (ILL Rept. 92FA0085)

C. Seyfert, D.A. Arms, H. Sinn, M. Schreckenberger,  
 R.O. Simmons, E. Burkel  
 ESRF Expt. Report HS-77 (1997)

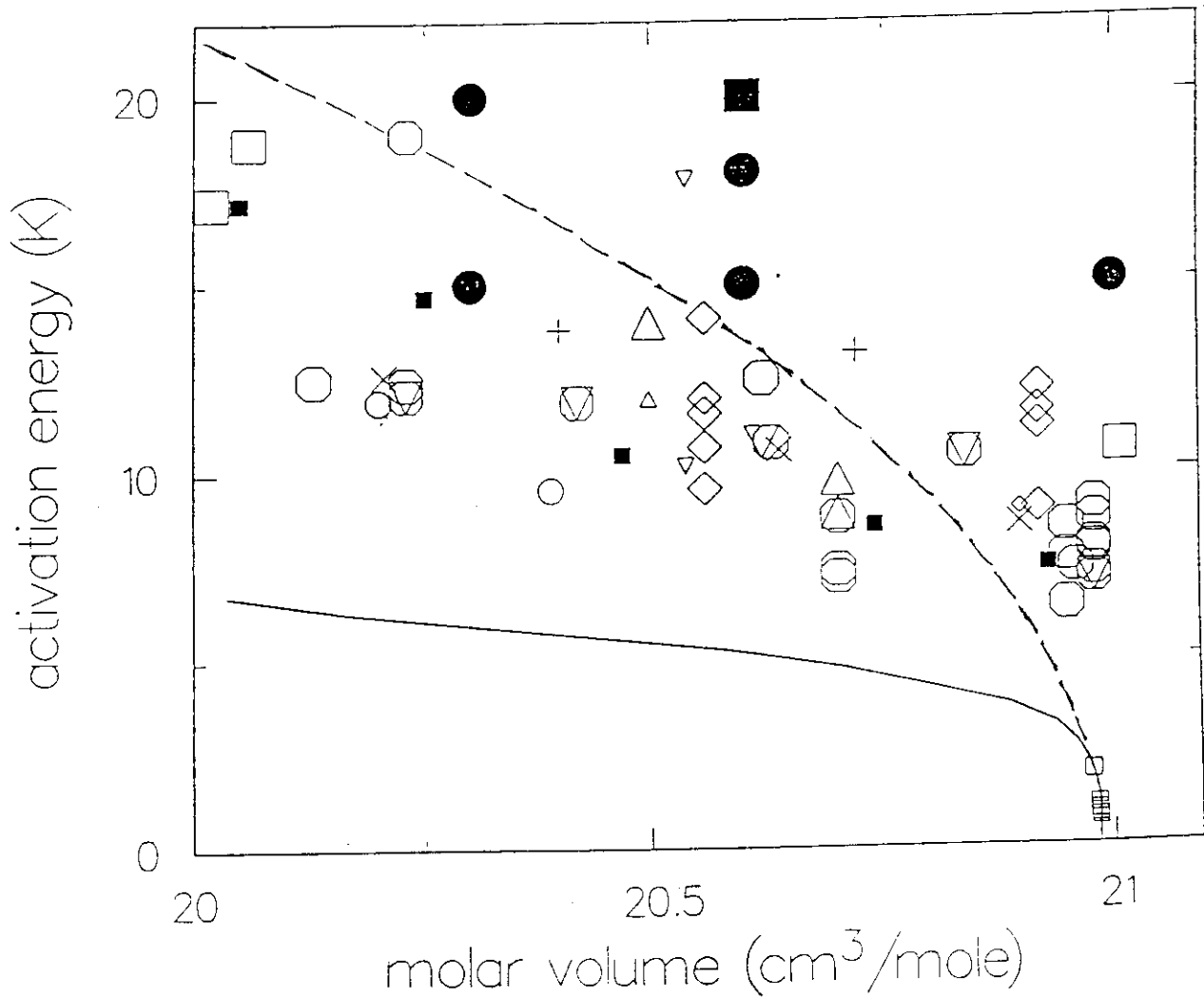
The diverse results for activation energies from  $^4\text{He}$  and  $^4\text{He}$ -rich systems are even more diverse than the techniques



The diverse results for activation energies from  $^4\text{He}$  and  $^4\text{He}$ -rich systems are even more diverse than the techniques

a search for unifying principles

'critical' behavior approaching the minimum density solid?



dashed line

Lengua & Goodkind, J. Low Temp. Phys. **79**, 251 (1990)

solid line

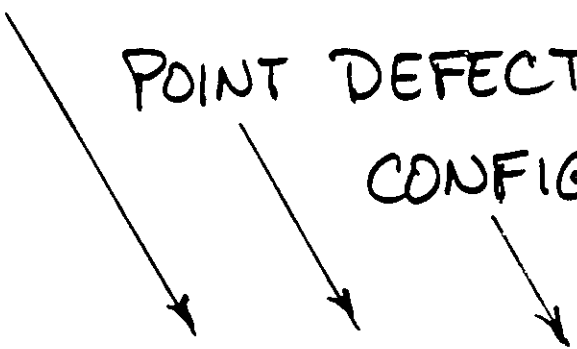
NO, the actual melting curve

# FREE ENERGY

PERFECT CRYSTAL

POINT DEFECTS

CONFIGURATIONS


$$F = F^o + \sum_k n_k f_k - TS_c,$$

$$(\partial F / \partial n_k)_{V,T} = 0$$

$$n_k = N \exp(f_k / k_B T),$$

## EQUILIBRIUM

LOCALIZED

$$x = \frac{\text{net added number of substitutional atomic sites}}{\text{total number of atoms}}$$

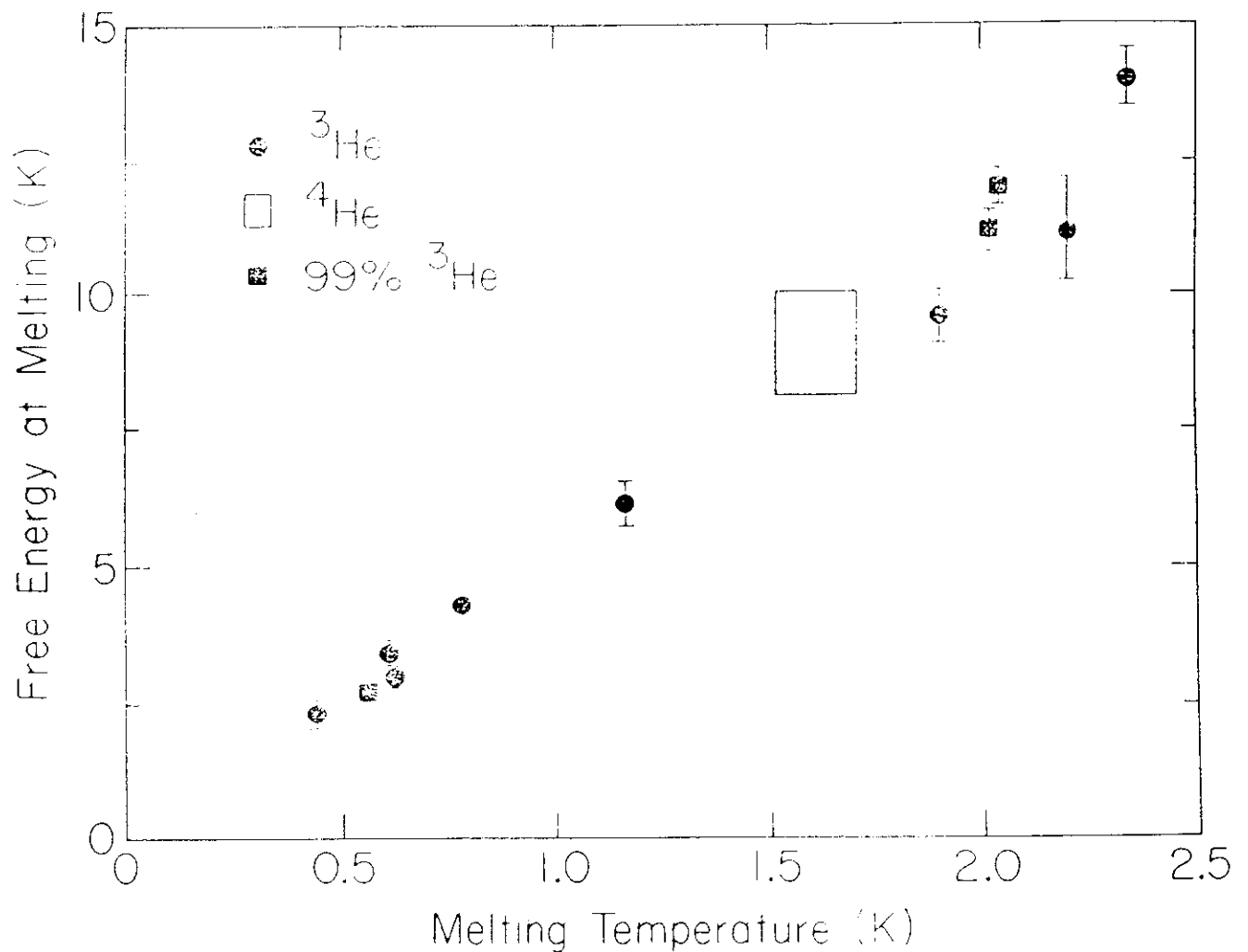
$$x(T) = \frac{\Delta V(T)}{V} - \frac{\Delta V_x(T)}{V_x}$$

For constant macroscopic volume,  $\frac{\Delta V(T)}{V} = 0$ .

Therefore x-ray measurements **alone** give vacancy content.

$$x(T) = - \frac{\Delta V_x(T)}{V_x}$$

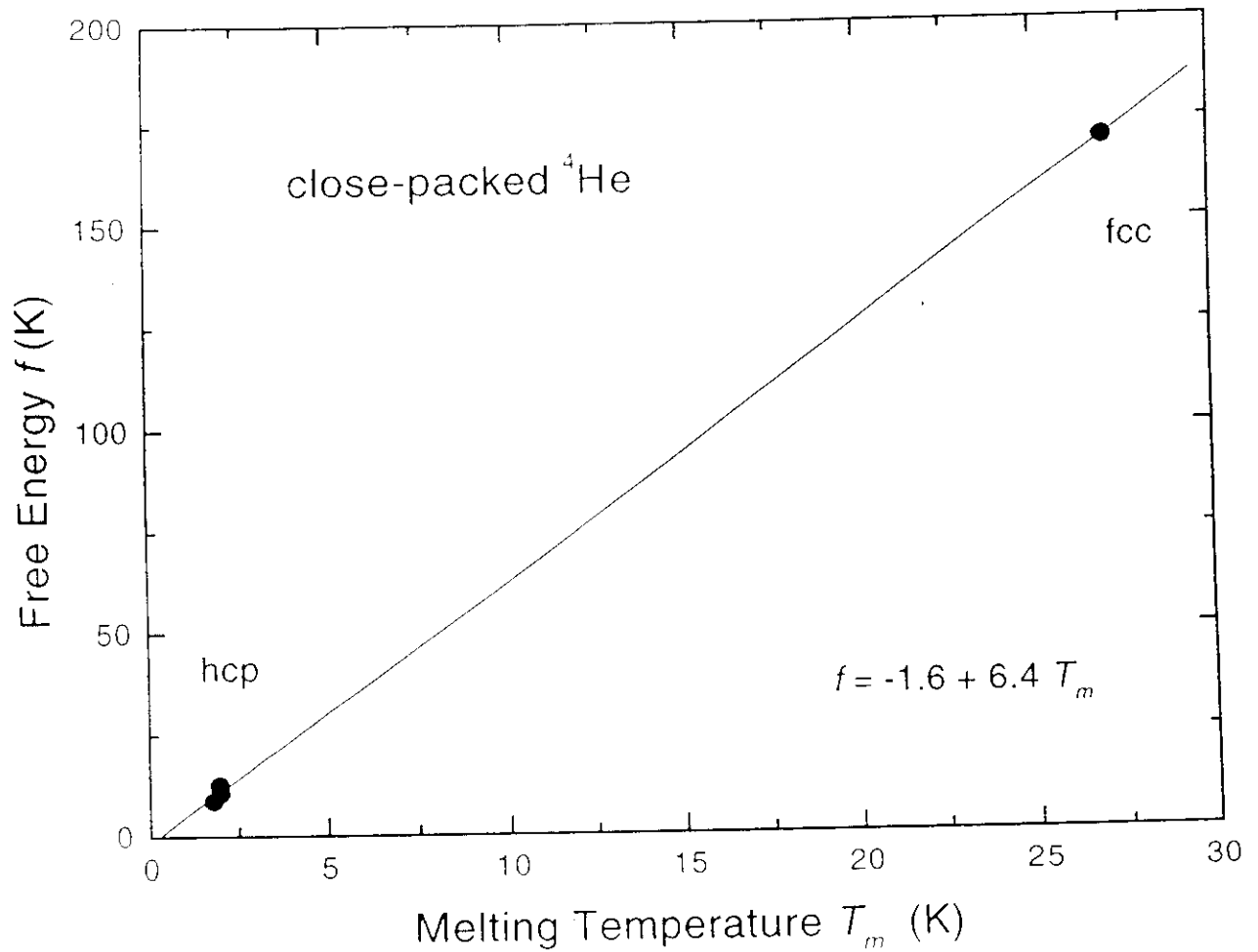
From X-ray measurements, an empirical result for bcc is  
the vacancy free energy is proportional to  $T_{melt}$



The net vacancy content appears to be about constant at melting, for temperatures above the minimum in the melting curve. The constant of proportionality is about 6.

## Direct X-ray measurement of thermal vacancy content

$$-(\Delta V / V)_x = \exp(-f / k_B T)$$



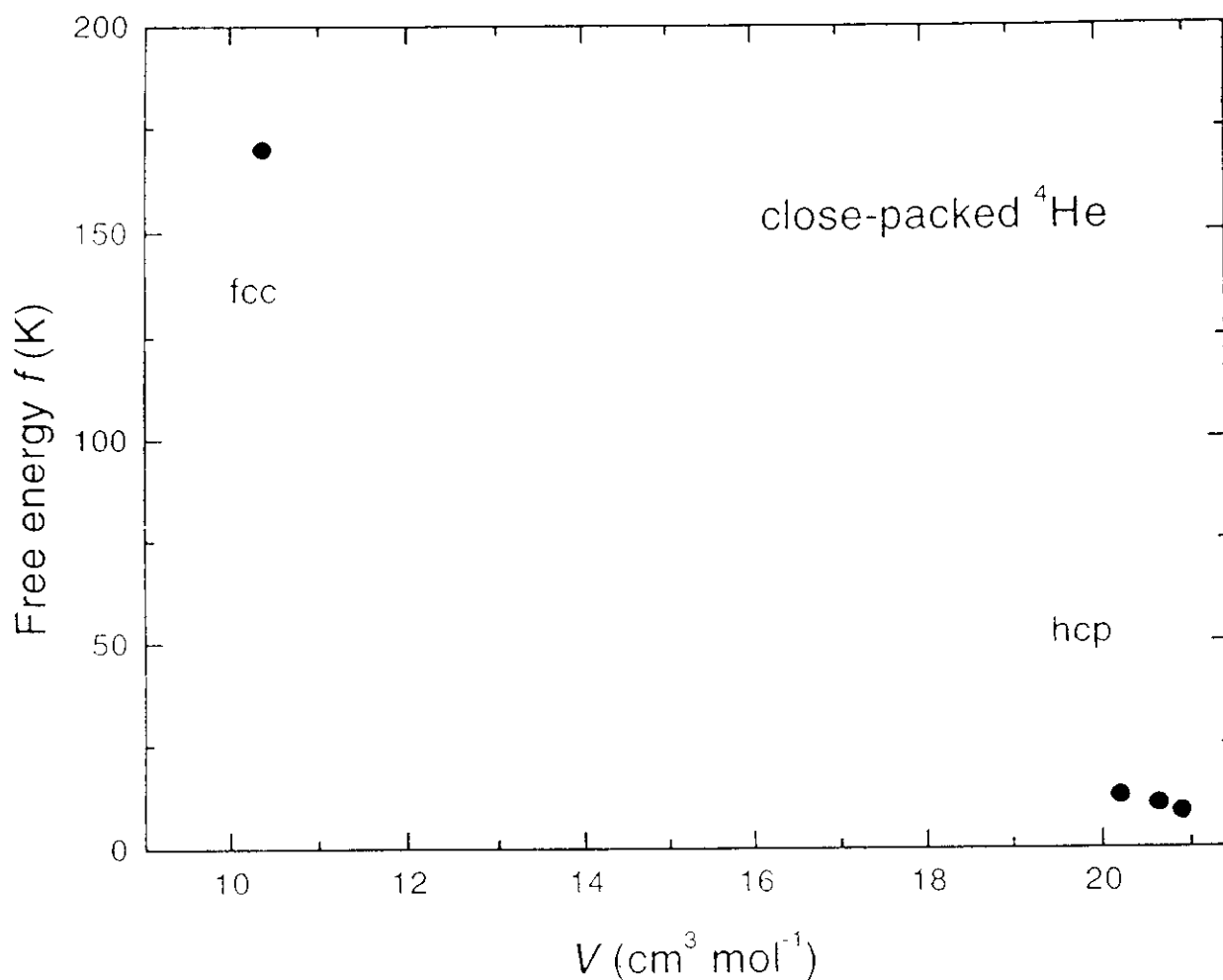
fcc C.T. Venkataraman, R.O. Simmons, Czech. J. Phys. **46**, S1, 461 (1966).

hcp B. Fraass, P. Granfors, R.O. Simmons, Phys. Rev. B **39**, 124 (1989).



## Direct X-ray measurement of thermal vacancy content

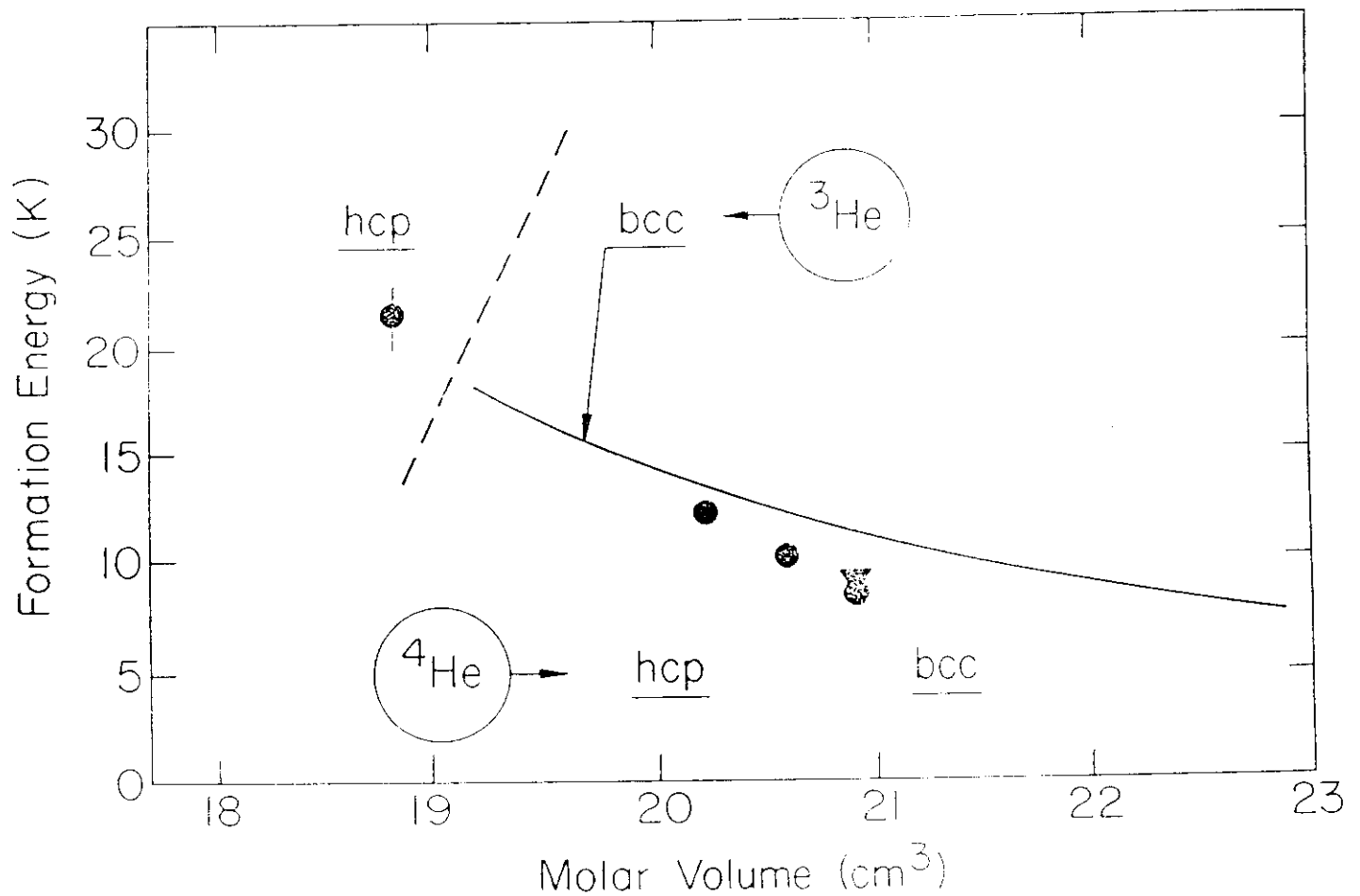
$$-(\Delta V / V)_x = \exp(-f / k_B T)$$



**fcc** C.T. Venkataraman, R.O. Simmons, Czech. J. Phys. **46**, S1, 461 (1966).

**hcp** B. Fraass, P. Granfors, R.O. Simmons, Phys. Rev. B **39**, 124 (1989).

From X-ray measurements, it appears that the vacancy formation energy,  $f(V)$ , is a 'smooth' function of density



If so, some inferences follow:

bcc <sup>3</sup>He tunneling mobility

hcp <sup>3</sup>He activated diffusion

<sup>4</sup>He? No 'pure' diffusion data available?

# PRESSURE A SENSITIVE INDICATOR

## PERFECT CRYSTAL

$$P(V, T) = P^{oo}(V) + P_p(V, T) + \underbrace{n(V, T) p}_{\text{DEFECTS}}$$

PHONONS

$$P_p(V, T) = (3\pi^4 k_B / 5v_0) \gamma(V, T) \underline{T^4} / \Theta_A(V)^3$$

## DEFECT PRESSURE

$$p = -(\partial f(V, T) / \partial V)_T = (B_T / V) v(V)$$

## VOLUME

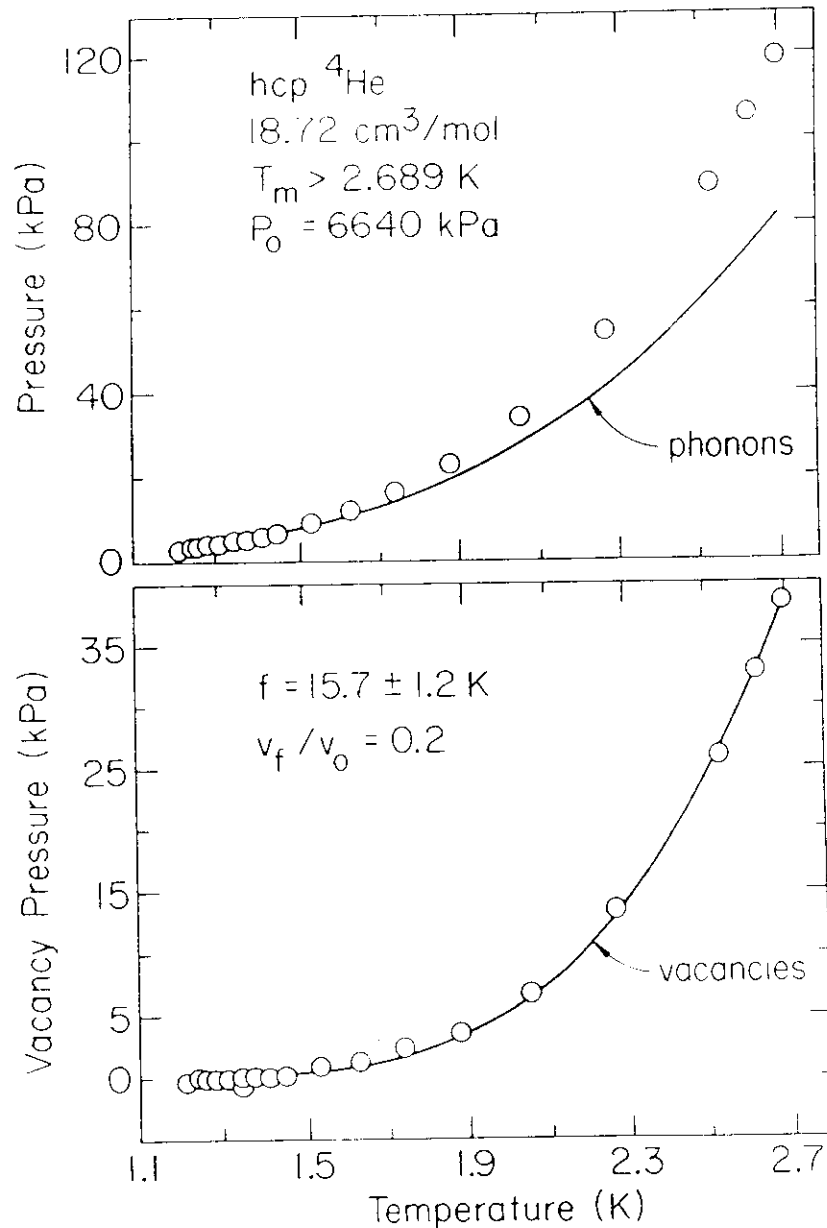
$$(v/V) = (g/\mu V) [\mu' - (\mu/B)]$$

## CONTENT

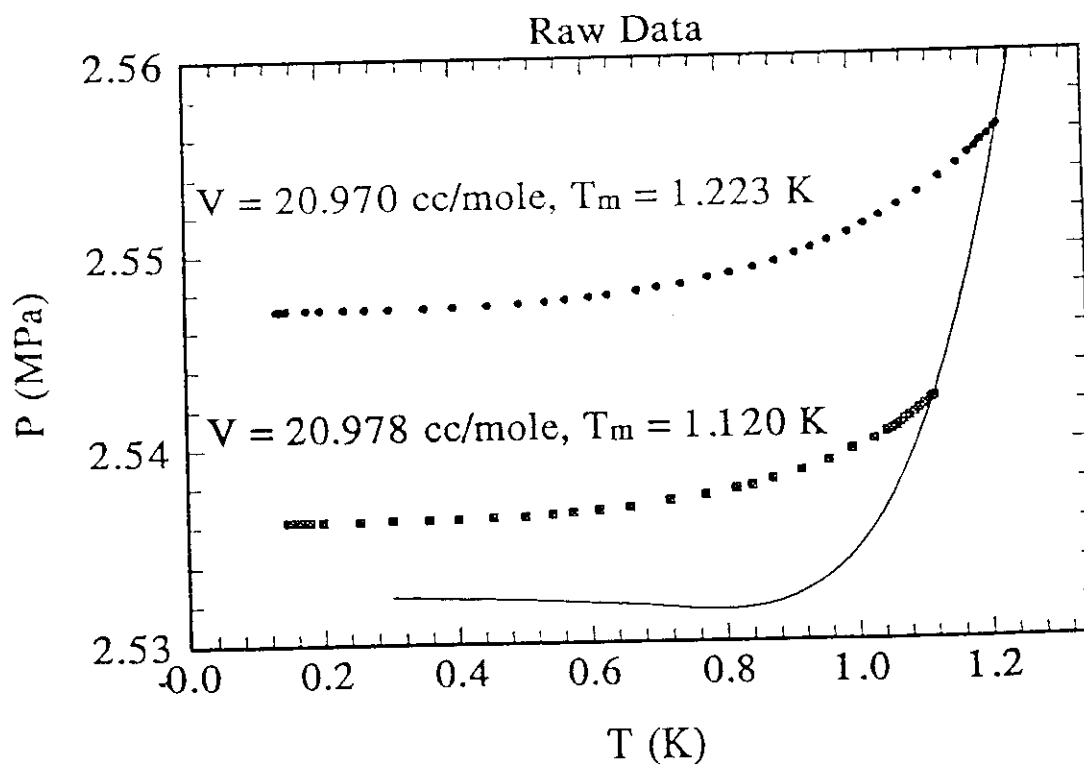
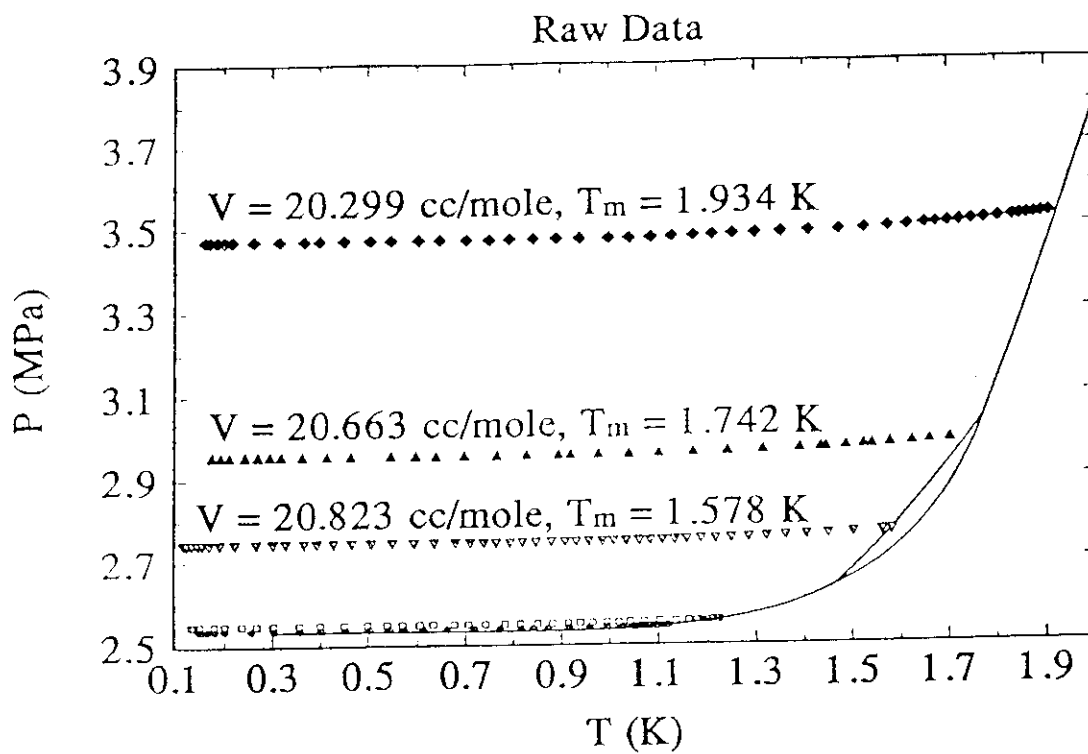
$$n = N \exp(f / k_B T)$$

Pressure measurements are a sensitive measure which includes all excitations.

However, separation of point defect properties may be equivocal and uncertain.



data and analysis from J. Thorpe, I. Fujita, R.O. Simmons (1996)



# Pressure measurements I. Fujita and R.O. Simmons (1997)

hcp  $^4\text{He}$ ,  $T_m = 1.130\text{ K}$ ,  $P_m = 2.5420\text{ MPa}$   $V = 20.9978\text{ cm}^3$

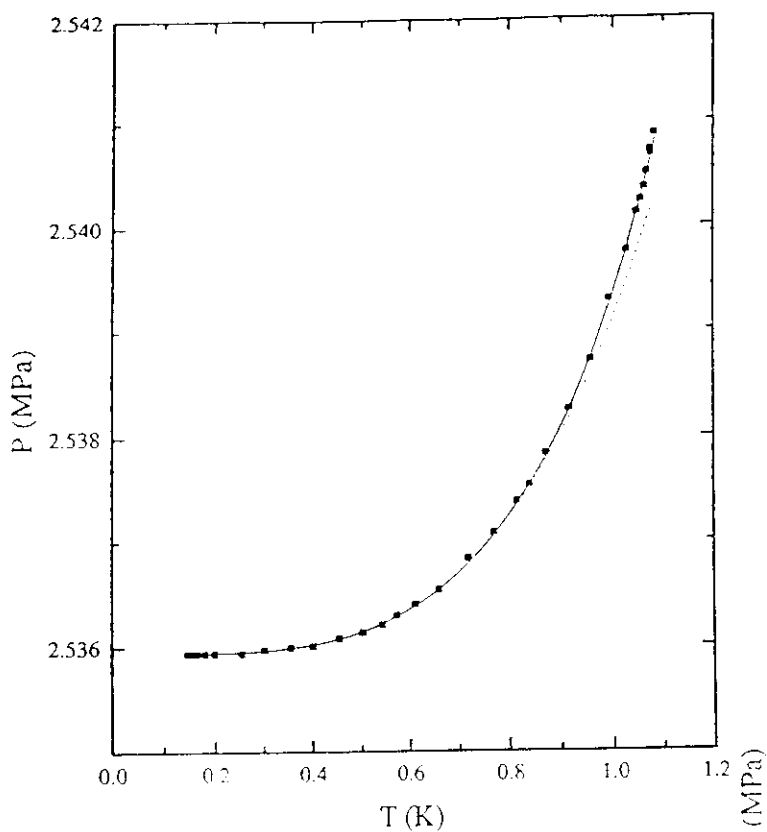


Figure 5.6 Localized model fit of crystal 2's  $P(T)$  data and associated zero-point and phonon pressure contributions.

- $P(T)$  data
- $P^l$  fit
- - -  $P_e^l + P_e^l$  fit

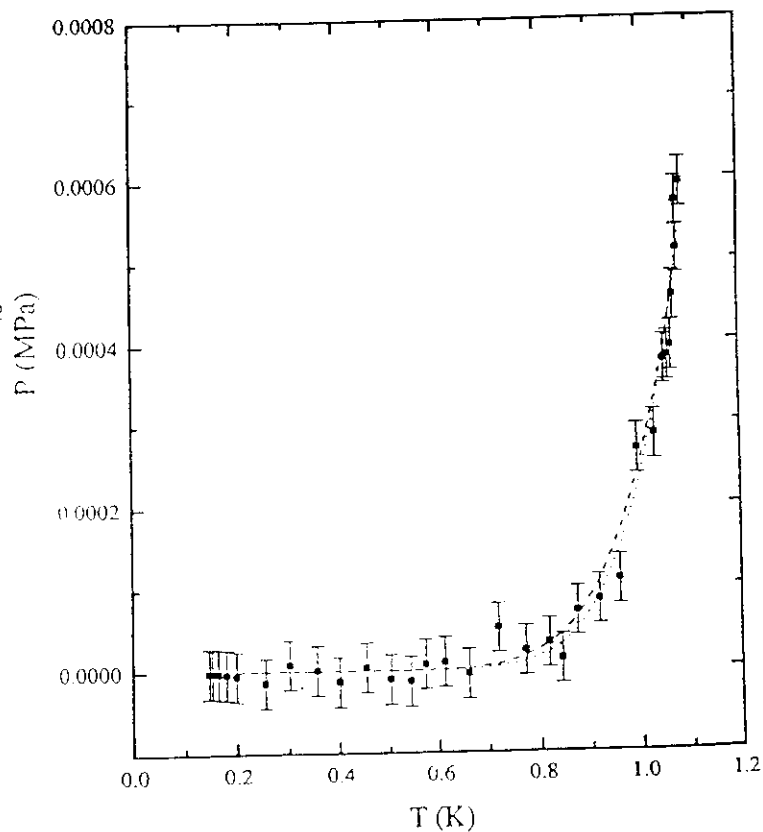
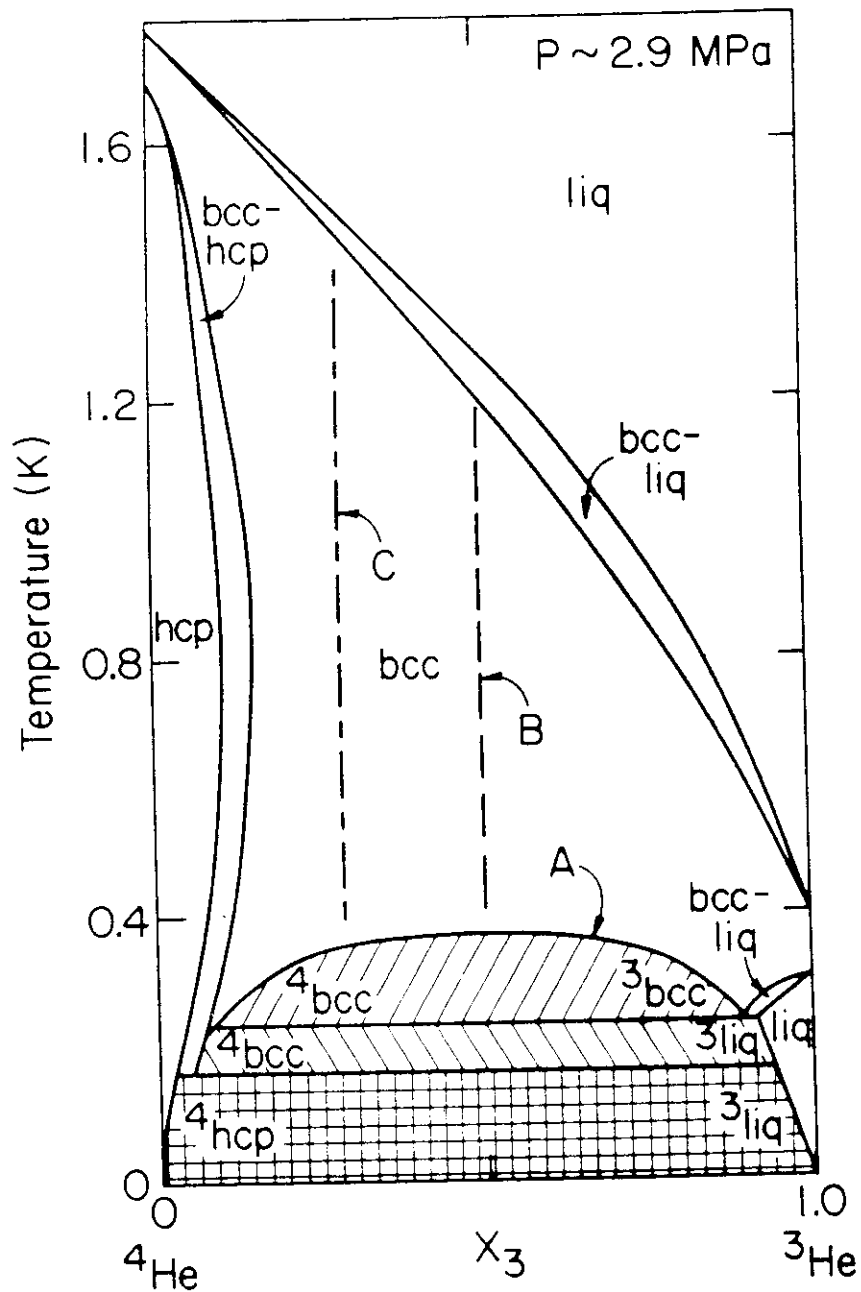


Figure 5.7 Vacancy pressure of crystal 2 in the localized model.

- localized vacancy pressure data,  $(P(T) - P_o^l - P_e^l)$
- - - localized vacancy pressure fit to data
- - - non-localized vacancy pressure fit to data

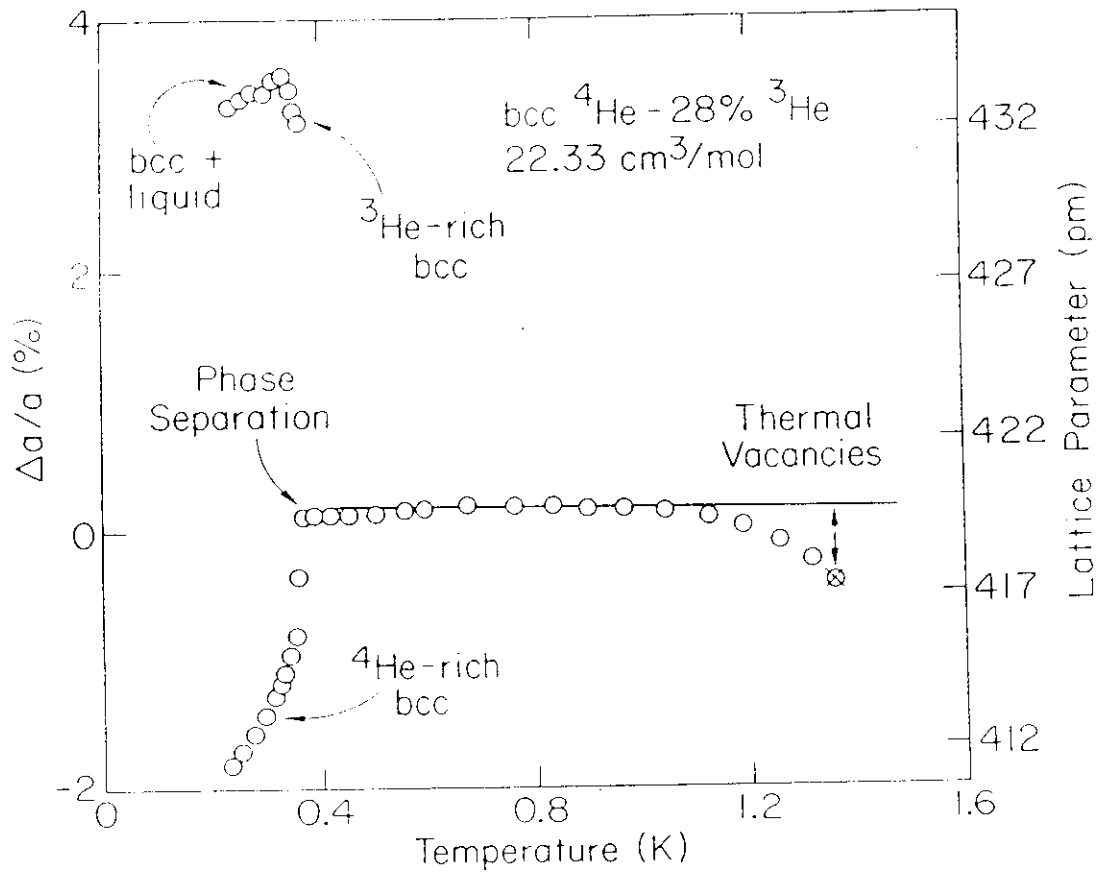
The  $^3\text{He}$ - $^4\text{He}$  mixture is a zoological garden.  
 There are substantial differences as a function of pressure  
 (density)



B.A. Fraass and R.O. Simmons, Phys. Rev. B **36**, 97 (1987)

The  $^3\text{He}$ - $^4\text{He}$  mixture is a zoological garden.

X-ray techniques can give information about these animals.



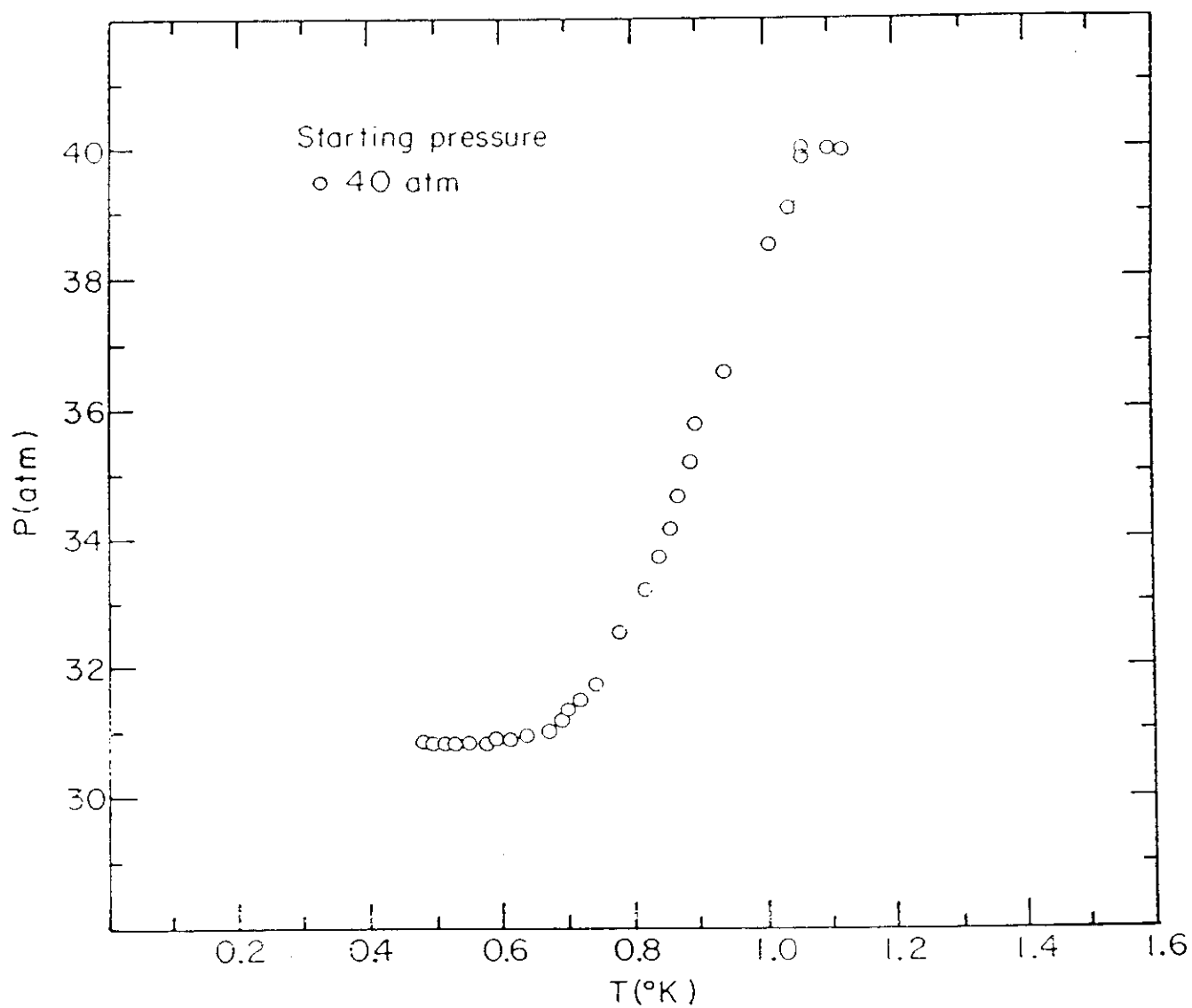
B.A. Fraass and R.O. Simmons, Phys. Rev. B **36**, 97 (1987)

When phase separation occurs, there appears to be atomic diffusion across an incoherent interface.



Large pressure changes in cooling of  
 $^3\text{He}$ - $^4\text{He}$  solid mixtures

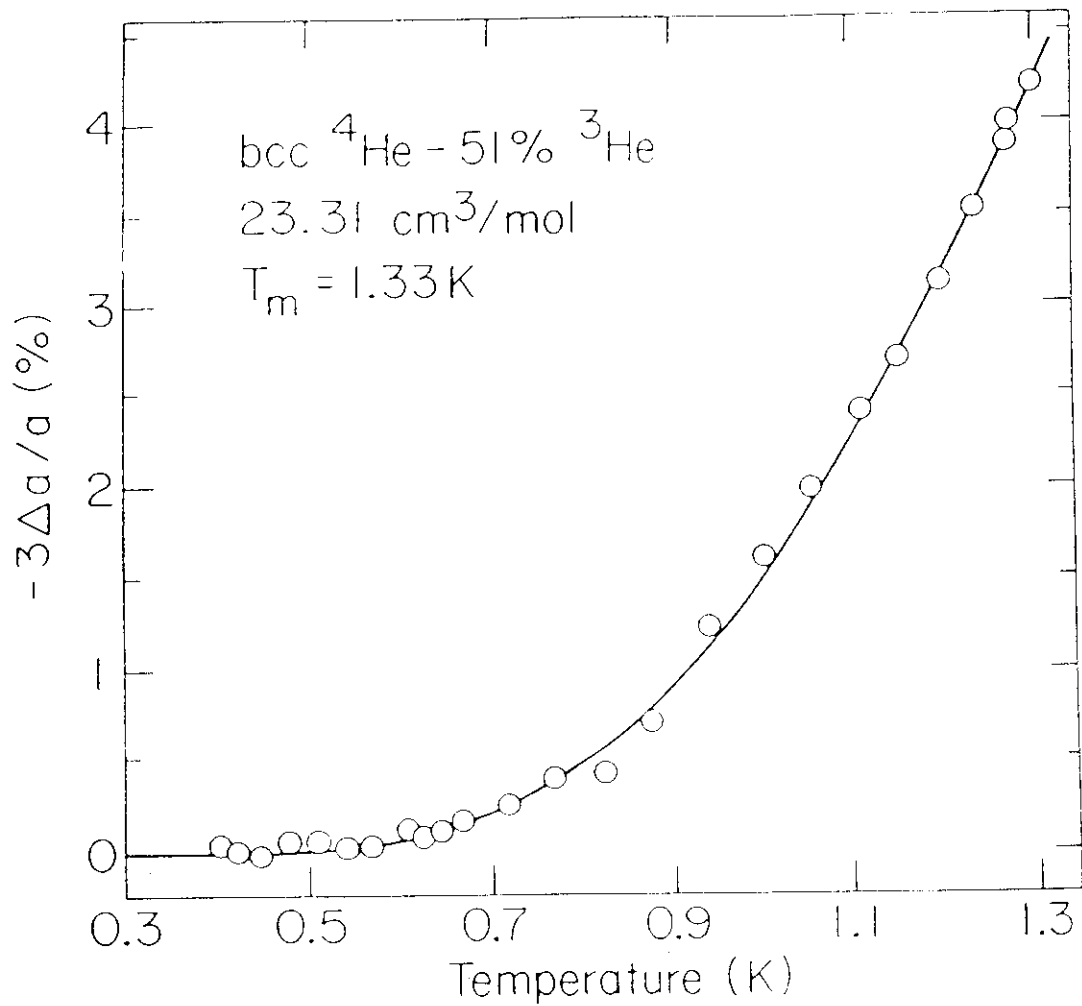
example: 78%  $^3\text{He}$



P.M. Tedrow and D.M. Lee, Phys. Rev. **181**, 399 (1969)

There are corresponding very large vacancy contents in  
homogenous solid  $^3\text{He}$ - $^4\text{He}$  mixtures

example: 51%  $^3\text{He}$

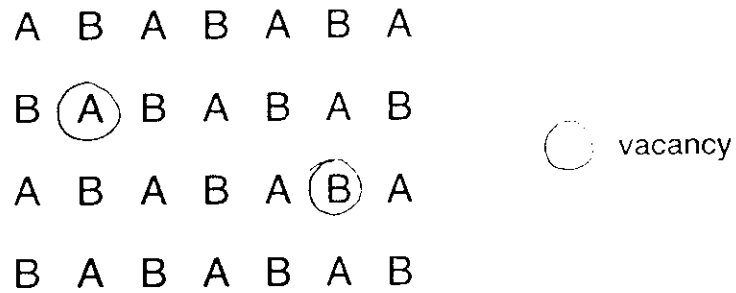


B.A. Fraass, R.O. Simmons, Phys. Rev. B **37**, 5058 (1988)

For macroscopically homogeneous solid mixtures, expressions for the crystal free energy,  $F$ , and the configurational entropy,  $S_C$ , are complicated.

There is some simplification on an ordered lattice.

[S.M. Kim, Phys. Rev. B **29**, 2356 (1984)]



$$\left. \begin{array}{l} N_{Aa} \\ N_{Bb} \end{array} \right\} \begin{array}{l} \text{site atoms} \\ \text{site atoms} \end{array} \quad \begin{array}{l} = N - N_{Ab} \\ = N - N_{Ba} \end{array}$$

$$\left. \begin{array}{l} N_{Ab} \\ N_{Ba} \end{array} \right\} \begin{array}{l} \text{anti-site atoms} \\ \text{anti-site atoms} \end{array}$$

$$\left. \begin{array}{l} N_{va} \\ N_{vb} \end{array} \right\} \begin{array}{l} \text{vacancies} \\ \text{vacancies} \end{array}$$

for example

$$\frac{N_{va}}{N + n} = \left( \frac{N_{Aa} N_{Ba}}{N_{Ab} N_{Bb}} \right)^{1/4} \exp[-4(e_{bb} - w) / k_B T]$$

where  $w = e_{34} - (1/2)(e_{33} + e_{44}) = 2T_c$ , measurable.

## **Motivations for phonon studies in $^3\text{He}$**

- Calorimetry shows that characteristic temperatures of  $^3\text{He}$  and  $^4\text{He}$  do not scale with the mass ratio  $(4/3)^{1/2}$ . Such results (low  $T$ ) weight the phonon spectrum by  $\omega^{-3}$ .
- Some indication that Debye-Waller effects for  $^3\text{He}$  and  $^4\text{He}$  do not scale either. These results weight the phonon spectrum by  $\omega^{-1}$  and  $\omega^{-2}$ , at low- and high- $T$ , resp.
- Anharmonicities are seen through ‘forbidden’ reflections in hcp  $^3\text{He}$  but not (so far) in hcp  $^4\text{He}$ .
- There may be qualitative differences in defect properties of  $^3\text{He}$  and  $^4\text{He}$ , and these may be related to the large contributions to atomic dynamics to the defect properties.

## **Motivations for studying other excitations in bulk solid heliums**

- First-principles calculations can be made of band structure.
- Exciton effects have been found (Frenkel) and possibly indicated (Wannier), and again, calculations are feasible.
- Many-body effects may be studied in the two pure isotopes  $^4\text{He}$  and  $^3\text{He}$  and their mixtures, and again modern calculations are feasible.
- Interesting soft X-ray and electron studies of clusters already exist, for comparison to bulk results. Through this, surface properties may be revealed.

# Kinetic Energy of Liquid and Solid $^4\text{He}$

D. M. Ceperley,<sup>1,2</sup> R. O. Simmons,<sup>2,3</sup> and R. C. Blasdel<sup>2,3</sup>

<sup>1</sup>*National Center for Supercomputing Applications, University of Illinois at Urbana-Champaign, 1110 W. Green Street, Urbana, Illinois 61801*

<sup>2</sup>*Department of Physics, University of Illinois at Urbana-Champaign, 1110 W. Green Street, Urbana, Illinois 61801*

<sup>3</sup>*Frederick Seitz Materials Research Laboratory, University of Illinois at Urbana-Champaign, 1110 W. Green Street, Urbana, Illinois 61801*

(Received 1 April 1996)

We report new path-integral calculations and measurements of the kinetic energy of condensed helium and construct an overall dependence of kinetic energy on temperature for densities less than 70 atoms  $\text{nm}^{-3}$ . In the solid phase we find the kinetic energy is almost temperature independent and, surprisingly, has a smaller kinetic energy than the fluid near freezing at the same density. In the high temperature fluid phase, the excess kinetic energy decreases to zero very slowly because of pair scattering from the repulsive interatomic potential. [S0031-9007(96)00592-3]

PACS numbers: 64.70.Dv, 61.12.Ex, 67.20.+k, 67.80.Gb

The momentum distributions of the condensed isotopes of helium have been a matter of widespread interest for many years because of their connections with the theories of Bose condensation and of Fermi liquids. In this Letter we consider only the second moment of the momentum distribution, the kinetic energy  $E_k$ . In contrast to the potential energy, the kinetic energy of a many-body system has distinctly different properties in the classical regime (Maxwellian), the quantum liquid, the crystal (Debye-like), the superfluid (Bose condensation), and for liquid  $^3\text{He}$  (Fermi-liquid behavior). Helium is a nearly ideal system in which to study the variation of these quantum effects because of the wide range of densities, temperatures, and phases that can be achieved experimentally and retained stably in the laboratory (unlike, for example, nuclear matter or laser-cooled ions). The kinetic energy is difficult to measure directly; inelastic (quasielastic) neutron scattering at high momentum transfers is probably the best way. On the theory side, the interatomic potential of helium is better known [1] than for any other atomic and molecular system, and for bosonic  $^4\text{He}$  one has a well-developed and highly accurate simulation method, path integral Monte Carlo (PIMC) [2]. Hence,  $^4\text{He}$  is the simplest quantum system for which to make accurate comparisons of theory and experiment.

Here we make a critical comparison between various experiments and the PIMC theory and draw conclusions about the behavior of the kinetic energy upon melting and at higher temperatures. We first recapitulate our experimental and theoretical methods, and show that the results are in agreement. We then summarize our comprehensive picture of the kinetic energy of  $^4\text{He}$  and comment on recent experiments.

With the advent of intense pulsed neutron sources, direct measurement of single-particle momentum distributions is possible within the limit of the impulse approximation [3]. Then the dynamic structure factor

$S(\mathbf{Q}, E)$  for a target of mass  $m$  can be scaled to the longitudinal neutron Compton profile  $J(y, \mathbf{Q})$  using the variable  $y = (m/\hbar^2 Q)(E - \hbar^2 Q^2/2m)\hat{\mathbf{O}}$ , where  $\hat{\mathbf{O}}$  is a unit vector in the direction of the wave-vector transfer  $\mathbf{Q}$ . Within this limit,  $S(\mathbf{Q}, E)$  is proportional to the longitudinal momentum distribution  $n(\mathbf{p})$ . An early search [4] for a change in kinetic energy upon melting in  $^4\text{He}$  used a comparison of pulsed neutron scattering from a liquid and solid sample at the same density so that the systematic effects of multiple scattering and final state effects (FSE) would largely cancel. Within the precision of these data (a few percent), no difference was found between the fixed-angle recoil scattering profiles of hcp and liquid  $^4\text{He}$  at a density of  $29 \text{ nm}^{-3}$ .

Measurements in solid and normal liquid  $^4\text{He}$  were considerably refined in a second generation of experiments using chopper spectrometers [5]. Special care was taken in the Monte Carlo simulation of the spectrometer-sample system [6]. Further, because the measurements were made at finite  $Q$  (mostly around  $237 \text{ nm}^{-1}$ ), the magnitudes of the FSE were measured and quantitatively compared with calculations over a range of sample densities. In particular, the leading asymmetric correction to the scaled profile  $J(y)$  [7] was computed using the pair potential and the PIMC-determined two-particle distribution function  $g(r)$ . A typical measured profile  $J(y)$ , shown in Fig. 1, allows a clean statistical analysis. The well-defined character of the wings of the profile can be contrasted, for example, to the results shown in Fig. 1 of Ref. [8].

During the past decade, the PIMC method has been developed to calculate a variety of thermodynamic properties of liquid and solid helium from first principles. This method allows calculations to be carried out using realistic interatomic potentials at precisely the density and temperatures of relevance without uncontrolled approximations. The new calculations reported here use a semiempirical potential [1]. We are able to do more precise calculations of the kinetic energy because we used an accurate

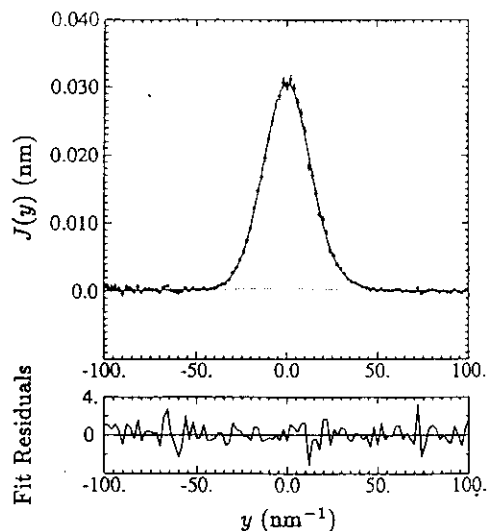


FIG. 1. Typical data of present pulsed neutron scattering experiment for liquid  $^4\text{He}$  at  $32.74 \pm 0.23 \text{ nm}^{-3}$  and  $4.20 \pm 0.04 \text{ K}$ . Shown is a fit of a Gaussian momentum distribution  $n(y)$  with Ref. [7] FSE corrections (solid line) to a measured neutron Compton profile  $J(y)$  corrected for multiple scattering (circles). An effective instrumental resolution function determined by Monte Carlo simulation is convolved with the model  $J(y)$ . The fit residuals are shown at the bottom. For the fit,  $\chi^2 = 87$  with 75 degrees of freedom.

pair density matrix to increase the time step to the value of  $0.00625 \text{ K}^{-1}$  at the higher densities and because we used the virial estimator [2] for energy instead of the thermodynamic estimator used previously. At a given temperature and density, the initial configurations of the paths were selected so as to match the proper experimental phase. Determination of the correct phase with PIMC would have been more difficult and possibly influenced by the neglected and ill-understood three-body potentials. In this Letter we neglect the effect of vacancies (or other defects) in the solid phase near melting. These could possibly raise the kinetic energy by  $\approx 1 \text{ K}$  at melting. Between 100 and 200 atoms were used in the present calculations. At the temperatures of concern in this Letter, we did not need to consider the effect of Bose statistics; that has been done in earlier calculations of the superfluid [2].

As a test, we have calculated the change in internal energy upon freezing and compared it with the value obtained from the experimental melting curve [9] and the Clausius-Clapeyron equation temperatures of 8.9 and 32 K. They differ by  $-0.3 \text{ K/atom}$  at the lower temperature and  $0.5 \text{ K/atom}$  at the higher temperature, which is close to the combined statistical, systematic, and experimental errors for this quantity. Hence, by explicit tests we have established that the errors in the kinetic energy arising from the interatomic potential, the finite number of atoms, the time step, Bose statistics, and Monte Carlo sampling are less than  $0.1 \text{ K/atom}$ .

We have calculated the kinetic energy at about fifty different physical states and fit the energies in each phase. We included in the fitted data the zero temperature

calculations [10,11]. In the solid phases we fit the kinetic energy by a form  $E_k = a\rho^{\gamma_1} + (T/\rho^{\gamma_2}\Theta)^4$  with  $\gamma_1 = 1.83$  and  $\gamma_2 = 2.2$  while in the liquid phase we used a polynomial of the form  $E_k = (3/2)T + \sum_{i,j} c_{i,j}\rho^i t^j$ , where  $t = [1 + (T/T_0)]^\eta$  and  $T_0 \approx 3 \text{ K}$  and  $\eta \approx -0.1$ . Fitting errors are less than  $0.2 \text{ K}$ . We will publish the PIMC energies and fits elsewhere.

Figure 2 is a contour plot of the kinetic energy of liquid and solid  $^4\text{He}$ . The superfluid phase (sf) and the liquid-gas region (l-g) are in the lower left-hand corner. (Note that the kinetic energy in the superfluid phase is given in Refs. [2,12,13]. In this Letter we do not address those regions of the phase diagram, concentrating instead on higher temperatures or densities.) First we discuss the kinetic energy in the solid, then at melting, and finally in the liquid. We remark that a purely classical system would have vertical, equally spaced contours, a behavior completely different from helium, at any density or temperature.

In the solid phase the kinetic energy depends almost entirely on density with only a small dependence on temperature, near melting, and only a small dependence

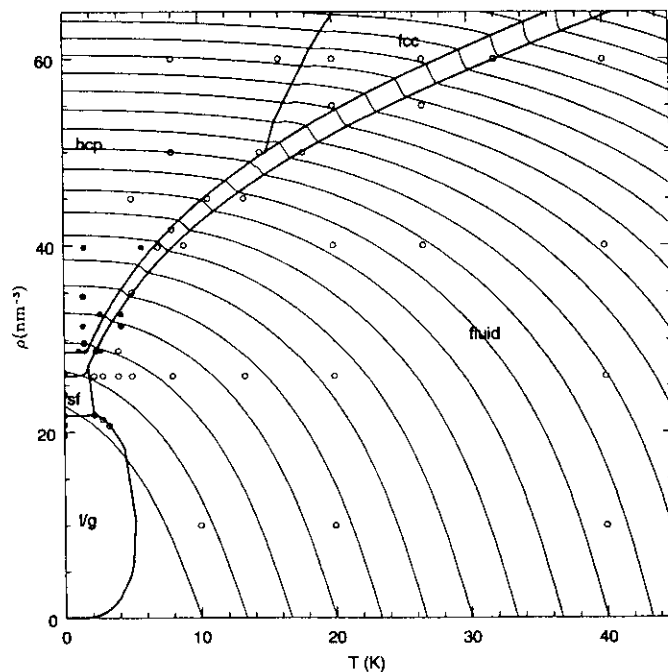


FIG. 2. Contour plot of the PIMC kinetic energy of  $^4\text{He}$  as a function of temperature and density. The experimental phase transitions (to fluid, superfluid, hcp, and fcc crystals) are shown as dark lines. The kinetic energy contours are shown every  $5 \text{ K}$ . Their values can be ascertained by their intercepts on the lower temperature axis since there  $E_k = 1.5T$ . The contours for  $5$  and  $10 \text{ K}$  are not shown since they go through the liquid-gas coexistence region. The  $15$  and  $20 \text{ K}$  contours graze the corners of the liquid-gas and superfluid regions, respectively. Values inside the liquid-solid coexistence region are shown to emphasize how the contours connect across the transition. The circles are locations of the PIMC runs used to construct the fit, and the stars the locations of the new neutron scattering experiments.

(less than 1 K) on crystal structure. Throughout the density range of our present measurements, and others using identical techniques [5], there is agreement between measured and PIMC values with an average difference of 0.6 K as shown in Fig. 3(a). Figure 3(b) explicitly shows the kinetic energy changes along melting-curve isochores.

Remarkably, the contours of kinetic energy are almost continuous (to within 5%) across the melting line. In fact, the kinetic energy at constant density *increases* slightly at melting on the order of 2–4 K as shown in Fig. 3(b). The positive jump upon melting extends up to room temperature [14]. Evidently, atoms are slightly more successful in avoiding each other in the solid. The near agreement of the kinetic energy in the liquid and solid at melting comes about because the local order in the two phases is so similar. Note the comparison of the pair correlation functions in Fig. 4. Inclusion of vacancies in the solid phase lowers the jump, but it still remains positive.

On the other hand, Bafle *et al.* [8] claim a contrary *decrease* in the kinetic energy on melting, on the basis of extrapolations of liquid and solid kinetic energies across the

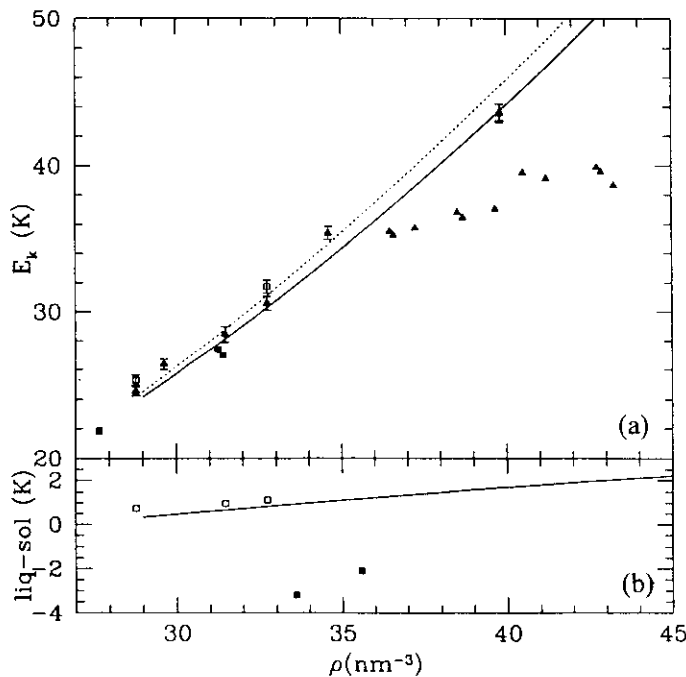


FIG. 3. (a) Density dependence of the kinetic energy of normal liquid and solid  $^4\text{He}$  along the melting curve. Our measured values are shown as open squares (liquid) and triangles (solid) (Ref. [5] and present work). The fitted PIMC kinetic energy is the dotted line in the liquid and full line in the solid. Kinetic energies from Ref. [8] are shown as filled triangles (solid) and filled squares (liquid). (b) The differences between the kinetic energies of solid and normal liquid  $^4\text{He}$  as a function of density. Our measured values are shown as open squares (present work and Ref. [5]). The solid line is the difference of the liquid and solid PIMC kinetic energies at melting. These are opposite in sign and different in magnitude from inferences made in Ref. [8], shown as filled squares.

physical density gap of their measured 4.35 K isotherm. We note that their “liquid” fit includes a substantial portion of the two-phase l-g region (see Fig. 2). As shown in Fig. 3(b), these contradictions with the present work are of sign, not just of magnitude. We believe their incorrect conclusions are based partly on measurement errors in the solid phase, and partly on inappropriate fitting functions in both phases. The solid-phase density dependence of  $E_k$  given by Bafle *et al.* [8] differs substantially from both the present results and all previous work [5,11,13,15,16], as shown in Table I. The previous results in the table apply to a variety of temperatures, but, as is evident in Fig. 2, temperature corrections are much smaller than the disagreement displayed between the Bafle *et al.* work and all others.

The liquid contours of kinetic energy are nearly horizontal at freezing indicating that, even at 40 K, helium is still a quantum liquid. We mean by this that the kinetic energy is much greater than the classical  $\frac{3}{2} k_B T$  value. Such quantum behavior continues at least up to room temperature melting (Ref. [14]).

In the high temperature fluid, the *excess kinetic energy*  $E_k - \frac{3}{2} k_B T$  drops off exceedingly slowly with increasing temperature as shown in Fig. 5, for low densities. In the high temperature regime, cluster expansion methods [17] are appropriate. The partition function, and hence the kinetic energy, can be expanded in powers of the fugacity,

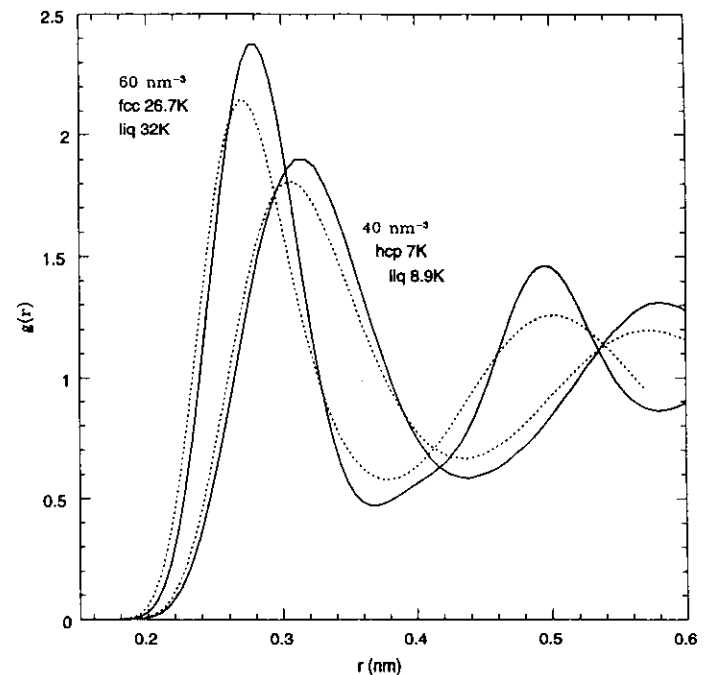


FIG. 4. Comparison of the pair correlation functions along the melting line computed with PIMC. The two left figures are at the higher density of  $60 \text{ nm}^{-3}$  and the right figures at  $40 \text{ nm}^{-3}$ . The solid lines are hcp (7 K) and fcc (26.7 K), and the dashed lines are liquid at 8.9 and 32 K.

TABLE I. Density dependences of previously published kinetic energies of hcp  $^4\text{He}$  near a density of  $35 \text{ atoms nm}^{-3}$ . From Fig. 2, temperature dependence is small so these results are quoted without temperature corrections, and we assumed  $E_k \approx 35 \text{ K/atom}$ .

Method	$d\ln(E_k)/d\ln(\rho)$	Reference	Year
Chopper spectrometer	1.50	[15]	1984
PIMC	1.52	[13]	1987
GFMC	1.34	[11]	1987
Chopper spectrometer	1.80	[5]	1993
SWFMC	1.76	[16]	1994
Resonance spectrometer	0.68	[8]	1995
Present fit	1.83		1996

obtaining

$$E_k \approx k_B T \left[ \frac{3}{2} + \frac{\rho}{2} \int d^3r \exp[-u(r, T)] \frac{du(r, T)}{d \ln m} + \mathcal{O}[\rho^2] \right], \quad (1)$$

where  $u(r, T)$  is the exact two-particle quantum action (on the diagonal) and  $m$  the atomic mass [2]. This virial correction is shown in Fig. 5. It decays roughly as  $T^{-0.3}$ . The near agreement at low density and high temperature shows that the slow decay of the excess kinetic energy arises from two-body scattering. By examining several similar repulsive potentials, we have observed that a steep

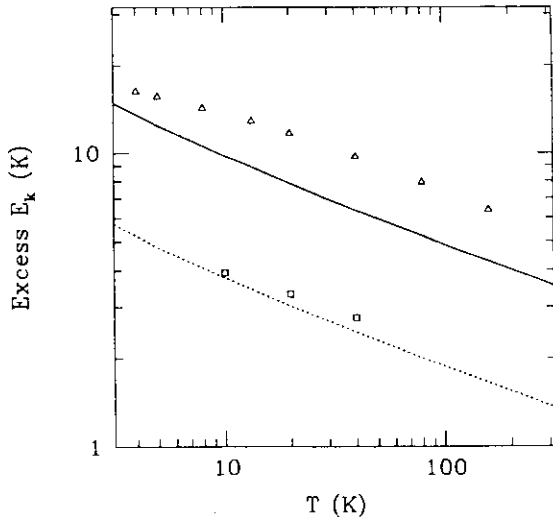


FIG. 5. The excess kinetic energy as a function of temperature at two densities: triangles ( $26 \text{ nm}^{-3}$ ) and squares ( $10 \text{ nm}^{-3}$ ). The solid and dashed lines are the excesses computed using the first-order cluster expansion, Eq. (1), at the same densities. The density matrix was calculated using the matrix squaring method [2].

intermolecular potential leads to a very slowly decaying excess kinetic energy. The exponent  $-0.3$  reflects the steepness of the potential that is sampled by thermal and quantum excitations in the range  $1.5 < r < 2.5 \text{ \AA}$ .

In conclusion, recent experiments and calculations have, for the first time, given a global picture of the dependence of kinetic energy on density and temperature of condensed helium, the prototypical many-body quantum system.

This work was supported by the U.S. National Science Foundation under Grant No. DMR 94-224-96 and by the U.S. Department of Energy, Basic Energy Sciences-Materials Sciences under Contract No. DEFG02-91ER45439. The experimental measurements were made at the Argonne National Laboratory Intense Pulsed Neutron Source, supported by U.S. Department of Energy Contract No. W-31-109-ENG-38.

- [1] R. A. Aziz, F. R. W. McCourt, and C. C. K. Wong, *Mol. Phys.* **61**, 1487 (1987).
- [2] D. M. Ceperley, *Rev. Mod. Phys.* **67**, 279 (1995), and references therein.
- [3] R. O. Simmons, *Z. Naturforsch.* **48a**, 415 (1993), and references therein.
- [4] R. O. Simmons, *Can. J. Phys.* **65**, 1401 (1987).
- [5] R. C. Blasdel, D. M. Ceperley, and R. O. Simmons (to be published).
- [6] R. C. Blasdel, J. M. Carpenter, and R. O. Simmons (unpublished).
- [7] V. F. Sears, *Phys. Rev. B* **30**, 44 (1984).
- [8] U. Bafle, M. Zoppi, F. Barocchi, R. Magli, and J. Mayers, *Phys. Rev. Lett.* **75**, 1957 (1995).
- [9] A. Driessen, E. van der Poll, and I. F. Silvera, *Phys. Rev. B* **33**, 3269 (1986).
- [10] S. Moroni, S. Fantoni, and G. Senatore, *Phys. Rev. B* **52**, 13 547 (1995).
- [11] P. Whitlock and R. M. Panoff, *Can. J. Phys.* **65**, 1409 (1987).
- [12] D. M. Ceperley and E. L. Pollock, *Can. J. Phys.* **65**, 1416 (1987).
- [13] D. M. Ceperley, in *Momentum Distributions*, edited by R. Silver and P. E. Sokol (Plenum, New York, 1987), p. 71; *Z. Naturforsch.* **48a**, 433 (1993).
- [14] M. Boninsegni, C. Pierleoni, and D. M. Ceperley, *Phys. Rev. Lett.* **72**, 1854 (1994).
- [15] R. O. Hilleke, P. Chaddah, R. O. Simmons, D. L. Price, and S. K. Sinha, *Phys. Rev. Lett.* **52**, 847 (1984).
- [16] T. McFarland, S. A. Vitello, L. Reatto, G. V. Chester, and M. H. Kalos, *Phys. Rev. B* **50**, 13 577 (1994).
- [17] B. Kahn and G. E. Uhlenbeck, *Physica (Amsterdam)* **5**, 399 (1938).





## THERMAL VACANCIES IN QUANTUM SOLID HELIUMS

R. O. SIMMONS

Frederick Seitz Materials Research Laboratory and Department of Physics, University of Illinois  
at Urbana-Champaign, Urbana, IL 61801, U.S.A.

**Abstract**—For a highly compressible crystal, the direct method of measuring thermal vacancy content by comparison of X-ray and macroscopic cell volumes over a range of temperature can be replaced by X-ray measurements alone, made on a sample constrained at constant volume. For both methods, the results are independent of assumptions about the nature and strength of the distortions introduced into the crystalline lattice by the presence of the point defects. This is especially important in quantum-solid heliums, in which some defects may be non-localized. X-Ray measurements of this type have been reported on many different solid helium phases: bcc  $^3\text{He}$ , hcp  $^3\text{He}$ , bcc  $^4\text{He}$ , hcp  $^4\text{He}$ , and bcc  $^4\text{He}$ - $^3\text{He}$  mixtures. The different solid heliums have identical interatomic interactions, but differ in their statistics and other properties, to provide a rich family of crystals for such studies. However, some of the vacancy contents measured directly have proven difficult to reconcile with less direct information inferred from some other types of measurements, such as heat capacity and pressure (which measure equilibrium properties) and on the other hand Nuclear Magnetic Resonance (NMR) relaxation and ion conduction (which relate to defect diffusion). The current situation is described and some suggestions for resolution of the apparent discrepancies made.

**Keywords:** D. Defects, D. diffusion, D. thermodynamic properties.

## 1. INTRODUCTION

Point defects in quantum solids continue to attract attention, because of their extraordinary properties. Relevant parts of the phase diagrams of both  $^3\text{He}$  and  $^4\text{He}$  are shown in Fig. 1. Owing to weak interatomic binding and small masses in solid heliums, excursions of atoms from their equilibrium positions are large enough that direct atomic interchange is significant, even at the lowest temperatures. Particle statistics therefore enters consideration of the crystalline properties, including the characteristics of possible point defects. Tunneling of vacancies into adjacent atomic sites in the boson solid  $^4\text{He}$  is expected to give rise to an allowed band of vacancy energies. In the fermion solid  $^3\text{He}$ , at temperatures of importance to thermal vacancies, nuclear spin disorder introduces additional elements into the tunneling model. In both solids, the widths of a possible vacancy band are unknown, however, and speculations about widths range over at least two orders of magnitude. Another intriguing possibility is that band dispersion may lead to states which have an energy lower than the energy per atom of a perfect crystal. The ground state of the crystal would then contain vacancies [1]. Searches for such zero-point vacancies have so far proven unsuccessful [2], perhaps because the concentration of such possible defects, if any, is very small.

Experimental studies potentially related to equilibrium defects in quantum solids have been made by

X-ray diffraction, calorimetry, sound velocity and attenuation, pressure, ion mobility, and plastic deformation. As in measurements made on usual solids, a common problem with all of these except X-ray diffraction is to isolate the defect contribution to the measured property from the influence of other excitations, such as phonons, on the property. It is often maintained, explicitly or implicitly, that this problem is minimized because the quantum solids melt at very low temperatures compared to their characteristic temperatures. We shall see below, however, that apparent contradictions remain between direct X-ray and the other methods which use assumptions about hypothetical crystal properties in the absence of defects.

Thermodynamic and structural properties of  $^4\text{He}$  have been studied over an extreme range of molar volumes,  $V$ , from the maximum (almost  $21\text{ cm}^3$ ) near the minimum of the melting curve at  $775\text{ mK}$  [3] to a value near  $4.5\text{ cm}^3$  for the solid melting near room temperature [4].

Solid  $^3\text{He}$  samples have also often been studied. Unlike bcc  $^4\text{He}$ , the bcc phase of  $^3\text{He}$  exists over a considerable range of molar volumes, from  $21$  to  $24.5\text{ cm}^3$  (Fig. 1). Further, in  $^3\text{He}$ , Nuclear Magnetic Resonance (NMR) methods can be used to investigate microscopic self-diffusion.

Isotopic mixtures are also of unusual interest, because they form systems in which chemical binding of the constituents is identical while both atomic

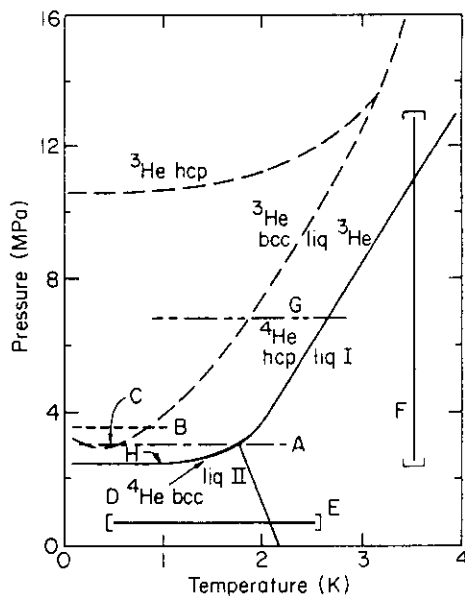


Fig. 1. Schematic  $P$ - $T$  diagrams for  $^3\text{He}$  (dashed lines) and  $^4\text{He}$  (solid lines). Both solids require applied pressure to crystallize, even at  $T = 0$  K, both exhibit minima in their melting curves, and both have bcc and hcp phases at relatively low pressure. Later figures correspond to the regions marked: A (Fig. 2, isotopic mixture), B (Fig. 3,  $^3\text{He}$ ), C (Fig. 4,  $^3\text{He}$ ), D (Fig. 5,  $^4\text{He}$ ), E (Fig. 6, bcc heliums), F (Fig. 7,  $^3\text{He}$  and  $^4\text{He}$ ), G (Fig. 11,  $^4\text{He}$ ), and H (Fig. 12,  $^4\text{He}$ ).

dynamics and statistics are different for the two isotopes. In these weakly bound crystals, atomic dynamics is heavily influenced by the masses, which differ by one-third. As to be expected from the complicated  $PVT$  relations for the pure heliums, the equilibrium phase diagrams for isotopic mixtures depend upon the pressure,  $P$ . An interesting case for defect studies is a solidification pressure near 2.9 MPa, shown in Fig. 2, for which the dominant crystalline phase is bcc [5]. In  $^4\text{He}$  containing dilute concentrations of  $^3\text{He}$ , NMR phenomena have been interpreted as yielding information about vacancy properties of the host  $^4\text{He}$ . Interesting NMR diffusion phenomena associated with  $^3\text{He}$  complexes have also been studied [6], but such impurity complexes are outside the scope of this paper. Also outside the scope are vacancy interpretations of phenomena occurring in restricted geometries [7].

In solid heliums, there have been many experimental and theoretical studies related to ideal crystal properties. For defects, on the other hand, a variety of experimental studies have dominated, with a lesser number of theoretical models. From this variety, a fully consistent and precise picture of defect phenomena is still lacking. In part, the occurrence of irreversible processes is responsible. Evidently, structure-sensitive effects are present in many experiments, and comparisons among different kinds of experiments, in different laboratories and upon different samples, is likely not to be straightforward. Helium

crystals are always subjected to applied pressure, and different sample holders may produce different inhomogeneous stress distributions on the samples.

## 2. PRINCIPLES

### 2.1. Localized vacancies

From the appropriate partition function for the imperfect crystal considered, one derives a Helmholtz free energy,  $F$ . For example, in the case of localized vacancy and interstitial defects, one has

$$F(V, T) = F^0(V, T) + \sum_k n_k f_k(V, T) - TS_c, \quad (1)$$

where  $F^0$  is the free energy of a hypothetical perfect crystal and  $n_k$  is the number of non-interacting defects of type  $k$  that have been added at constant macroscopic volume  $V$ , temperature  $T$ , and number of atoms  $N$ .  $f_k(V, T)$  is the partial Helmholtz free energy of formation of the defect of type  $k$ , and  $S_c$  is the configurational entropy of the system. At equilibrium, the number of defects of type  $n_k$  satisfies the condition

$$(\partial F / \partial n_k)_{V, T} = 0, \quad (2)$$

which after manipulation yields the familiar expression for exponential generation of defects with increasing temperature

$$n_k = N \exp(-f_k / k_B T), \quad (3)$$

provided the defect concentration is very small,  $n_k \ll N$ .

Under conditions of constant macroscopic volume, these thermodynamic relations hold for localized thermal monovacancy formation parameters [8]:

$$f(V, T) = u(V) - TS(V) \quad (4)$$

$$s(V) = -(\partial f(V, T) / \partial T)_V \quad (5)$$

$$p(V) = -(\partial f(V, T) / \partial V)_T. \quad (6)$$

Here,  $u$  is the energy of formation of the vacancy and  $s$  is the non-configurational entropy of formation. The pressure of formation at constant volume,  $p$ , is related to the more familiar free volume of formation at constant pressure,  $v$ , by the relation

$$p = (B_T / V)v, \quad (7)$$

where  $B_T$  is the isothermal bulk modulus.

Thermal vacancy contributions to thermodynamic properties of a solid are calculated analogously. For a monovacancy concentration  $n/N \ll 1$ , where  $n$  is the number of noninteracting localized monovacancies, useful results are

$$C_V - C_V^0 = nk_B \left( \frac{\partial u}{\partial T} + \left( \frac{u}{k_B T} \right)^2 \right), \quad (8)$$

and

$$P - P^0 = np. \quad (9)$$

Here,  $C_V$  is the isochoric specific heat and  $P$  is the pressure. The superscript zeroes denote properties of a hypothetical defect-free solid at the same macroscopic volume. Note that in principle the macroscopic properties of the hypothetical defect-free solid are inaccessible to direct measurement unless such a measurement can quickly be made in a quasi-equilibrium manner after bringing the solid from a state without defects in a time very short compared to the time for microscopic processes to generate the equilibrium defect concentration. In the quantum solid heliums, however, atoms exhibit considerable mobility even at low temperatures, so that such measurement conditions are unlikely to be met.

## 2.2. Non-localized vacancies

An interesting possibility in quantum solid helium is that defects can easily move from site to site, because the atomic position probabilities are not tightly localized at the atomic sites. A partition function,  $Z$ , for the vacancy excitations in the case of  $^3\text{He}$  may then be [9]

$$Z = \sum_{\{m_x\}} \exp \left( -\beta \sum_x m_x E_x \right), \quad (10)$$

where  $\beta = (1/k_B T)$  and  $m_x$  is the occupation number of the vacancy state of energy  $E_x$ . If one limits the sum to a single excitation and replaces the sum by an integral, one obtains after some manipulation

$$\ln Z = N \int \rho(E) e^{-\beta E} dE, \quad (11)$$

where  $\rho(E)$  is the density of single-particle vacancy states. Such states include some local phonon modes which presumably have been extracted from the high frequency part of the phonon spectrum.

From this partition function, expressions for the vacancy contributions to the thermodynamic properties of the solid then follow. For the energy  $E$ , one has

$$E = -\frac{\partial \ln Z}{\partial \beta} = N \int E \rho(E) e^{-\beta E} dE, \quad (12)$$

and the associated specific heat is

$$C_V = -\beta^2 \frac{\partial E}{\partial \beta} = N \beta^2 \int E^2 \rho(E) e^{-\beta E} dE. \quad (13)$$

The pressure is given by

$$P_V = \beta^{-1} \frac{\partial \ln Z}{\partial V} = \beta^{-1} \int \frac{\partial \rho(E)}{\partial V} e^{-\beta E} dE. \quad (14)$$

And finally, the concentration of single-particle excitations is

$$n = N \int \rho(E) \frac{e^{-\beta E}}{1 + e^{-\beta E}} dE. \quad (15)$$

Because the single-particle states may include, as noted above, some local phonon modes, the role of the quantities  $C_V^0$  and  $P^0$  in eqns (8) and (9) may be different than in the localized vacancy discussion.

To illustrate the influence of statistics, a simple model can be constructed, which also uses a non-configurational entropy [10]. Then one finds for the vacancy concentration an expression

$$n = N e^{1/k_B} \int \frac{\rho(E)}{e^{\beta E} \pm 1} dE, \quad (16)$$

where the plus and minus signs refer to fermions and bosons, respectively, that is, to  $^3\text{He}$  and  $^4\text{He}$ .

The density of states  $\rho(E)$  is unknown from any first principles calculation, although an interesting microscopic model for the vacancy in bcc  $^3\text{He}$  was constructed long ago [11]. One form which has been used to represent specific heat data on bcc  $^3\text{He}$  is

$$\rho(E) = (1/2) \Phi^3 (E - \Phi)^2, \quad E > \Phi, \quad (17)$$

and  $\rho(E)$  equal zero for  $E$  below the "band edge" at  $\Phi$  [9]. Using this empirical form the relations, eqns (15), (14), and (13), become approximately

$$n = N(T/\Phi)^3 \exp(-\Phi/T), \quad (18)$$

$$C_V = nk_B [(\Phi/T)^2 + 6\Phi/T + 12], \quad (19)$$

$$P = nk_B (-\partial \Phi / \partial V) (1 + 3\Phi/T), \quad (20)$$

respectively.

Other semi-empirical forms have been given with the excitation energy being  $\Phi = e - \Delta/2$ , where  $e$  is an energy,  $\Delta$  is a bandwidth of the tunneling defects, the condition  $\Delta > T$  holds, and the defects have an effective mass [12]. One of the fascinations of the non-localized vacancy picture is the possibility that the energy  $e$  might be less than half the band width in a significant fraction of the Brillouin zone [1]. This has led, for example, to an argument that "the melting of helium at  $T=0$  is associated with the emergence of a nonideal gas of zero-point vacancies whose Bose condensation leads to superfluidity in the case of liquid  $^4\text{He}$ " [13]. However, as noted above, searches for "zero-point vacancies" have so far been unrewarded [2].

### 2.3. Mixed isotopic crystals

Relations for defects in isotopic mixture crystals are complicated. There is no general statement, valid for all isotopic concentrations and structures. For present purposes, however, a nearest neighbor bond energy approximation for localized vacancy defects illustrates some elements to be taken into account in an analysis. Assume bond energies  $e_{33}$ ,  $e_{44}$  and  $e_{34}$ , where each subscript denotes a particular isotope,  $^3\text{He}$  or  $^4\text{He}$ , respectively. From these bond energies (or quasi-chemical models) a parameter to measure the ordering energy can be constructed. It is

$$w = e_{34} - (1/2)(e_{33} + e_{44}). \quad (21)$$

If the  $^3\text{He}$  and  $^4\text{He}$  atoms form a homogeneously disordered system with localized vacancies, elaborations and modifications of expressions from Section 2.1 can be constructed, beginning from the partition function. In general, one expects  $^3\text{He}$ -vacancy binding to be preferred, from their opposite dilatational fields. However, only for very dilute cases are the resulting expressions straightforward.

On the other hand, suppose that there is an ordered structure consisting of two sublattices,  $i$  and  $j$ , one for each of the isotopes,  $^3\text{He}$  and  $^4\text{He}$ , respectively. In this case, denote occupancy of the  $i$  sublattice by  $^3\text{He}$  atoms by  $N_{3i}$ , and of the  $j$  sublattice by  $^4\text{He}$  atoms by  $N_{4j}$ . The numbers of vacant  $^3\text{He}$ -atom sites is then  $N_{vi}$ , etc. One proceeds by minimizing the free energy of the crystal as a function of the independent variables  $n$ ,  $N_{3j}$ , and  $N_{4j}$ , noting that  $N_{3j} = N - N_{3i}$ ,  $N_{4j} = N - N_{4i}$ ,  $N_{vi} = n + N_{3i} - N_{4i}$ , and  $N_{vj} = n - N_{3j} + N_{4j}$  [14]. One result is, for example,

$$\frac{N_{vi}}{N + n} = \left[ \frac{N_{3i} N_{4i}}{N_{3j} N_{4j}} \right]^{1/4} \exp[-4(e_{44} - w)/k_B T], \quad (22)$$

and there is a similar formula for the number of vacant sites on the  $^4\text{He}$ -atom sublattice,  $N_{vj}$ , except it has  $e_{33}$  in the exponential factor. The expressions for  $N_{3j}$  and for  $N_{4i}$  are more complicated.

Independent values for the parameters appearing in this analysis can sometimes be obtained. For example, from the observed cohesive energies of the pure He isotope crystals at large molar volume,  $|e_{33}| > |e_{44}|$ . The formalism then indicates that essentially all the vacancies will be located on  $^3\text{He}$  sites, while the  $^4\text{He}$  sites will contain  $(1/2)N_{vi}$  excess  $^3\text{He}$  atoms (i.e. about  $N_{3j} - N_{4i}$  of them). In case the ordering on the two sublattices is incomplete in the presence (or indeed the absence) of vacancies, this possibility can be treated by introducing another parameter, an order parameter [14]:

$$\eta = \frac{N_{3i} - N_{4i}}{2N} - \frac{N_{4j} - N_{3j}}{2N}. \quad (23)$$

The configurational part of the vacancy free energy then varies with  $\eta$  through the probabilities of occurrence of local configurations, unlike the case of a localized vacancy in a pure crystal, in which there is a constant configurational entropy. Further, if  $\eta$

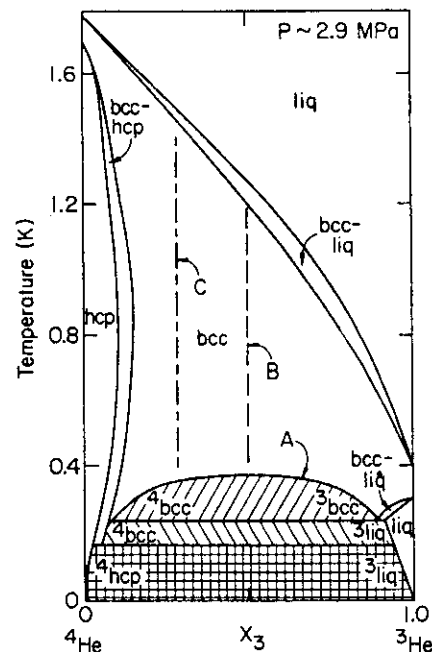


Fig. 2. Schematic temperature-composition diagram for  $^4\text{He}$ - $^3\text{He}$  mixture solidified at about 2.9 MPa.  $x_3$  is the fraction of  $^3\text{He}$ . The main area of the diagram is bcc solid, although bcc is very limited in extent for nearly pure  $^4\text{He}$ . The system shows isotopic phase separation, according to regular solution behavior, with a critical temperature  $T_c$  below 0.4 K (curve A). The  $^3\text{He}$ -rich daughter phase melts as the temperature is lowered below about 0.3 K. After Fraass and Simmons [5]. Other figures of the present paper correspond to the composition marked C and A (Fig. 8) and B (Fig. 9), although Figs 8 and 9 represent data on samples at different pressures.

varies with temperature, then the apparent vacancy free energy will also.

Now, from Fig. 2 one sees that at low temperature there is isotopic phase separation, not the ordering just discussed. From equilibrium X-ray measurements, it has been shown for the bcc mixture the coexistence line is of the form  $x(1-x)$ , where  $x$  is the concentration of one of the isotopes, and that therefore the solid solution is regular [15]. Moreover, the upper limiting temperature,  $T_c$ , of the coexistence curve gives a value for the parameter in eqn (21), namely  $T_c = 2w$ .

### 3. DIRECT AND INDIRECT EXPERIMENTAL METHODS

#### 3.1. X-ray method and procedure

Because solid  $^3\text{He}$  and  $^4\text{He}$  are extremely compressible, they can be held at essentially constant macroscopic volume in a cell thin enough so that quantitative X-ray diffraction study of the sample crystal can be carried out. Samples can be crystallized from the liquid, oriented, their subgrain structure characterized, their lattice parameters determined, and variations in their lattice parameters with changes in cells temperature measured [16, 17]. The key principle of direct measurements is that the net additional concentration of substitutional atomic sites,  $n/N$ , is given by

$$\frac{n}{N} = \frac{\Delta V}{V} - \frac{\Delta V_x}{V_x} \rightarrow -\frac{\Delta V_x}{V_x}, \quad (24)$$

where  $V_x$  is the unit cell molar volume determined by X-ray diffraction and the  $\Delta$ s denote changes in the measured volumes with respect to a reference state. With macroscopic constraint  $\Delta V/V$  becomes zero in eqn (24), and only an X-ray measurement is required, as indicated to the right. For cubic crystals,  $\Delta V_x/V_x = 3\Delta a/a$ . When the crystal is not cubic, determination of  $V_x$  requires the measurement of more than one lattice parameter, or else use of an assumption. In hcp  $^4\text{He}$ , experiments show that the crystals are ideally-packed, with fixed  $c/a$  ratio, so both parameters do not have to be followed in every run.

Temperature dependence of thermal vacancy content is given by eqn (3) or, alternatively, by eqn (18). In the former (localized) case, the vacancy partial free energy has two components as given in eqn (4), where it is assumed that the energy  $u$  and the non-configurational entropy  $s$  depend only upon the volume.

The guiding principle, eqn (24), depends upon a number of postulates. Important among them are (i) that the dilatational field of the force tensor describing the vacancies, in a real crystal, makes equal

contributions to the macroscopic and Bragg X-ray dilatations of the crystal lattice, and (ii) that the defect population is sufficiently dense and homogeneous to make surface elastic irregularities relatively unimportant [18]. Many treatments of the principle, both theoretical and experimental, are in the literature [19]. These treatments are static; they do not explicitly include point defects which are microscopically considered to be non-localized. However, it is likely that models which in regions far from the defect core treat the point defect as a singularity in an elastic continuum, and assign tensor components to this singularity, can include this possibility, even when the non-localization, in the sense of Andreev [1], is *not* static.

Preparation of the best helium crystals for vacancy studies is by directional solidification from liquid at essentially constant melting pressure,  $P_m$ , on the liquid-solid interface [20]. For pressure up to about 30 MPa, PMMA cells are strong enough to provide essentially constant volume conditions while transmitting sufficient X-rays for direct vacancy concentration measurements on cylindrical samples of 1–2 mm diameter [21]. Elapsed time for solidification of good crystals > 1 cm length can be from a few minutes to a few hours. The experimental method can be arranged so that (a) the cell maintains essentially isochoric conditions over the temperature range for the applicable pressures, and (b) the production of any significant content of other point defects by the measuring X-rays in the solid He specimens by photoelectric and Compton processes is negligible [22].

X-Ray measurements have been made with a special instrument designed for the purpose [23]. Success of X-ray techniques depends upon reasonable orientational and positional stability of the crystal in the diffractometer. Figure 3 shows that thermal vacancies can be directly observed, for example in bcc  $^3\text{He}$  [21]. Given the stability just noted, direct X-ray measurements can even be carried out under extreme conditions very near the melting line. Data of this kind for bcc  $^3\text{He}$  are shown in Fig. 4 [24] (taken in region C of Fig. 1). Note that this sample had *both* upper and lower melting temperatures.

When a large temperature range is not available for determining the reference lattice parameter, as for the constricted region of the phase diagram for bcc  $^4\text{He}$  shown in Fig. 1, one can sometimes use other methods. Two such methods are mentioned in the Fig. 5 caption [25]. One is obvious in principle and difficult in practice: the absolute comparison of macroscopic and microscopic volumes,  $V$  and  $V_x$ , respectively. The other recognizes that in a sample consisting of a fixed number of atoms, a reference  $V_x$

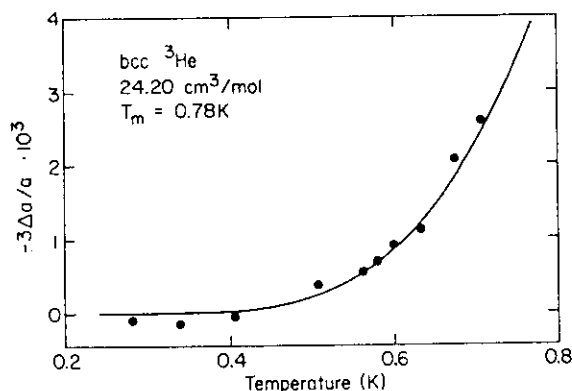


Fig. 3. Changes in the X-ray lattice parameter are direct evidence for thermal vacancies in bcc  $^3\text{He}$  confined at constant macroscopic volume, according to eqn (24). The solid line is an exponential of the form, eqn (3), with free energy  $4.25 \pm 0.1 \text{ K}$ . After Heald *et al.* [21]; the data were taken upon warming.

for the application of eqn (24) can be obtained even in another phase, in this case the hcp at low temperature, if that phase is expected to have a vanishing vacancy content. In view of the disagreements about vacancy content noted below, it is important to note that these two independent direct methods agree in bcc  $^4\text{He}$  [25].

There is a well defined pattern in results from X-ray measurements of vacancy content in  $^3\text{He}$ ,  $^4\text{He}$ , and dilute mixtures [24]. One could express this by saying that the net content is about constant along the melting line. An equivalent and somewhat more informative expression is shown in Fig. 6. Because of the limited sensitivity of X-ray measurements of this type, I have taken the view that characterization of the results by a single parameter, for example a free energy  $f$ , eqn (4), is a reasonable first step. The resulting  $f$ s show a linear dependence upon the melting temperature,  $T_m$ , of the samples.

There are further interesting coincidences in the properties of these solids. The deduced free energies

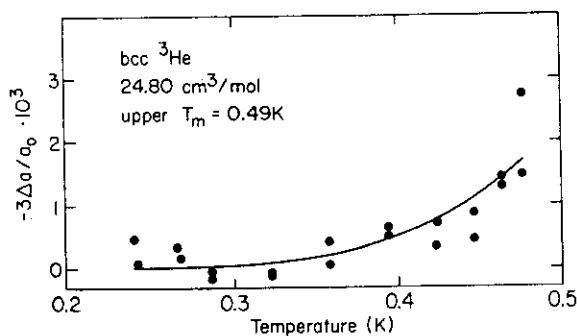


Fig. 4. At extremely low densities, near the minimum of the melting curve of bcc  $^3\text{He}$ , thermal vacancies can still be detected by X-rays, although the relative insensitivity of the measurement does not allow a quantitative determination of the temperature dependence over a narrow range of molar volumes near the maximum one. After Granfors *et al.* [24].

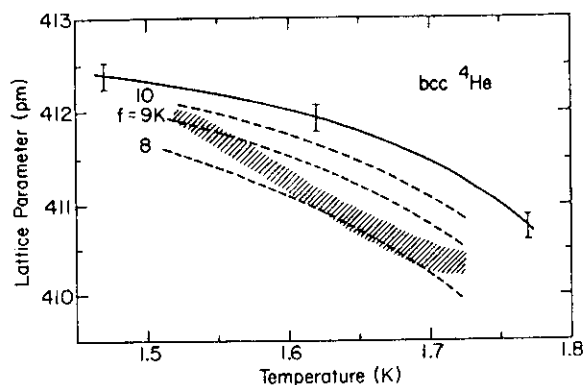


Fig. 5. The bcc phase in pure  $^4\text{He}$  is very narrow, so two methods have been used to determine the vacancy content [25]. One is to compare the absolute lattice parameters of crystals in contact with liquid (shaded band represents 80% of the measurements) with the macroscopic molar volume of the solid determined from *PVT* measurements (—). The dashed lines (----) represent  $f$ -values in eqn (3). The other method is to recognize that for a constant number of  $^4\text{He}$  atoms confined in a constant volume, the reference (thermal vacancy-free) volume can be measured after cooling the sample into the hcp phase at low temperature. The two independent methods agree.

show an apparent systematic variation with volume  $V$ . As for the solid *PVT* behavior, the energy decreases with increasing volume. Further, it is remarkable that the  $f$ s are similar at the same volume for all three solids: bcc  $^3\text{He}$ , bcc  $^4\text{He}$ , and hcp  $^4\text{He}$ . The temperature ranges are very different for  $^3\text{He}$  and for  $^4\text{He}$ , of course, because of the different zero-point pressures. This scaling by  $V$  rather than by  $T$  is characteristic for a quantum system. The vacancies themselves, therefore, can be justifiably called a quantum phenomenon. It should be noted that this characterization is further supported by measurements of the kinetic energies,  $\langle E_k \rangle$ , of bcc and of hcp  $^4\text{He}$  using neutron Compton profiles [26]. These measurements show both a similarity in  $\langle E_k(V) \rangle$  values for different phases at the same volume and a

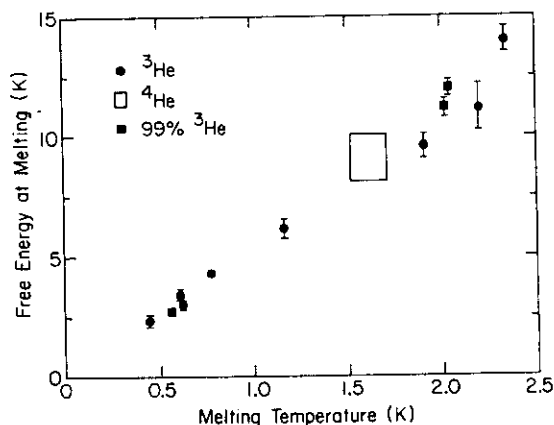


Fig. 6. Systematic relation between the apparent free energy,  $f$ , and the melting temperature for three kinds of bcc crystals, pure  $^3\text{He}$ , pure  $^4\text{He}$ , and lightly doped  $^3\text{He}$ . After Granfors *et al.* [25].

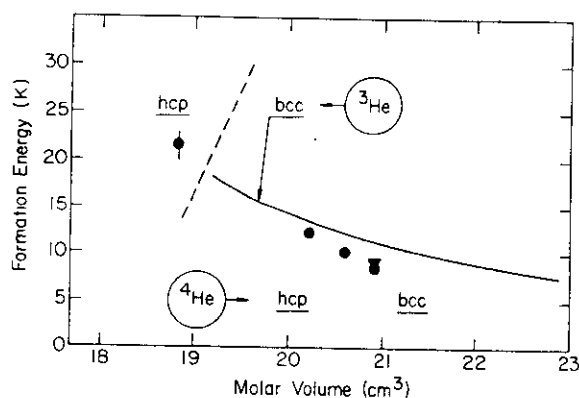


Fig. 7. Another trend is apparent in thermal vacancy properties of He crystals (after Simmons [27]). Qualitatively, the volume dependence of the vacancy free energy and of the crystal kinetic energy show a similar magnitude and a similar volume dependence.

decrease in  $\langle E_k(V) \rangle$  with increasing  $V$ . Finally, the magnitudes of the  $f_s$  and of the  $\langle E_k(V) \rangle$ s are similar [27]. The magnitudes of the vacancy properties are shown in Fig. 7.

Another very remarkable feature of an isotopic He mixture is shown in Fig. 8, namely, an extremely large thermal vacancy concentration, indicated by the exponentially decreasing lattice parameter in the specimen constrained at constant macroscopic volume. At the solidus (1.33 K) the vacancy content is  $\exp(-4.4 \text{ K}/1.33 \text{ K})$  or almost 4% [28]. In other solids, such thermal vacancy content is unknown except in ordered CsCl structure (B2) metallic alloys like Fe-Al, Ni-Ga, Ni-Al, Co-Ga, and Co-Al [29]. As noted in Section 2.3, such vacancies may appear on one sublattice or both. The situation, while complicated, is better defined than one in which the vacancies appear in a homogenous alloy without long-range order. In that case,

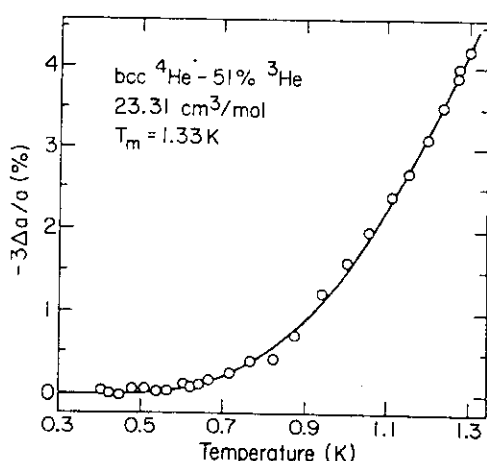


Fig. 8. The equilibrium vacancy content of bcc  ${}^3\text{He}$ - ${}^4\text{He}$  mixture containing 51%  ${}^3\text{He}$  at a molar volume of  $23.31 \text{ cm}^3$  is extraordinarily large. It is more than 4% at the solidus temperature of  $T_s = 1.33 \text{ K}$  (schematically, line B of Fig. 2, although this sample was at  $P$  about 3.57 MPa, which shifted  $T_s$  up). After Fraass and Simmons [28].

one would expect  ${}^3\text{He}$ -vacancy binding and other effects.

It is to be noted that such ordering in isotopic He mixtures would be contrary to the sign of  $w$  given in Section 2.3, for the (low) temperature near  $T_c$ . Searches for long-range order in  ${}^3\text{He}$ - ${}^4\text{He}$  at high temperature by my group have so far been unsuccessful. X-Ray diffraction appears unsuitable because the atomic form factors for  ${}^3\text{He}$  and  ${}^4\text{He}$  are identical; one would be looking for subtle dynamical effects in a weakly scattering sample. Neutron diffraction suffers from the practical problem of extremely large absorption by the  ${}^3\text{He}$  nucleus. If there is B2 type order at high temperatures, then  $w$  (remarkably!) changes sign as temperature is changed from high to low. If there is no such ordering, then the extraordinary vacancy content shown in Figs 8 and 9 needs some other explanation.

Apparent large thermal vacancy contents are not limited to approximately 50-50 mixtures, although the contents at the solidus are somewhat less than shown in Fig. 8. X-Ray studies of 12 and 28%  ${}^3\text{He}$  mixtures [28] also show significantly enhanced vacancy content compared to pure bcc  ${}^3\text{He}$ . In addition, measurements of pressure, motivated by a study of the phase diagrams of the mixtures at various densities, also showed a large pressure drop

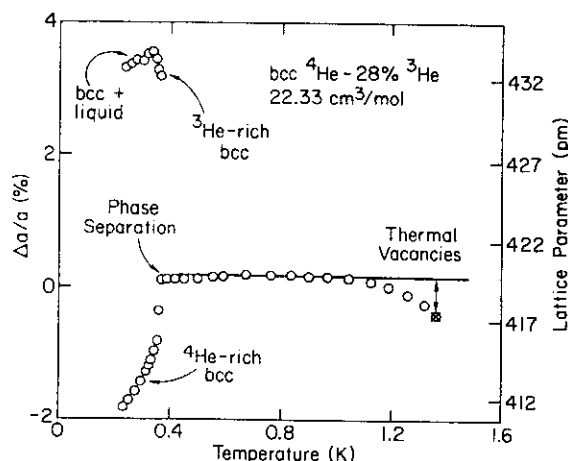


Fig. 9. Overall behavior of the X-ray lattice parameter,  $a$ , of a bcc crystal of 28%  ${}^3\text{He}$  in cooling from the solidus near 1.58 K in a cell at constant macroscopic volume  $22.33 \text{ cm}^3/\text{mol}$  (lines C and A of Fig. 2). An initial absolute lattice parameter ("x") was taken near 1.4 K. At high temperature,  $T$ , thermal vacancies compress the lattice because they add substitutional atomic sites. At intermediate  $T$ , the parameter  $a$  is constant if the sample cell is stiff enough to prevent contraction as the thermal pressure decreases. At phase separation, two lattice parameters appear, corresponding to the  ${}^4\text{He}$ -rich and  ${}^3\text{He}$ -rich daughter phases, respectively. Decrease of the temperature produces growth of  ${}^3\text{He}$ -rich and  ${}^4\text{He}$ -rich daughter phases, which have the different lattice parameters shown as they are enriched at lower temperatures. Finally, the  ${}^3\text{He}$ -rich phase melts and the liquid compresses the bcc phase in which it is embedded. After Fraass and Simmons [5].

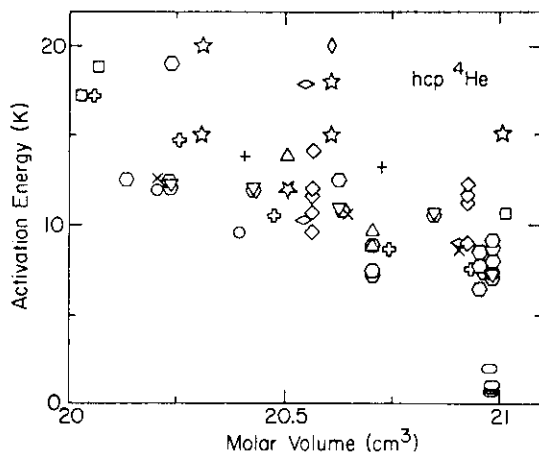


Fig. 10. As the kinds of experiments on solid heliums have multiplied, the diversity of results for apparent activation energies has increased. This figure is taken from published values for hcp  $^4\text{He}$  [31–48] and cited in specific detail in [48]. It illustrates the very wide variety of deductions which have been made from experiments which may individually have high sensitivity but at the same time each require an indirect path for the deduction of thermal defect properties. Values from localized vacancy model-fitting to direct X-ray data [22] are shown as “×” symbols.

from high temperatures in a sample of 78%  $^3\text{He}$  content [30]. The magnitude of this drop (0.9 MPa!) is consistent with a vacancy content of several percent at the solidus.

Although the magnitudes of these vacancy effects are enormous, by the standards of most solids, they produce lattice parameter changes which are moderate compared to the lattice parameter differences between isotopic samples at the same pressure. This is shown dramatically in Fig. 9 which gives an overall view of X-ray measurements on an isotopic mixture crystal [5].

### 3.2. Indirect methods for formation parameters

X-Ray measurements concerning defects in solid heliums, as described in the preceding Section 3.1, have been published only from Illinois. Other investigators have sought more sensitive measurements, although interpretation of such work is indirect. The overall results from these other kinds of measurements are that extremely diverse values for the apparent activation energies for defects have been found. For example, for hcp  $^4\text{He}$ , studies have been reported from measurements of pressure [31], sound velocity and attenuation [32, 33], NMR on  $^3\text{He}$  impurities [34–38], positive ion mobility [39–44], plastic deformation and diffusive creep [45, 46], and recovery of thermal conductivity after deformation [47]. For  $^3\text{He}$ , a similarly large collection of references could be cited.

Specifically, results in hcp  $^4\text{He}$  over a narrow volume range are shown in Fig. 10 [48]. An extraordi-

nary range of values is illustrated. Again, for  $^3\text{He}$  a similar scattered figure could be constructed. Clearly, one needs to have criteria to make some choices among possibilities, if one is going to obtain useful understanding of defects in the solid heliums.

In the search for defect contributions to thermo-physical properties, the measurement of pressure has some practical advantage. Highly sensitive capacitative pressure gauges can be incorporated into cells for other measurements (X-ray or NMR, for example). Simultaneous calorimetry would not be as practicable, because it requires careful thermal isolation. In a localized vacancy picture, the crystal pressure consists of three terms:

$$P(V, T) = P^0(V) + P_p(V, T) + n(V, T)p, \quad (25)$$

where  $P^0(V)$  is the zero-point pressure of the hypothetical perfect crystal,  $P_p(V, T)$  is the pressure due to phonons in the perfect crystal, and  $n(V, T)p$  is the increase in pressure due to the added vacancies.

Unfortunately, neither thermodynamic considerations, nor dynamical experiments, nor theory alone can be used to find the phonon pressure  $P_p(V, T)$  in the hypothetical perfect crystal. In a general way, experimentally measured phonon spectra in bcc, hcp, and fcc He phases [49] agree with self-consistent phonon calculations [50]. However, they do not agree in detail, that is, with an accuracy sufficient to make any inferences about vacancy content. One reason for this failure is scarcity of coherent-inelastic neutron scattering data at energy transfers corresponding to the higher energy parts of the expected one-phonon spectrum. It is these phonons that contribute most of the phonon pressure. Moreover, it is these phonons which may be concerned with non-localized vacancy states, as noted after eqn (11).

Another kind of measurement, neutron scattering, Compton profile does include all high-energy phonons in the determination of the atomic momentum distribution. By this direct method [26], it has been found that hcp  $^4\text{He}$  kinetic energies are considerably underestimated by self-consistent phonon calculations. Therefore, in order to analyze pressure data for possible defect contributions, a semi-empirical method is required to estimate  $P_p$ .

In these circumstances it is common to use an approximate form:

$$P_p(V, T) = (3\pi^4 k_B / 5v_0) \gamma(V, T) T^4 / \Theta_A(V)^3, \quad (26)$$

in which a constant characteristic temperature  $\Theta_A$  is used at each volume. This is usually an average value  $\Theta_A(V)$ , defined using actual temperature-dependent heat capacity measurements, calculated from the



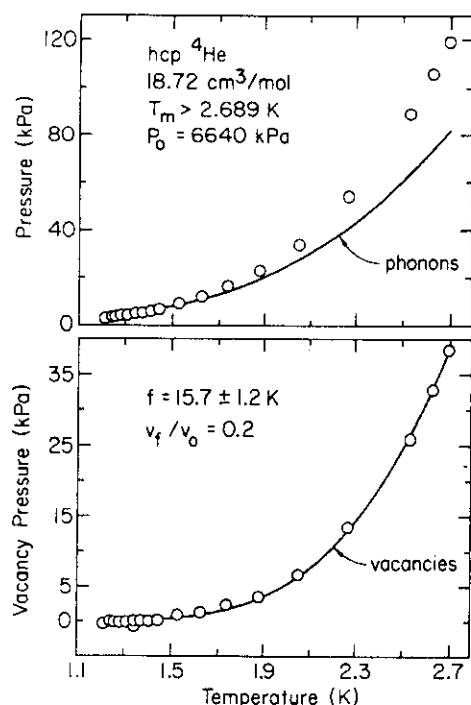


Fig. 11. Measurements of pressure of an isochoric sample are a sensitive way to detect the presence of thermal excitations, which include both phonons and vacancies. See eqns (3), (7), (26) and (27). These measurements on hcp  $^4\text{He}$  by Thorpe *et al.* [54] show the relative sizes of the inferred phonon and vacancy effects.

empirically derived temperature-dependent characteristic temperature,  $\Theta(V, T)$ . Better would be use of the actual  $\Theta(V, T)$ . These are available from precise experiments, for example on hcp  $^4\text{He}$  [51] and on bcc  $^3\text{He}$  [52], but not at precisely the values of  $V$  of a given pressure experiment. An interpolation is therefore required, which can be done with some confidence using the Grüneisen parameter defined as

$$\gamma(V, T) = -\partial \ln \Theta(V, T) / \partial \ln V, \quad (27)$$

with values set from calorimetry extrapolated to  $T = 0$  [53]. For the largest molar volumes, quantum solid heliums do not exhibit the corresponding states behavior of usual solids, that is,  $C_V$  is not represented by a universal function of  $\Theta/\Theta_0$  versus  $T/\Theta_0$  for all  $V$ . At smaller volumes, however, this is the case for the heliums, so that eqn (28) can be replaced by a relation with a fixed  $\gamma$ .

Deductions about thermal vacancies, made using this kind of host phonon analysis, are shown in Fig. 11 [54]. The crystal is hcp  $^4\text{He}$  at middling  $V$ . In this case, one expects a significant vacancy content at melting, but also one finds that the phonon pressure is significant. In the case shown, measurements could not be extended to a temperature low enough to reach a condition where the total phonon pressure was of the same order as the sensitivity of the pressure

measurements. Therefore the deduced values of  $P^{00}(V)$  for different  $V$ s were correlated through the known dependence of the bulk modulus,  $B(V)$ .

The very high sensitivity of pressure measurements allows studies to be carried out under extreme conditions, for example at the largest molar volumes. An example of precise data is shown in Fig. 12 [55]. The pressure scale is so highly expanded that the slight minimum in the melting curve of this heavier isotope,  $^4\text{He}$ , is easily visible.

Analysis of Illinois data of this kind using a localized vacancy model (Section 2.1) yields intermediate values of  $f$  for volumes, for example, the case shown in Fig. 11. On the other hand, analyses using non-localized vacancy models (Section 2.2) have been published both for bcc  $^3\text{He}$  [9] and for hcp  $^4\text{He}$  [46]. Both these analyses have used selected pressure, heat capacity, and diffusion data, and have concluded that the  $P$ ,  $C_V$ , and NMR or diffusive flow data are mutually consistent. They have also concluded that "an exception... is formed by X-ray experiments, which give a vacancy concentration substantially larger..." [46].

### 3.3. Vacancy migration energies, $^4\text{He}$

Self-diffusion in pure  $^4\text{He}$  is difficult to study directly, because plastic deformation experiments cannot be interpreted unambiguously and NMR cannot be applied in the pure system. Deformation experiments are becoming more sophisticated, and Dyumin *et al.* [46] claim not only to obtain information about migration but also to determine that  $s$  is non-zero. They continue their work, with further mass diffusion data.

Study of conductivity of samples into which ions have been injected by radioactive sources has also yielded activated behavior [56]. Both negative and

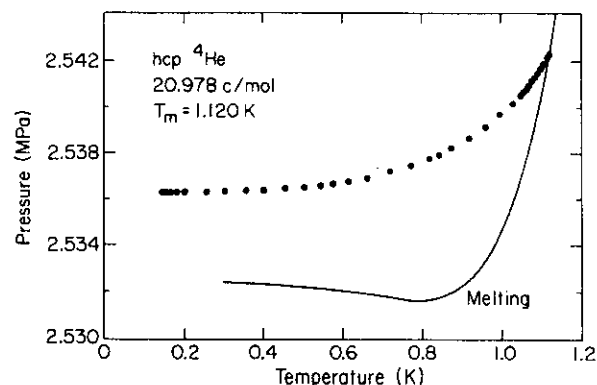


Fig. 12. The high sensitivity of pressure measurements is especially valuable under extreme conditions near melting. These data are on ultrapure hcp  $^4\text{He}$  (after Fujita and Simmons [55]). The maximum equilibrium  $V$  for  $^4\text{He}$  is  $V_{\text{max}} = 20.984 \pm 0.001 \text{ cm}^3 \text{ mol}^{-1}$ , which occurs at a pressure of 2.532 MPa and a temperature of  $0.775 \pm 0.005 \text{ K}$  [3].

positive ions have been studied. The negative ions are probably microvoids containing an electron; if so, their mobility may not be related to bulk thermal vacancies. The positive ions are thought to have the best possibility for relation to bulk monovacancy properties, although the structure(s) of such ions may be complex [57]. From different experiments the activation energies for positive ion mobility generally cover a range of values at a given  $V$ . This may simply be due to uncontrolled variability in experimental conditions. More interesting is the possibility that the ion mobility in hcp  $^4\text{He}$  is anisotropic. Lau *et al.* [43] fitted their data on specimens of fixed  $V$ , but of unknown crystallinity and orientation, with an assumed anisotropic mobility. Their derived values for the mobility could be described by two (limiting) activation energies and an angle. On Fig. 10 these limiting energies are shown as horizontal diamonds at  $V = 20.54 \text{ cm}^3 \text{ mol}^{-1}$ .

At  $V$ 's between 20 and  $21 \text{ cm}^3$  in hcp  $^4\text{He}$ , localized vacancy formation energy  $f$  values from both X-ray and pressure measurements lie near the bottom of the range exhibited by positive ion mobilities. Suppose that the activation energy for defect diffusion is the sum of activation energies for formation and for motion of the defects. Then if the range of mobility activation energies is indeed due to anisotropy, perhaps the vacancies tunnel in one orientation while, on the other hand, a thermally activated step is needed in the orthogonal direction. Speculations like this may be too simple: careful studies have shown that the ion mobilities are field dependent [58]. Andreev [59] proposes that this can be understood using a distribution of compact ion clusters.

Pressure measurements for vacancy analysis have been made at smaller  $V$ 's, down to about  $18 \text{ cm}^3$  [54].  $f$  values, from a localized vacancy analysis of these pressure data, lie at least 10 K below energies from NMR, positive ion diffusion, and deformation experiments. The apparent discrepancy is larger than the estimated uncertainty arising from choice of phonon model in the  $P$  analysis. Unfortunately, no X-ray data exist for these smaller  $V$ 's.

As cited above, NMR data on  $^3\text{He}$  impurities in hcp  $^4\text{He}$  have been collected in the region up to melting and also in the zero-point regime, where the relaxation times are temperature-independent. In the high-temperature region, activation energies have usually been obtained from  $T_1$  measurements although some  $T_2$  analysis has also been made. The range of activation energies reported by the different investigators is wide, but there is an apparent moderate dependence on  $V$ . None of the NMR studies had any independent information about sample crystallinity or orientation.

### 3.4. Vacancy migration energies, $^3\text{He}$

In  $^3\text{He}$ , for which NMR measurements of self-diffusion are available, comparison of the  $V$ -dependence of vacancy free energies leads to an interesting conclusion [21]. In the bcc phase the X-ray (formation) activation energies and the NMR (formation plus motion) activation energies agree within the uncertainties in the respective measurements. The barrier to motion in bcc is therefore about 1 K at the most; the vacancies may indeed be tunneling.

The formation  $f$  values from X-ray work and eqn (3) follow a smooth trend upward with decreasing  $V$  in successive samples, even into the hcp phase, as shown in Fig. 7. On the other hand, in the hcp phase there is a clear 11 K upward jump in the NMR values. This difference between the two energies can be attributed to a thermally activated barrier to migration in the close-packed phase.

### 3.5. Other measurements on hcp $^4\text{He}$

In ultrasonic work at  $V$ 's near the limiting value in the  $^4\text{He}$  phase diagram [33], (the  $P$ - $T$  range, but not the data, of Fig. 12), a complicated response is shown in samples of ultrapure  $^4\text{He}$ . Among the parameters of the data analysis were activation energies,  $f_u$ , with values very small compared to all previous studies on hcp  $^4\text{He}$ . (These values are visible as symbols near the axis at  $V = 21 \text{ cm}^3$  on Fig. 10.) It was found that these  $f_u$ 's were also proportional to the melting temperatures of the respective samples, but with a constant offset. A later search for an influence on the thermal conductivity of samples of similar purity did not detect any effect attributable to defects [60]. At present there appears to be no clear connection between these interesting studies and others aimed at thermal defects in hcp  $^4\text{He}$ .

## 4. CONCLUSION

Direct X-ray studies have shown that measurable net thermal vacancy contents exist in hcp and bcc  $^4\text{He}$  and  $^3\text{He}$  and in bcc isotopic mixtures. Analyses of these contents using thermoelastic models give a reasonable free volume of formation for these defects, regarded as localized. Various correlations in vacancy energies can be made, as functions of molar volume in a given phase, as a function of structure for a given isotope, and between isotopes. Some of these correlations are expected, some are surprising. Even for a localized model for vacancies, the defects are clearly quantum entities, because mass and volume effects appear much more important than temperature in determining characteristic energies.

However, attempts to harmonize the X-ray measurements with other studies in pure  $^3\text{He}$  and  $^4\text{He}$

have run into difficulty. Direct X-ray work generally finds a larger vacancy content than can be inferred from the temperature dependence of deduced deviations of other properties (specific heat, pressure, etc.) from postulated properties of a hypothetical defect-free crystal. These inferences [for example, Refs 9 and 46] use a fairly generalized form of non-localized model for the excitation energy spectrum of the thermal defects. A preliminary impression might be that this difficulty could be surmounted either by more secure knowledge of the hypothetical defect-free crystal properties, by use of other models for the vacancy excitation spectrum, by consideration of possible vacancy aggregation, or by microscopic consideration of which local vibrational modes have been abstracted from the defect-free crystal. But this difficulty is not small, since the analyses appear rather insensitive to variations in these assumptions within the few quantitative calculations available. Intriguing as the notion of non-localized vacancies may be, convincing experimental determination of the bandwidth and of the density of states of vacancies in a given solid helium phase is still not available.

These difficulties are joined by those presented by the much larger vacancy contents seen using X-rays in concentrated mixtures, as shown in Figs 8 and 9, although suitable pressure measurements have not yet been carried out with such a comparison in mind. The thermal defect population in a concentrated mixture is diverse, which complicates comparisons between measurements of different physical properties.

It is clear that much remains to be learned about these exotic defects in quantum solid heliums. More experiments on well characterized samples and new microscopic theories of the defects would be useful.

*Acknowledgement*—I am very pleased to acknowledge the inspiration of Bob Balluffi, with whom I first spent much time concerned with direct thermal vacancy measurements. My work on helium reported here was supported by the U.S. Department of Energy, BES-Materials Sciences under Grant DEFG02-91ER45439.

## REFERENCES

1. Andreev A. F. and Lifshitz, I. M., *Zh. Eksp. Teor. Fiz.* **56**, 2057 (1969). [*Sov. Phys.-JETP* **29**, 1107 (1969)]; A. F. Andreev in *Progress in Low Temperature Physics* (Edited by D. F. Brewer), Chap. 2. North Holland Pub. Co., New York (1982).
2. van de Haar P. G., Woerkens C. M. C. M., Meisel M. W. and Frossati G., *J. Low Temp. Phys.* **86**, 349 (1992); M. W. Meisel, *Physica B* **178**, 121 (1992).
3. Grilly E. R., *J. Low Temp. Phys.* **11**, 33 (1973).
4. Loubeyre P., Le Toullec R., Pinceaux J. P., Mao H. K., Hu J. and Helmley R. J., *Phys. Rev. Lett.* **71**, 2272 (1993).
5. Fraass B. A. and Simmons R. O., *Phys. Rev.* **B36**, 97 (1987).
6. Andreev A. F., *J. Physique* **39**, C6-1257 (1978) and experimental references therein.
7. See as recent example, Beamish J. R., Mulders N., Hikata A. and Elbaum C., *Phys. Rev.* **B44**, 9314 (1991).
8. Varotsos P. A. and Alexopoulos K. D., *Thermodynamics of Point Defects and Their Relation with Bulk Properties*, Elsevier, New York (1986).
9. Bernier M. E. R. and Hetherington J. H., *Phys. Rev.* **B39**, 11285 (1989).
10. Granfors P. R., Ph.D. thesis, University of Illinois (1982, unpublished). See also D. I. Pushkarov, *Zh. Eksp. Teor. Fiz.* **59**, 1755 (1970) [*Sov. Phys.-JETP* **32**, 954 (1971)] and *J. Phys. C: Sol. State Phys.* **19**, 6873 (1986).
11. Hetherington J. H., *Phys. Rev.* **176**, 231 (1968).
12. See for example Dyumin N. E., Zuev N. V. and Grigor'ev V. N., *Fiz. Nizk. Temp.* **19**, 33 (1993) [*Low Temp. Phys.* **19**, 23 (1993)].
13. Volykhin K. F. and Khrapak A. G., *Fiz. Nizk. Temp.* **19**, 93 (1993) [*Low Temp. Phys.* **19**, 67 (1993)].
14. Kim S. M., *Phys. Rev.* **B29**, 2356 (1984).
15. Ehrlich S. N. and Simmons R. O., *J. Low Temp. Phys.* **68**, 125 (1987); *Can. J. Phys.* **65**, 1569 (1987).
16. Balzer R. and Simmons R. O. in *Low Temperature Physics*, LT13, Vol. II, (Edited by Timmerhaus D. K., O'Sullivan W. J. and Hammel E. F.), p. 115. Plenum, New York (1974).
17. Heald S. M. and Simmons R. O., *Rev. Sci. Instrum.* **48**, 316 (1977).
18. Balluffi R. W. and Simmons R. O., *J. Appl. Phys.* **31**, 2284 (1960).
19. For further discussion, with historical references, see for example Dederichs P. H., *J. Phys. F* **3**, 471 (1973); and Hartwig J. and Holy V., *Phys. Stat. Sol. B* **135**, 37 (1986).
20. Fraass B. A., Heald S. M. and Simmons R. O., *J. Cryst. Growth* **42**, 370 (1977).
21. Heald S. M., Baer D. R. and Simmons R. O., *Phys. Rev.* **B30**, 2531 (1984).
22. Fraass B. A., Granfors P. R. and Simmons R. O., *Phys. Rev.* **B39**, 124 (1989).
23. Fraass B. A., Granfors P. R., Hilleke R. O. and Simmons R. O., *Rev. Sci. Instrum.* **55**, 1455 (1984).
24. Granfors P. R., Fraass B. A. and Simmons R. O. (unpublished).
25. Granfors P. R., Fraass B. A. and Simmons R. O., *J. Low Temp. Phys.* **67**, 353 (1987).
26. Blasdel R. C., Ceperley D. M. and Simmons R. O., *Z. Naturforschung* **48a**, 433 (1993).
27. Simmons R. O., *Can. J. Phys.* **65**, 1401 (1987).
28. Fraass B. A. and Simmons R. O., *Phys. Rev.* **B37**, 5058 (1988).
29. Kim S. M., *Phys. Rev.* **B29**, 2356 (1984), and references therein.
30. Tedrow P. M. and Lee D. M., *Phys. Rev.* **181**, 399 (1969).
31. Jarvis J. F., Ramm D. and Meyer H., *Phys. Rev.* **170**, 320 (1968).
32. Tsuruko F. and Hiki Y., *Phys. Rev.* **B20**, 2702 (1979).
33. Lengua G. and Goodkind J., *J. Low Temp. Phys.* **79**, 251 (1990).
34. Miyoshi D. S., Cotts R. M., Greenberg A. S. and Richardson R. C., *Phys. Rev. A* **2**, 870 (1970).
35. Grigor'ev V. N., Esel'son B. N. and Mikheev V. A., *Zh. Eksp. Teor. Fiz.* **39**, 321 (1974); [*Sov. Phys.-JETP* **39**, 153 (1974)].
36. Allen A. R. and Richards M. G., *Phys. Lett.* **65A**, 36 (1978).
37. Allen A. R., Richards M. G. and Schratter J., *J. Low Temp. Phys.* **47**, 289 (1982).
38. Mikheev V. A., Maidanov V. A. and Mikhiv N. P., *Fiz. Nizk. Temp.* **8**, 1000 (1982). [*Sov. J. Low Temp. Phys.* **8**, 505 (1982)].

39. Ifft E., Mezhev-Deglin L. and Shal'nikov A., in *Proc. 10th Int. Conf. on Low Temperature Physics*, Vol. I, p. 224. Viniti Publishing House, Moscow (1967).
40. Sai-Halasz G. A. and Dahm A. J., *Phys. Rev. Lett.* **28**, 1244 (1972).
41. Marty D. and Williams F. I. B., *J. Physique* **34**, 989 (1973).
42. Keshishev O., *Zh. Eksp. Teor. Fiz.* **72**, 521 (1977). [*Sov. Phys.-JETP* **45**, 273 (1977)].
43. Lau S. C., Dahm A. J. and Jeffers W. A., *J. Phys.* **39**, C-686 (1978).
44. Golov A. I., Efimov V. B. and Mezhev-Deglin L. P., *Zh. Eksp. Teor. Fiz.* **40**, 293 (1984). [*JETP Lett.* **40**, 1080 (1984)].
45. Suzuki H., *J. Phys. Soc. Japan* **42**, 1865 (1977).
46. Dyumin N. E., Zuev N. V., Boiko V. V. and Grigor'ev V. N., *Fiz. Nizk. Temp.* **19**, 9846 (1993); [*Low Temp. Phys.* **19**, 696 (1993)].
47. Levchenko A. A. and Mezhev-Deglin L. P., *Pis'ma Zh. Eksp. Fiz.* **37**, 173 (1983) [*JETP Lett.* **37**, 205 (1983)]; *Zh. Eksp. Teor. Fiz.* **86**, 2123 (1984) [*Sov. Phys.-JETP* **59**, 1234 (1984)].
48. Fujita I., Thorpe J. C. and Simmons R. O. (unpublished).
49. Glyde H. R. and Svensson E. C., in *Neutron Scattering, Methods of Experimental Physics*, Vol. 23, Part B (Edited by D. L. Price and K. Skold), p. 303. Academic Press, New York (1987).
50. Koehler T. R., in *Dynamical Properties of Solids*. (Edited by G. K. Horton and A. A. Maradudin) Vol. 2, p. 1. North-Holland Pub. Co., New York (1975).
51. Ahlers G., *Phys. Rev.* **A2**, 1505 (1970).
52. Greywall D., *Phys. Rev.* **B15**, 2604 (1977); **B16**, 5129 (1977).
53. For example, for hcp  $^4\text{He}$ , precise interpolation formulae are given by Gardner W. R., Hoffer J. K. and Phillips N. E., *Phys. Rev.* **A7**, 1029 (1973).
54. Thorpe J., Fujita I. and Simmons R. O. (unpublished).
55. Fujita I. and Simmons R. O. (unpublished).
56. Dahm A. H., in *Progress in Low Temperature Physics*, Vol. X. (Edited by D. F. Brewer), p. 73. North-Holland Pub. Co., New York (1985) and the references cited earlier.
57. Potapov S. G. and Sukhanov L. P., *Fiz. Nizk. Temp.* **16**, 1363 (1990) [*Sov. J. Low Temp. Phys.* **16**, 773 (1990)].
58. Efimov V. B. and Mezhev-Deglin L. P., *Fiz. Nizk. Temp.* **4**, 857 (1978) [*Sov. J. Low Temp. Phys.* **4**, 406 (1978)].
59. Andreev A. F. (personal communication).
60. Burns C. A. and Goodkind J., *J. Low Temp. Phys.* **93**, 15 (1993).

SYNCHROTRON X-RAY STUDY OF DEBYE-WALLER FACTORS  
IN FCC HELIUM-3 AND HELIUM-4

D.A. Arms, R. Shah, R.O. Simmons

Department of Physics, University of Illinois at Urbana-Champaign, Urbana, IL 61801 U.S.A.  
dohnarms@uiuc.edu, r-shah2@uiuc.edu, ros@uiuc.edu

M. Schwoerer-Böhning

Advanced Photon Source, Argonne National Laboratory, Argonne, IL 60439 U.S.A.  
schwoere@aps.anl.gov

Comparative study of the crystal dynamics of the fcc phases of the helium isotopes has faced the difficulty of measurements at pressures above 100 MPa. Adiabatic calorimetry on high-density  $^4\text{He}$  and  $^3\text{He}$  was first carried out by Dugdale and Franck [1], who also studied the hcp-fcc transition. However, because of this transition, calorimetry on fcc phase cannot be carried to low temperature. Quantitative temperature-dependent studies for high density therefore exist only for the hcp phases of  $^3\text{He}$  [1,2] and  $^4\text{He}$  [1,3]. When the heat capacity for these hcp phases was represented by an equivalent Debye characteristic temperature [2], it was found that the ratio of the low-temperature-limiting values of the characteristic temperatures at a given molar volume was 1.18, apparently larger than the simple dynamical ratio of the isotopic masses,  $(4/3)^{1/2} = 1.1547$ . That is, although the isolated interatomic pair potential is identical for the two isotopes, there appeared to be some dynamical modification of the potential in the crystalline state. No comparative isotopic studies of fcc dynamics by means of Brillouin, Raman, neutron, or x-ray scattering have appeared, although inelastic neutron studies of fcc  $^4\text{He}$  alone have been published [4].

Here we report the results of synchrotron X-ray measurements of Bragg intensities from both fcc  $^3\text{He}$  and fcc  $^4\text{He}$  over very large ranges of  $q = (4\pi/\lambda)\sin\theta$ , using a wavelength of 0.07749 nm, at beamline X-14 of the Brookhaven National Synchrotron Light Source. The results directly yield values for the mean-square atomic displacement from the lattice site,  $\langle u^2 \rangle$ . The applicable formula for a Gaussian distribution of displacements is

$$I(q) = I_0 |F(q)|^2 L (1 + \epsilon_{DS}) \exp(-\langle u^2 \rangle q^2) \quad (1)$$

Here  $I(q)$  is the measured intensity relative to an incident reference  $I_0(q)$ ,  $F(q)$  is the form factor, of which the atomic factor  $f$  is a part,  $L$  is the Lorentz factor, and  $\epsilon_{DS}$  is a diffuse scattering correction. It should be noted that such a measurement is complementary to a measurement of the atomic momentum distribution,  $\langle p^2 \rangle$ , which is accessible through data on the neutron Compton profile [5].

High-purity samples were prepared *in situ* in a cylindrical Be cell, from a sealed all-metal gas-handling and pressurization system which preserves the purity of the original sample gases. Data were taken on single crystals, for which the mosaic half-widths were near 0.02 deg. Because the x-ray absorption length in helium at this density is large compared to the 0.8 mm diameter of the samples, no corrections for absorption or extinction were made.

Data were obtained from fcc  $^3\text{He}$  at 18.13 K with molar volume 11.545 cm<sup>3</sup>, including Bragg peaks (111), (200), (220), (311), (222), (420), (422), (333), and (511), a range of  $q$  from

251 through 768 nm<sup>-1</sup>. The raw integrated intensities, compared to the reference (111), covered the remarkable range almost exp(10), in part because of the very strong dependence of  $f(q)$ . This range could not have been achieved without the very clean signals made possible using synchrotron radiation. Data obtained from fcc <sup>4</sup>He at 20.25 K with molar volume 10.953 cm<sup>3</sup>, covered a similar number of Bragg peaks. The raw data were corrected for the effects noted in Eq. (1), to produce values of  $\langle u^2 \rangle$ . The values were  $11.376 \pm 0.102$  and  $9.838 \pm 0.320 \times 10^{-4}$  nm<sup>2</sup>, for <sup>3</sup>He and <sup>4</sup>He, respectively. In neither solid is there evidence for crystalline anisotropy of  $\langle u^2 \rangle$ .

For a first comparison, it is convenient to convert these displacements to Debye characteristic temperatures,  $\Theta^M(V,T)$ . The results are  $\Theta_{\text{3}}^M = 121.3 \pm 0.9$  K and  $\Theta_{\text{4}}^M = 111.4 \pm 2.6$  K. Because the data were taken at somewhat different sample densities and temperatures, one must consider corrections in order to compare the isotopes strictly. For the volume correction, we took the Grüneisen relation with a value of 2.0 [2], which at the measured <sup>4</sup>He density produces a value for  $\Theta_{\text{3}}^M = 133.7$  K. The temperature corrections are more problematical. An empirical approach in the actual anharmonic solids is limited because the fcc phase covers only a very limited temperature range at these molar volumes. For the present, we neglect temperature corrections, because the two samples were measured at very similar reduced temperature, namely 0.167 and 0.163 for <sup>3</sup>He and for <sup>4</sup>He, respectively.

Finally, the ratio of Debye temperatures at a reduced temperature near 0.165 becomes  $(133.7 \pm 1.0)/(111.4 \pm 2.6) = 1.200 \pm 0.036$ . This result is centered above the calorimetric ratio for hcp phase [2], and also appears to be significantly above the dynamical ratio of the masses. It should be noted that the calorimetric ratio is of values integrated over the phonon frequency spectrum weighted by a factor  $\omega^3$ , while the Debye-Waller ratio is of values weighted by a factor near  $\omega^{-1}$ . We are reanalyzing our data to establish whether the limits of uncertainty given, dominated by some scatter in the <sup>4</sup>He data, are too conservative. Separately, with a similar goal of investigating dynamical effects owing to mass changes, we are examining an extensive set of Debye-Waller data on the hcp phases of <sup>3</sup>He and <sup>4</sup>He [6]. Finally, just as in the case of momentum distributions, which produced excellent agreement with path-integral Monte Carlo calculations [5], the values of  $\langle u^2 \rangle$  should be subject to comparison with such fundamental theory.

This research was supported by the U.S. Department of Energy, Office of Energy Research, Basic Energy Sciences contract DEFG02-96ER45439.

- 
- [1] J.S. Dugdale and J.P. Franck, Phil. Trans. Roy.Soc. Lond. **257**, 1 (1964).
  - [2] H.H. Sample and C.A. Swenson, Phys. Rev. **158**, 188 (1967) and references therein.
  - [3] G. Ahlers, Phys. Rev. A **2**, 1505 (1970), and references therein.
  - [4] E.R. Dobbs, *Solid Helium Three* (Clarendon Press, Oxford, 1994).
  - [5] D.M. Ceperley, R.O. Simmons, and R.C. Blasdel, Phys. Rev. Lett. **77**, 115 (1996).
  - [6] D.A. Arms, R. Shah, M. Schwoerer-Böhning, and R.O. Simmons (to be published).

FIRST DETERMINATION OF THE PHONON DISPERSION RELATION  
IN HCP HELIUM-3

C. Seyfert, H. Sinn, E. Burkel

FB Physik, Universität Rostock, August-Bebel-Str. 55, 18055 Rostock, Germany  
seyfert@desy.de, sinn@desy.de, burkel@villa.physik1.uni-rostock.de

D. A. Arms, R. O. Simmons

Dept. of Physics, University of Illinois, Urbana-Champaign, IL 61801, USA  
dohnarms@aps.anl.gov, ros@uiuc.edu

The phonon dispersion relation in hcp  $^3\text{He}$  was determined by inelastic x-ray scattering. Beforehand, there was a striking lack of experimental data on the dispersion relation in solid  $^3\text{He}$  while the dispersion relations in the different modifications, bcc, hcp and fcc of solid  $^4\text{He}$  had been the subject of many experimental studies<sup>1</sup>. This is caused by the very high absorption cross section for thermal neutrons, the commonly used probe to study the dynamics in solids. In contrast, the new technique of inelastic x-ray scattering with meV resolution<sup>2</sup> is not hindered by absorption, thus allowing the direct comparison of  $^3\text{He}$  and  $^4\text{He}$  lattice dynamics.

The experiment was performed at the very high resolution inelastic x-ray scattering beamline ID16 at the ESRF. The instrument<sup>3</sup> is a triple-axis spectrometer placed at an undulator source. It uses high order reflections of perfect silicon crystals in backscattering geometry to obtain a relative energy resolution better than  $10^{-6}$ . During this experiment, the energy resolution was 8.6 meV at a photon energy of 13.8 keV, corresponding to the Si(777) reflection. The triple axis spectrometer was used in the constant-Q mode with fixed final energy and a momentum resolution of  $0.08 \text{ \AA}^{-1}$ . Scans were performed in the momentum transfer range between  $Q=0.6 \text{ \AA}^{-1}$  and  $Q=2.1 \text{ \AA}^{-1}$ . During the scans the incident energy was tuned by varying the lattice parameter of the monochromator crystal, rather than its scattering angle which stays fixed in backscattering geometry. This variation was achieved by changing the crystal temperature in steps of 0.01 K, corresponding to energy steps of 0.35 meV.

The data presented here were measured on hcp  $^3\text{He}$  single crystals with molar volumes of  $13.2(1) \text{ ccm}$ , the same molar volume as in previous studies<sup>4</sup> on hcp  $^4\text{He}$ . The crystals were grown in situ inside a beryllium sample cell situated in a closed-cycle refrigerator. The beryllium cell was pressurized with  $^3\text{He}$ -gas via a capillary from an external pressure generating system. At a constant pressure of 90 MPa, the cell was slowly cooled down below the melting temperature of 11.8 K. The crystals were characterized and oriented using their Bragg reflections. The mosaic spreads of the crystals were typically about  $0.05^\circ$ .

Longitudinal phonons along along the a- and c-axis, the two principal directions in hexagonal closed packed crystals, were observed. In the (00q)-direction, the dispersion

relation for the LA and LO branch was determined in two different Brillouin zones. The dispersion shows the expected symmetry around the zone centre  $\Gamma$ , where the highest phonon energy of 10.7(4) meV has been measured. Along the other principal direction, the (q00)-direction, the LA and LO branches could not be separated due to the limited energy resolution. The data analysis was done assuming single-phonon excitations, thus ignoring any multi-phonon effects. The spectra could be described by a convolution of the resolution function with a line-shape model suggested by Fåk and Dorner<sup>5</sup>. However, the increasing width of the excitations at higher momentum transfers suggests to include multi-phonon contributions into a final analysis.

Comparison with the available <sup>4</sup>He data shows a ratio of the phonon energies between <sup>3</sup>He and <sup>4</sup>He of 1.15(8). That is the precise value expected from the mass difference alone. However, the estimated uncertainty covers other predictions, as well.

We thank C. Masciovecchio from the ESRF for his valuable help performing the experiment. Work supported by BMBF Projektnr. 05 - 650 HRA 1 and by U.S. DOE BES-MS, Contract No. DEFG02-91ER45439.

## References:

- <sup>1</sup> H. R. Glyde, *Excitations in solid and liquid helium* (Clarendon Press, Oxford, 1994) and references therein.
- <sup>2</sup> E. Burkel, *Inelastic scattering of x-rays with very high energy resolution*, Springer tracts in modern physics, Vol. 125 (Springer-Verlag, Berlin, 1991).
- <sup>3</sup> F. Sette, in *ESRF Beamline handbook*, ed. R. Mason (ESRF, Grenoble, 1995), p. 99.
- <sup>4</sup> C. Seyfert, D. A. Arms, H. Sinn, R. O. Simmons and E. Burkel, Czech. J. Phys. **46**, 471 (1996).
- <sup>5</sup> B. Fåk and B. Dorner, ILL technical report No. 92FA0085 (1992).



## DEVELOPMENT OF COORDINATED METHODS TO STUDY VACANCIES IN LOW-DENSITY HCP HELIUM-4

I. Fujita, J.C. Thorpe, R.O. Simmons

Department of Physics and Frederick Seitz Materials Research Laboratory  
University of Illinois at Urbana-Champaign, Urbana, IL 61801, U.S.A.  
ros@uiuc.edu

The measurement of equilibrium vacancy content in hcp  $^4\text{He}$  at densities near the minimum density depends upon finding a sensitive and reliable signature of vacancy presence. Unfortunately, physical properties which can be measured with potential high precision, such as heat capacity, pressure, ultrasonic attenuation, thermal conductivity, etc., are sensitive not only to vacancy content but also to the presence of other excitations and of other defects. Further, for such sensitive properties, separation of the vacancy contribution from others is equivocal and difficult both in the case of thermodynamic properties and of transport or nonequilibrium properties. On the other hand, the direct method which measures the difference between number of atoms and the number of atomic sites, using x-ray diffraction, is limited in its sensitivity. Finally, complications also arise in many cases because sample conditions may depend on the history of the sample. It appears that some of the disparate results in the literature originated in differences between the sample characterizations.

A constructive approach can be to combine a direct x-ray measurement with one of the sensitive but indirect methods. This has the advantage of offering the possibility of a common sample, with better sample characterization. The present paper describes development of coordinated x-ray and sensitive pressure measurements on a single sample. The pressure measurement capabilities are illustrated by results on a  $^4\text{He}$  sample very close to the minimum density of the hcp phase.

To permit x-ray study of a single-crystal sample, the central part of the sample cell followed the pattern used successfully in previous work [1]. That part is a polished PMMA cylinder with 1.59 mm i.d. and 3.81 mm o.d. Because our x-ray methods, using a tail-type cryostat with multiple thermal radiation shields, have been thoroughly described previously, we focus on pressure measurements here. At the upper end of the cylinder a capacitive strain gauge made of BeCu was mounted with a Ge resistance thermometer and connection to the dilution refrigerator mixing chamber. At the lower end a Cu chamber filled with sinter provided both entrance for the sample fill capillary and thermal connection to another Ge resistance thermometer. Typical temperature differences across the whole PMMA cell assembly were about 1 mdeg.

For the present work, the resolution of the strain gauge was chosen to be 0.03 kPa, appropriate to the total pressure range to be covered and high enough that overall sample irreproducibilities were not a factor. Our pressure scale was both calibrated against an external standard Bourdon gauge and checked under actual sample conditions against the melting curve

minimum, assumed to be at 2532.1 kPa [2]. Along the lower part of the melting curve our measurements were offset from the values of Grilly [3] typically by 0.3 kPa. A further check of both pressure and temperature, rather far from the present-measurements, was made at the lower bcc-hep-fluid triple point. Our Ge thermometers were calibrated against a certified superconducting fixed point device.

We report here results on an hep  $^4\text{He}$  sample having melting coordinates of  $T_m = 1.130 \pm 0.004$  K,  $P_m = 2542.0 \pm 0.0002$  kPa (molar volume  $20.9773 \text{ cm}^3$ ) [3]. Sample isotopic impurity was  $< 1$  ppb. The solid was prepared by directional solidification of liquid, with constant pressure on the solid-liquid interface, until a plug was formed in the fill capillary. After growth the solid sample was annealed by a series of cooling and warming cycles; this was more effective than extended time spent at a constant temperature just below melting. Over 40 pressures were measured along the final data isochore from 150 mK to melting. Pressure rise along this isochore was about 7 kPa, of which about 700 Pa appeared to be vacancy contribution.

The pressure data can be well-represented by the relation

$$P = P_0 + P_\Theta + P_{\text{vac}} = P_0 + BT^4 + C\phi \exp(-\phi / T), \quad (1)$$

with the parameter  $B$  in the phonon term required to be consistent with low-temperature limiting values of the Debye temperature, Grüneisen parameter, and molar volume from independent work [2,3]. The simple form of the third term on the right corresponds to a localized vacancy model with formation energy  $\phi = 7.6$  K. Various non-localized vacancy models have been proposed, with different numbers of parameters. One with a minimum number of parameters [4], produced a  $P_{\text{vac}}$  never different from the one in Eq. (1) by more than 12 Pa, and the exponential term with a value of 7.5 K. The two models could therefore not be distinguished. Refinement of the capacitance sensitivity would not in our opinion improve the ability to discriminate between models, however, because of the uncertainty in the phonon contribution.

One clear conclusion can be drawn. The defect excitation energy for such a low density hep  $^4\text{He}$  sample is consistent with extrapolation of volume dependence deduced from direct x-ray work [5]. On the other hand, it is far too large to fit the postulated form

$$\phi = \text{const.} \left(1 - (V / V_{\text{max}})\right)^{1/2}. \quad (2)$$

with  $V_{\text{max}} = 20.984 \text{ cm}^3$  [6]. From this, we conclude that the excitations studied in the cited ultrasonic work [6] are unrelated to thermal vacancies.

This research was supported by the U.S. Department of Energy, Office of Energy Research, Basic Energy Sciences contract DEFG02-96ER45439.

[1] See review in R.O. Simmons, J. Phys. Chem Solids **55**, 895 (1994).

[2] J.K. Hoffer, *et al.*, J. Low Temp. Phys. **23**, 63 (1976).

[3] E.R. Grilly, J. Low Temp. Phys. **11**, 33 (1973), in which the minimum is  $2.5316 \pm 0.0005$  MPa.

[4] D. Dyumin, *et al.*, Low. Temp. Phys. **19**, 696 (1993).

[5] B.A. Fraass, P.R. Granfors, R.O. Simmons, Phys. Rev. B **39**, 124 (1989).

[6] G.A. Lengua and J.M. Goodkind, J. Low Temp. Phys. **79**, 251 (1990).